UNIVERSITY OF CALGARY

The Effects of Patellofemoral Kinematics on Joint Congruence and Cartilage Stresses

by

Barbara Jean Kralovic

A THESIS

SUBMITTED TO THE FACULTY OF GRADUATE STUDIES

IN PARTIAL FULFILLMENT OF THE REQUIREMENTS FOR THE

DEGREE OF MASTER OF SCIENCE

DEPARTMENT OF MECHANICAL AND MANUFACTURING ENGINEERING

CALGARY, ALBERTA

JANUARY, 2000

ABSTRACT

Altered patellofemoral (PF) kinematics, associated with joint malalignment, muscle imbalances, or ligament injury, is speculated to be a potential cause of abnormal stresses, possibly leading to cartilage degeneration. The relation between kinematics and joint mechanics has not been well established. The purpose of this research was to investigate relations between kinematics, joint congruence, and cartilage stresses in a cat PF joint. Firstly, the congruence was quantified as a function of flexion angle, for a range of medial to lateral patellar tracking positions. Secondly, the effect of lateral versus central tracking on cartilage stresses and strains was quantified using a finite element model. Congruence and cartilage stresses were sensitive to patellar position. Lateral tracking decreased contact area by approximately 40%, and increased cartilage stresses and strains between 100% and 200%. This preliminary work suggests that patellar alignment may have important implications in terms of joint function and cartilage health.

ACKNOWLEDGEMENTS

The years spent working on my Masters thesis was a wonderful time for me. I found the Human Performance Laboratory a great place to work, learn, and to grow. I had the opportunity to interact with many capable people whom I both respect and admire for their competence and dedication to research. I met fascinating people from all over the world. It was their enthusiasm and openness that I found so motivating. I fondly remember the ski trips, hiking excursions, rafting adventures on the Kicking Horse, the ABCs, hacky sack club meetings on the roof, the HPL-international soccer games, tennis and squash matches, the lunches on the patio, barbeques, get-togethers, searching for Sid, the aching muscles (not so fondly) after core conditioning!! and most importantly I remember the laughter and comedy. Thank you, all of you!!

I would like to express special thanks to:

My supervisor, Dr. Janet Ronsky, for your enthusiasm, support and guidance, your grasp of the big picture, and forcing me to "run with it".

Dr. M. Epstein, Dr. N. Shrive, and Dr. R. Zernicke for taking the time to serve on my examination committee.

Steve Boyd, Dr. Salkauskas, and Dr. John Wu for technical assistance.

Alberta Heritage Foundation for Medical Research, Natural Sciences and Engineering Research Council of Canada, The Province of Alberta Scholarship Fund, and the Department of Mechanical Engineering for financial support.

Rich, for your crazy energy!!! for your love and support, ...for showing me the other side of the coin.

and last, but certainly not least!!, I would like to thank my family: my Mom, my Dad, and my brother, Paul. Thank you for everything! For understanding (and putting up with) me. For your love, support, and encouragement. For the years and years of comedy and laughter. You have always been there for me. Thank you!

for Mom and Dad

TABLE OF CONTENTS

LIST OF TABLES

LIST OF FIGURES

LIST OF ABBREVIATIONS

ACL: anterior cruciate ligament

CMC: carpometacarpal

CT: computed tomography

GCS: global coordinate system

MDPG: multi-station digital photogrammetry

MRI: magnetic resonance imaging

OA: osteoarthritis

PF: patellofemoral

RMS: root-mean square

SCS: surface coordinate system

SD: standard deviation

SPG: stereophotogrammetry

TPS: thin-plate spline

1.0 INTRODUCTION

A synovial joint is defined as a junction between two or more bones. Synovial joints function to permit movement with minimal friction and to transfer forces from one articulating bone to another. Synovial joints are important biomechanically because of their role in movement and locomotion. The patellofemoral (PF) joint is the articulation between the patella and the intercondylar groove on the distal aspect of the femur. The PF joint is made up of several structures: bone, articular cartilage, synovial fluid, muscle tendon units, and ligaments. Each of these structures contributes to the overall function of the joint.

The PF joint and its contributing structures function under demanding conditions. Mathematical models have predicted that the PF contact force may be several times body weight. The PF contact force in humans was calculated to be as high as three times body weight during stair climbing and descending (Matthews et al., 1977). For the cat, PF contact forces during walking were estimated to be 1.5 to 3.5 times body weight (Hasler and Herzog, 1998a). The joint can function successfully for an entire lifetime. However, frequently, the PF joint malfunctions, possibly due to injury or disease.

The following clinical disorders frequently affect the PF joint:

- chondromalacia,
- patellofemoral pain syndrome,
- patellar subluxation and dislocation, and
- osteoarthritis.

Briefly, chondromalacia is roughening, softening, and fibrillation of the surface of the retropatellar cartilage (Bentley and Dowd, 1984). Chondromalacia of the patella has been cited as the most frequently encountered cause of knee pain in young people (Insall et al., 1976). Patellofemoral pain syndrome is associated with anterior knee pain (Stergiou, 1996). Subluxation and dislocation of the patella are associated with instability of the joint and abnormal joint kinematics (Fulkerson and Shea, 1990). Subluxation is characterized by pain, swelling, locking-popping, and giving out of the knee (Hughston, 1968). Complete dislocation of the patella often results in gross articular damage (Fulkerson and

Shea, 1990). These clinical disorders may lead to osteoarthritis (OA). OA is the disease associated with joint and cartilage degeneration. OA is characterized by fibrillation and softening of the articular cartilage, as well as changes in the subchondral bone. OA poses a significant health risk. It is estimated that 63% of North Americans aged 55 or older suffer from OA (Lawrence et al., 1989). These pathologies have motivated study of the PF joint, to understand the underlying mechanisms of disease. Studies have been performed to determine the mechanical and biological variables that contribute to cartilage health and function. Knowledge of these variables will be useful in predicting, diagnosing, and treating joint disorders and disease.

Abnormal stresses acting on or within a joint are thought to be one of the causes of PF disorders (Radin et al., 1978; Moskowitz, 1992). Internal stresses, resulting from external loading, affect the health of articular cartilage. Cartilage degeneration has been initiated experimentally in animals by excessive loading. Impact loading, as well as chronic overuse, have led to cartilage degeneration (Dekel and Weissman, 1978; Moskowitz, 1992). Similarly, insufficient loading and joint immobilization have resulted in degenerative responses (Palmoski et al., 1980; Jurvelin et al., 1986). Osteoarthritic degeneration has also been found in normally unloaded regions in human hips (Bullough et al., 1973). These studies support the concept of a window of optimal loading to maintain adequate cartilage health (Bullough and Jagannath, 1983; Bullough, 1992). The distribution of stress within the joint is thought to maintain cartilage health by affecting the nutrition of the solid matrix and cartilage cells. Loading causes pressure gradients that stimulate the flow of pore fluid within the tissue. Movement of the pore fluid allows an influx of essential nutrients and an efflux of waste (Shrive and Frank, 1994). In addition, movement of pore fluid allows lubrication of the articular surfaces, thereby decreasing friction. Mechanical loading has also been shown to affect the metabolic activity of cartilage cells (Wong et al., 1997). Understanding the differences in joint loading and the resulting stress distributions between normal and abnormal joints may provide information on the mechanism of cartilage degeneration.

The distribution (i.e., magnitude and location) of joint stresses is a function of the following variables:

- joint geometry (of cartilage and subchondral bone),
- joint kinematics,
- material properties (of cartilage and subchondral bone), and
- external loading.

Physiologically, all of the above factors are highly interrelated. Knowledge of how these factors relate to joint stress, and their relative importance is necessary in understanding what changes occur in an abnormal joint to increase the risk of disease.

Abnormal joint kinematics has been frequently cited as a potential cause of clinical disorders, such as chondromalacia, patellar subluxation, dislocation, and osteoarthritis (Insall et al., 1976; Paulos et al., 1980; Huberti and Hayes, 1984; Fulkerson and Shea, 1990). Joint kinematics is affected by ligaments and muscles, as well as the geometry of the knee extensor mechanism. Ligaments passively restrain joint movement. Laxity or rupture of the restraining ligaments may lead to abnormal kinematics. For example, rupture or transection of the anterior cruciate ligament (ACL) has been associated with altered joint tracking and contact patterns (Ronsky et al., 1995; Herzog et al., 1998). Changes in joint tracking may be responsible for the osteoarthritic changes in the PF and tibiofemoral joints induced by ACL transection (Pond and Nuki, 1973). Also, excessive tightness of the ligaments, may contribute to lateral patellar tilt and joint malalignment (Paulos et al., 1980). Deficiencies in the quadriceps muscles, particularly the vastus medialis oblique, result in lateral tracking that may be linked to subluxation, chondromalacia, and patellofemoral pain syndrome (Paulos et al., 1980; Ahmed et al., 1983b). Abnormalities in the extensor geometry, such as abnormal patellar tendon length, patellar tendon alignment, and tibial tubercle height, have been proposed to affect patellar kinematics and stability (Insall et al., 1976; Paulos et al., 1980, Hirokawa, 1991). The alignment between the tibia and femur, described as the Q-angle (Figure 1.1), has also been studied (Huberti and Hayes, 1984; Hirokawa, 1991). A large and small Q-angle has been associated with medial or lateral tracking of the patella and chondomalacia (Paulos et

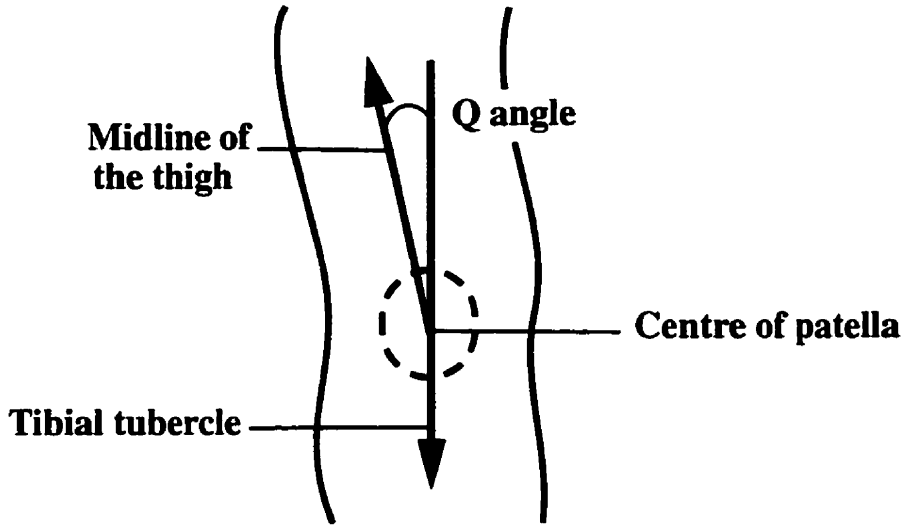

Figure 1.1: The frontal view of an extended knee joint. The Q-angle, used to describe joint alignment, was measured between a line connecting the middle of the patella to the centre of the tibial tubercle, and a line extending from the centre of the patella to the centre of the anterior-superior iliac spine on the pelvis.

al., 1980; Huberti and Hayes, 1984). Joint kinematics, specifically medial and lateral tracking of the patella, is therefore, an important variable associated with clinical disorders.

Abnormal joint kinematics has been proposed to cause mechanical loading outside the window of optimal loading, possibly leading to cartilage disorders and degeneration. Joint kinematics, together with the geometry of the articular surfaces, determine the contact geometry. Contact geometry is defined by the relative geometries of the two surfaces in the region of interaction. Joint congruence has been used to characterize contact geometry. Joint congruence describes the similarity of the geometries of the opposing surfaces. It has been suggested that joint congruence is an important factor affecting joint function. Joint congruence is believed to play a large role in the transmission of joint loads and the distribution of stresses. In addition, joint congruence affects joint movement and possibly joint stability. Therefore, there are a number of design criteria that determine the optimal joint congruence. The optimal congruence for joint function and cartilage health is not well understood. It has been suggested that higher congruence results in larger contact

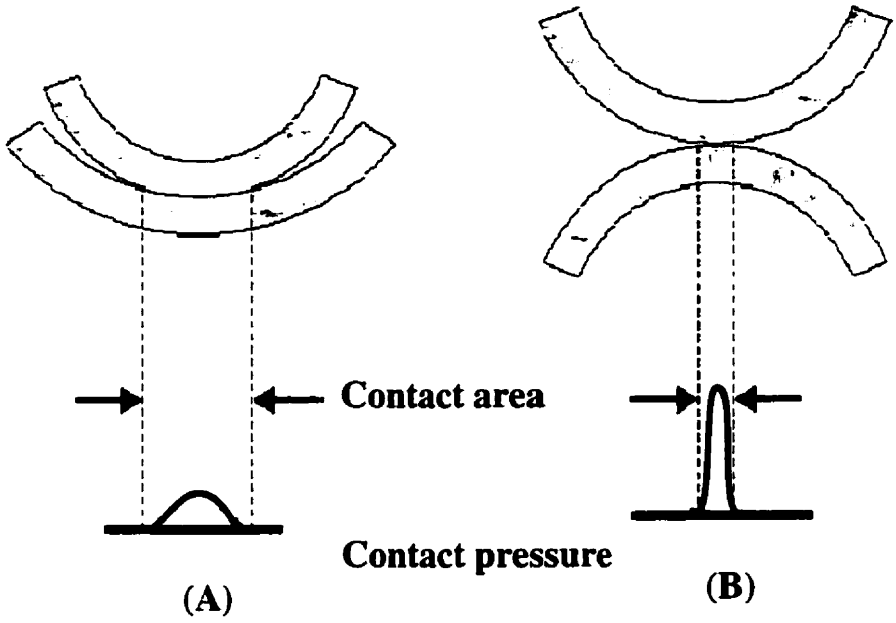

Figure 1.2: A cross-sectional representation of A) two highly congruent surfaces and B) two highly incongruent surfaces. Possible contact areas and contact pressure are shown (adapted from Mow et al., 1990).

areas (Figure 1.2). The joint loads would be distributed over a larger region resulting in a more uniform stress distribution and lower contact pressures. Lower congruence has been suggested to result in a smaller contact area, leading to a less uniform stress distribution and higher contact pressures. The congruence of the joint may change, however, as a function of loading and movement, due to the deformability of articular cartilage. Theoretical finite element models suggested that a certain amount of incongruence in the unloaded joint may allow a more equal distribution of stress under higher loads than a perfectly congruent joint (Eckstein et al., 1994). Incongruity is also speculated to promote pore fluid movement to provide nutrition to the cartilage matrix and cells as well as to allow joint movement. The optimal congruence and optimal patellar tracking to maintain joint function and cartilage health has not been well established.

In summary, patellar kinematics affects the joint congruence, thereby affecting joint stresses. The relations between joint congruence, joint stresses, and cartilage health have not been well established. Investigating the relations between kinematics, joint

congruence and the resulting joint stresses is useful in understanding the changes that occur in a destabilized or injured joint that may increase the risk of disease.

Both experimental and theoretical studies have investigated the effects of joint kinematics and contact geometry on joint stresses. Experimental studies have analysed the effects of

- Q-angle (Huberti and Hayes, 1984),
- flexion angle (Ronsky, 1994; Boyd, 1997),
- ACL integrity (Ronsky, 1994; Boyd, 1997; Herzog et al., 1998), and
- quadriceps loading and muscle imbalances (Ahmed et al., 1983b)

on contact area and peak contact pressures. The results indicated that changes in patellar kinematics affect the magnitude and location of the contact area and peak contact pressures. In general, central tracking was associated with a larger contact area and lower peak contact pressure. There are several limitations to these experimental studies. Firstly, the resulting PF kinematics is complex and difficult to classify. This makes it difficult to establish relations between joint kinematics and joint stresses. Secondly, an insufficient number of positions were investigated. To establish relations between joint alignment and joint stress, it is necessary to perturb the patella systematically throughout a full range of flexion angles and patellar orientations. This is difficult to do experimentally. Lastly, with experimental techniques it is not possible to measure the distribution of stress throughout the depth of the cartilage or bone.

While several studies have characterized the geometry of the PF joint surfaces (Kwak et al., 1997), to date, no studies have incorporated kinematics to quantify the contact geometry. Few models have been used to study the effects of theoretically perturbing joint kinematics. One model (Hirokawa, 1991) showed that both an increase and decrease in Q-angle results in changes in contact geometry and substantial increases in cartilage stresses. The effects of perturbing joint surface geometries on cartilage and bone stresses have also been investigated using numerical models (Eckstein et al., 1994; Stone and Yu, 1997). Results indicate that the magnitude and distribution of joint stress vary considerably depending on joint geometry. However, these models are typically oversimplified, using non-specific geometry. While indicating general trends, they do not accurately simulate

the complex surface interactions expected in real joints. In addition, simplified material properties limit the validity of the models.

In summary, the experimental and theoretical studies suggest that joint kinematics and joint congruence play large roles in the distribution of joint stresses. However, these investigations have not been sufficient in establishing relations between patellar alignment and stresses in the cartilage. To date, the effects of incrementally perturbing the patellar orientation on joint congruence and cartilage stress has not been investigated. Understanding the relations between kinematics, joint congruence and cartilage stress may provide insight into joint function, the effects of injury, and the mechanisms of cartilage degeneration. Knowledge of optimal tracking patterns would be useful to establish rehabilitation and treatment protocols.

The purpose of this research was to investigate the complex relations between patellar orientation, joint congruence, and the resulting cartilage stresses. The goal was to gain a better understanding of how kinematics affects joint mechanics. This would provide further insight into the effect of muscle imbalances and ACL injuries, and possibly the causes of joint degeneration.

This research investigated three speculations:

Speculation 1. joint congruence varies throughout the flexion/extension range of motion,

Speculation 2. joint congruence is highest for central tracking, and decreases with medial or lateral tracking,

Speculation 3. lateral tracking, compared to central tracking results in decreased contact area, increased contact pressure, increased principal stresses, increased Tresca stresses, and increased principal strains.

There were two main objectives of this research. The first objective was to quantify the congruence of a PF joint, with the following specific aims:

Specific aim 1. to quantify congruence index for a range of flexion angles (30° to 90°),

Specific aim 2. to quantify congruence index for a range of medial to lateral patellar tracking positions.

Specific aim 1 investigated speculation 1, while specific aim 2 investigated speculation 2. A geometric model of a cat PF joint was used (Boyd, 1997). The range of joint congruence values indicated how sensitive the PF joint is to changes in patellar kinematics. The values of joint congruence for different patellar orientations were compared to assess cartilage stresses indirectly. It was assumed that a more congruent joint would result in lower cartilage stresses.

The second objective was to assess cartilage stresses and contact mechanics, with the following specific aim:

Specific aim 3. to quantify the contact area, contact pressure, principal stresses, Tresca stresses, and principal strains for a central and a lateral patellar position.

Specific aim 3 investigated speculation 3. A finite element model of a cat PF joint was used. The range of joint stresses provided an indication of how sensitive the PF joint is to changes in patellar kinematics. It was hypothesized that the changes in joint stress would be directionally consistent with the changes in congruence index.

The thesis continues with a review of the PF joint anatomy (Chapter 2). The thesis is divided into two parts, each dealing with one of the objectives stated above. Each part has a separate literature review, methods, results, and discussion. The effect of joint kinematics on joint congruence is presented in Chapter 3. The effect of joint kinematics on cartilage stresses is presented in Chapter 4. A general summary (Chapter 5) concludes the thesis.

2.0 PATELLOFEMORAL JOINT ANATOMY

The knee is a complex structure consisting of two synovial joints; the tibiofemoral joint and the PF joint. Both joints affect the global function of the knee. Focusing on the PF joint, the patella, embedded in the patellar tendon, slides in the intercondylar groove on the distal anterior aspect of the femur. The main functions of the patella (Heegaard et al., 1995) include:

- improving efficiency of the extensor muscles by increasing the moment arm,
- centralizing the forces of the quadriceps muscles, and
- providing a smooth sliding mechanism with low friction.

The patellar cartilage is frequently inflicted with disease and degeneration (Ficat and Hungerford, 1977). The high incidence of disease has motivated research of the PF joint.

The following is a general description of PF joint anatomy. The PF joint consists of many unique structures, each contributing to the function of the joint. The PF joint consists of subchondral bone, articular cartilage, synovial fluid, muscles, tendons, ligaments, and menisci. The above structures and their role in the healthy function of the joint will be described.

Bone is dense, hard connective tissue that makes up the majority of the skeleton. Bones have two major mechanical functions:

- to provide support for soft tissue, and
- to act as a lever system to transfer forces.

Bone, at the articulating regions, provides the foundation for calcified cartilage and articular cartilage. The shape of the subchondral bone surface influences joint congruence and contact stresses in the joint. The bone also provides attachment for ligaments and muscle tendon units.

Articular cartilage is a thin layer of connective tissue that lines the articular surface of bones in synovial joints.

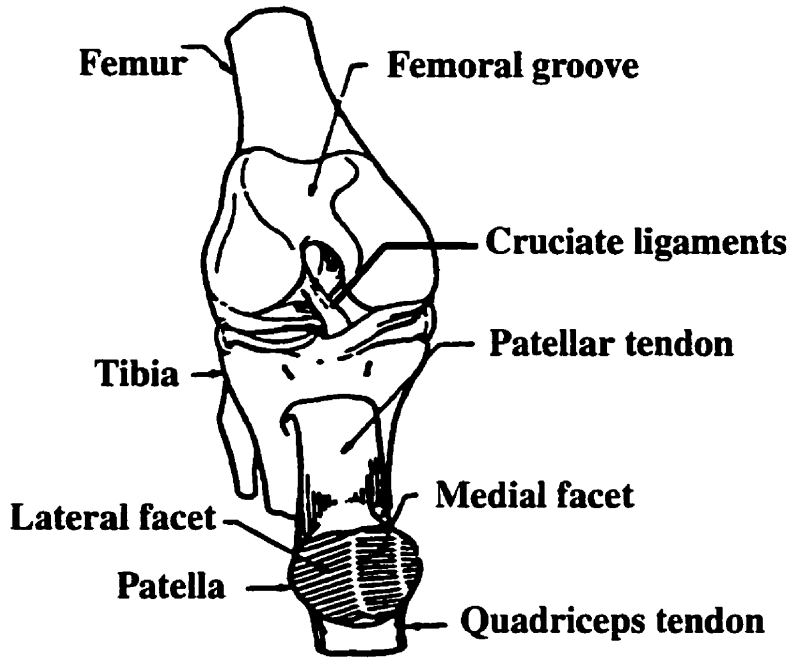

Figure 2.1: The knee is comprised of two joints; the tibiofemoral joint and the patellofemoral joint (from Ahmed et al., 1983b).

The major functions (Shrive and Frank, 1994) of cartilage include:

- painlessly transferring forces between articulating bones,
- distributing forces in the joint, and
- allowing joint movement with minimal friction.

Articular cartilage is a complex material. It behaves as a non-linear, inhomogeneous, and anisotropic material (Newman, 1998). The structure of articular cartilage contributes to its material properties and affects the ability of cartilage to transmit and distribute force. Understanding its structure and material properties is necessary to model tissue behaviour theoretically.

Articular cartilage is a biphasic material. It is made up of porous extra-cellular matrix (20-40% of the wet weight of cartilage), tissue fluid (60-80%) and chondrocytes or cells (5%). The extracellular matrix is a complex arrangement of structural macromolecules consisting of collagen, proteoglycans, and other proteins. The collagen provides the structural framework of the cartilage and gives it much of its tensile strength.

Proteoglycans are meshed in the network of collagen. The proteoglycans consist of a protein core with multiple sulfated glycosaminoglycan chains. The glycosaminoglycan chains have a negative electrostatic charge, producing two consequences. First, the proteoglycans attract water, and second, the chains repel each other keeping them at a distended state. The result is a viscoelastic gel, responsible for the low permeability, as well as the compressive strength of cartilage.

Tissue fluid plays a large role in cartilage material properties, joint lubrication, and tissue nutrition and health. The fluid can move in and out of the cartilage. Fluid movement causes an influx of nutrients, and an efflux of waste, thereby promoting tissue health. The permeability of the matrix is low. This prevents the fluid from being squeezed out quickly under compression, protecting the solid matrix during impact loading. It is estimated that in healthy cartilage, for the first few seconds of loading the compressive stress is borne mostly by the fluid phase. Only after a period of continuous loading (hundreds of seconds) is equilibrium reached. At equilibrium all the fluid has been exuded and the load is supported by the solid matrix (Newman, 1998).

The structure and composition of articular cartilage varies with distance from the joint surface. Four zones can be identified; superficial, transitional, deep, and calcified zone (Shrive and Frank, 1984). In the superficial zone, cartilage fibres lie parallel to the joint surface (Figure 2.2). It is speculated that the fibres at the surface are oriented to resist tensile stress. In the transitional zone the fibres have a more random orientation. In the deep zone the collagen bundles are oriented perpendicular to the subchondral bone. It is speculated that the fibres in the deep zone are oriented to resist shear stress. In addition, the solid to fluid ratio varies with depth (Maroudas, 1979). The superficial zone has the highest fluid concentration, and this concentration decreases linearly with depth. As well, the permeability of the cartilage varies with depth. Since the deep zone has the highest content of proteoglycans, it has the lowest permeability (Maroudas, 1979). The structure and composition of articular cartilage results in a highly non-linear, inhomogeneous, anisotropic material (Shrive and Frank, 1984). Due to the complex nature of cartilage, it is difficult to quantify the material properties necessary to model the tissue theoretically.

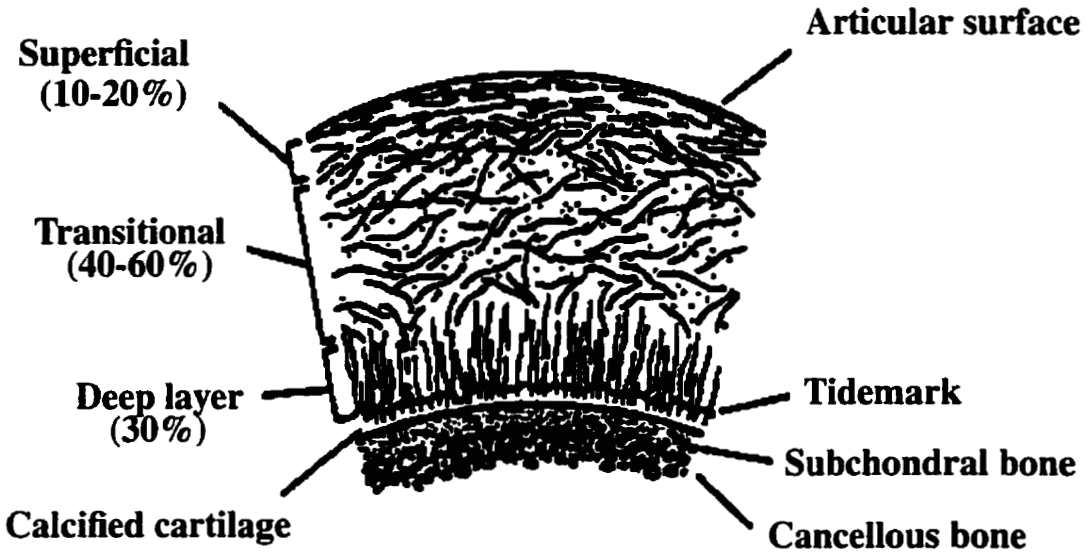

Figure 2.2: Schematic drawing of the structure of articular cartilage (from Mow and Proctor, 1989).

A review of methods used to quantify the material properties, as well as the material property values reported in the literature, is presented in Chapter 4.

In addition to structure and material properties, the geometry of the cartilage surfaces plays a large role in force transmission and distribution (Eckstein et al., 1994; Stone and Yu, 1997). The articular surfaces of the PF joint are saddle-shaped (Ateshian et al., 1991; Boyd, 1997; Kwak et al., 1997). The complex shape of the articular surfaces affects joint congruence and joint stresses. As well, non-uniform cartilage thickness (Ateshian et al., 1991) is thought to influence the distribution of stresses within the joint.

Synovial fluid is a viscous fluid secreted by the synovial membrane in joints. Its main functions are to

- lubricate the articulating joint surfaces, and
- provide nutrients to the cartilage.

The synovial fluid influences the behaviour of cartilage. It permits the diffusion of gases

and nutrients and lubrication, making it essential to the health of the tissue. The degree of fluid movement is affected by the joint congruence and loading conditions between articular surfaces.

Muscles and tendons have an important role in joint function. Muscles are attached to bone by tendons. Muscle tendon units have two main functions:

- to transfer forces across joints to effect movement, and
- to stabilize the joint actively.

Muscles and tendons affect the kinematics of the bones. By affecting the relative position of the articulating surfaces, muscles influence the contact geometry and the distribution of joint stresses. All muscles affecting the position of the patella, femur, and tibia play a role in PF mechanics. The knee extensor mechanism has a large effect on the patella. The quadriceps femoris is the extensor muscle of the leg and is comprised of four individual muscles (Ahmed et al., 1983b); the rectus femoris, vastus intermedius, vastus medialis (longus and oblique), and vastus lateralis (Figure 2.3). The tendons of the vastus medialis and lateralis insert at the medial and lateral borders of the patella, respectively. Therefore, the alignment of the patella is particularly influenced by these muscles (Ahmed et al., 1983b). The tendons of the rectus femoris and vastus intermedius insert at the base of the patella. The continuation of the quadriceps tendon is the patellar tendon, which attaches to the tibial tubercle. The height of the tibial tubercle and the length of the patellar tendon also influence joint mechanics (Ferguson et al., 1979).

Clinically, abnormal function of the extensor mechanism has been related to chondromalacia, patellofemoral pain syndrome, subluxation and dislocation of the patella, and as a possible factor contributing to diseases that cause cartilage degenerative, such as osteoarthritis (Insall et al., 1976; Paulos et al., 1980; Huberti and Hayes, 1984). Therefore, the quadriceps muscles have an important role in joint function and health. It is also speculated that tendons may provide proprioceptive feedback for joint position, thus assisting with stabilizing the joint.

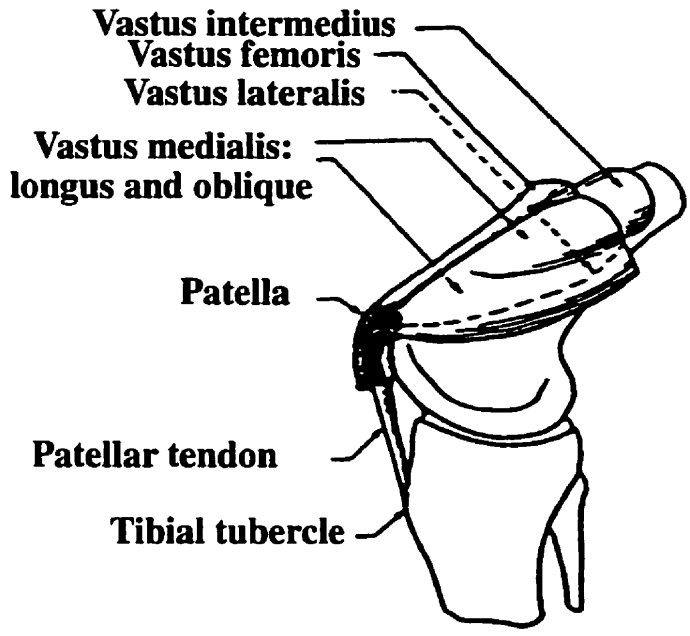

Figure 2.3: The knee extensor mechanism. Muscle imbalances and the geometry of the mechanism (muscle attachment sites, elevation of tibial tubercle, and length of the patellar tendon) influence joint function and knee stability (From Ahmed et al., 1983b).

Ligaments attach one articulating bone to another across a joint. The main functions of ligaments are to guide motion, and constrain relative movement of the bones to stabilize the joint. In the knee the intra-articular cruciate ligaments function to restrain anterior and posterior tibial displacement and tibial rotation. The collateral ligaments, found outside the joint capsule, restrain varus/valgus angulation and rotation. Ligament laxity and rupture may lead to joint instability, affecting the articular contact mechanics and distribution of joint stresses. It is also speculated that nerves in ligament tissue may permit sensing of joint position, possibly initiating protective reflexes (Frank and Shrive, 1994).

Menisci are crescent-shaped fibrocartilaginous bodies attached to the tibial plateau. Their major functions are to

- distribute compressive pressure, and
- help stabilize the articulation between the tibia and femur.

Their function is related to the tibiofemoral joint, but has been shown to affect the global function of the knee (Fujikawa et al., 1983).

Each of the above structures plays an integral role in the healthy and function of the PF joint. Failure or disease of any of the supporting structures may drastically alter joint function.

3.0 PATELLOFEMORAL JOINT CONGRUENCE

3.1 LITERATURE REVIEW

Joint geometry plays a large role in joint function (Bullough, 1992; Bullough and Jagannath, 1983). The shape of the joint is a key factor determining the transmission of joint loads and the distribution of stresses (Eckstein et al., 1994; Stone and Yu, 1997). In addition, the joint geometry affects the freedom of movement between the articulating surfaces, as well as the stability of the joint (Bullough, 1992; Bullough and Jagannath, 1983). Joint congruence has been used to characterize contact geometry. The goal of this literature review is to

- define joint congruence,
- present the implications of joint congruence on joint function, and
- present the ways to analyse joint congruence, and to discuss the advantages and limitations of each.

3.1.1 Definition and Implications of Congruence

Joint congruence is defined as the mechanical property of surface coincidence when the joint surfaces are superimposed (Hamilton, 1996). A joint position in which the surfaces coincide is a perfectly congruent joint position. Conversely, a joint position in which the surfaces do not coincide is called an incongruent position. Joint congruence depends on the joint geometry, as well as the position and orientation of the joint surfaces, the mechanical properties of the bone and cartilage, and joint loading.

Joint congruence is an important factor affecting contact mechanics and joint function. Joint congruence affects the transmission and distribution of joint loads, which in turn affects cartilage health. Joint congruence also plays a role in determining the relative motion between the articulating surfaces affecting joint movement. Therefore, there are a number of design criteria that determine the optimal joint congruence. It has been suggested that optimal congruence results in a uniform distribution of stress and hydrostatic pore fluid pressures under large loads (Greenwald and O'Conner, 1971; Eckstein et al., 1994). Conceptually, for a more congruent joint position, loading results in

a larger contact area. Since, the joint loads are distributed over a larger surface area, presumably lower peak stresses result (Fujikawa et al., 1983; Ateshian et al., 1992). Conversely, for a less congruent joint position, a smaller area of contact may result in higher peak stresses. However, due to the biphasic properties of articular cartilage, as the joint is loaded the articular cartilage deforms and the joint congruence changes. The optimal unloaded joint congruence is not well established.

Theoretical analyses have shown that a perfectly congruent unloaded geometry does not permit equal distribution of stress (Greenwald and O'Conner, 1971; Eckstein et al., 1994). A perfectly congruent ball and socket joint, like the hip joint, yielded a "bell-shaped" stress distribution with peak values in the depth of the socket, falling to zero peripherally. A slightly incongruous joint with a deeper socket yielded a better distribution of stresses. At smaller loads the incongruous joint resulted in two contact regions located towards the joint margins, rather than a single contact region in the deepest part of the joint. Under increasing load, the two distinct contact regions gradually merged, until the deepest part of the joint came into contact. The slightly incongruent joint resulted in lower peak stresses and a more equal stress distribution. It has also been suggested that a certain amount of incongruence may be necessary for pooling and movement of synovial fluids affecting cartilage nutrition (Eckstein et al., 1994; Bullough and Jagannath, 1983). In addition, incongruence may facilitate the relative movement of the joint surfaces. However, the PF joint is a saddle joint and its function is very different than a ball and socket joint. It is not clear whether the PF joint demonstrates the same type of bicentric contact pattern. In conclusion, the optimal PF joint congruence for efficient load distribution and joint health is currently not well understood. The study of joint congruence may provide an indication of its importance in terms of joint function and health.

Abnormal joint congruence may be a result of abnormal kinematics, abnormal geometry, or abnormal mechanical properties of the bone and cartilage. Abnormal kinematics may be caused by

- muscle imbalances (Ahmed et al., 1983b),

- injuries to ligaments and joint stabilizers (Ronsky et al., 1995),
- joint malalignment (Paulos et al., 1980; Bentley and Dowd, 1984; Huberti and Hayes, 1984), and an
- abnormal extensor mechanism (Ferguson et al., 1979; Hirokawa, 1991).

Abnormal joint geometry may be due to:

- natural morphology (Ateshian et al., 1992),
- remodelling with age (Eckstein et al., 1994),
- remodelling due to joint atrophy (Goodfellow and Mitsou, 1977),
- fibrillation and geometric changes related to disease (Bentley and Dowd, 1984), and
- geometric changes associated with injury.

Finally, abnormal mechanical properties of cartilage and bone are associated with disease, for example, chondromalacia (Bentley and Dowd, 1984) and osteoarthritis (Bullough, 1992). One focus of this thesis is to analyse the effects of abnormal kinematics on joint congruence.

3.1.2 Quantification of Congruence

While the term congruence is used frequently to describe the relative geometries of two objects qualitatively, it has not been well-defined in the biomechanics literature. The calculation of congruence for two joint surfaces with complex geometry is not a trivial problem. Ideally, congruence should be a global measure taking into account the differences between the complex 3D geometry of both joint surfaces.

An example of a global measure of relative joint geometries was the index of sphericity used to quantify the congruence of the hip joint. The global 3D geometries of the acetabulum and the femoral head were characterized by an index of sphericity (Bullough et al., 1973). The index was taken as a measure of the departure from sphericity of each surface. The comparison of the two indices indicated the global congruence of the hip joint. However, this method only applied to ball and socket joints. It could not be used to characterize the complex geometries of saddle joints, such as the PF joint. In addition, the global measure of the sphericity was independent of joint position. To investigate the effect of abnormal kinematics on joint mechanics it is necessary to quantify congruence as a function of joint orientation.

While the quantification of relative joint geometries on a global level is a complex problem that has not been solved in the biomechanics literature, numerous measures have been used to investigate congruence. Both 2D and 3D measurements of joint geometry, as well as contact area, have been used to indicate PF joint congruence. The advantages, limitations, and application of each measure will be discussed. While contact pressure and cartilage stress may also be used to indicate joint congruence, they will be discussed in Chapter 4.

3.1.2.1 Two Dimensional Geometric Measures

Two dimensional measures of joint geometry have been useful indicators of how the PF joint surfaces interact at a given position. Congruence angle, lateral PF angle, and the comparison of the patellar facet angle and the femoral sulcus angle have been used by clinicians to identify joint instabilities, such as subluxation and the potential for patellar dislocation (Bentley and Dowd, 1984). These geometric measures have been used to indicate joint congruence. These angles typically have been measured from transversely oriented radiographs, and more recently from magnetic resonance images (MRI).

The congruence angle described the orientation of the patella within the femoral groove (Merchant et al., 1974). To calculate the congruence angle, the sulcus angle defining the femoral groove, was bisected, and a line between the lowest point in the femoral groove and the vertex of the patella was drawn (Figure 3.1). The angle between these two lines was defined as the congruence angle. Large positive congruence angles indicated less congruent joint positions associated with malalignment and subluxation (Merchant et al., 1974). The sulcus angle was a measure of the femoral geometry. While the femoral geometry constrained the patella and was associated with patellar instability, the sulcus angle alone did not indicate joint congruence, and therefore will not be discussed.

The lateral PF angle also provided an indication of patellar orientation within the femoral groove (Bentley and Dowd, 1984). The lateral PF angle typically was measured from a transverse radiograph of the PF joint in 20° flexion. The lateral PF angle was defined as the angle between a line connecting the highest points on the femoral condyles, and a line

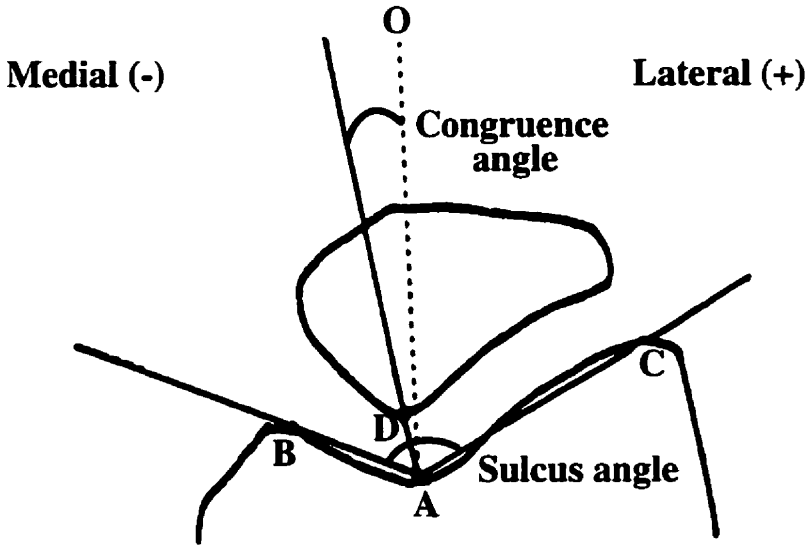

Figure 3.1: The congruence angle (∠DAO) was defined as the angle between the zero reference line (dotted line), bisecting the sulcus angle, and a line drawn between the lowest point in the femoral groove (point A) and the vertex of the patella (D). The sulcus angle (∠BAC) was the angle between the highest points on the femoral condyles and the lowest point in the groove. (from Merchant et al., 1974).

connecting the two ends of the lateral facet (Figure 3.2). Typically, normal knees exhibited a small lateral PF angle. Parallel lines or an angle opening medially have been associated with patellar subluxation and indicated less congruent joint positions (Laurin et al., 1978). Koskinen et al. (1991) used lateral PF angle as one of the criteria to evaluate knees with subluxation and dislocation of the patella pre-operatively, and post-operatively after combined lateral release and tibial tuberosity transposition. Therefore, the lateral PF angle indicated how the PF joint surfaces interact.

Another measure of congruence was the comparison of the patellar facet angle and the femoral sulcus angle. In congruent joints the angles are very similar. In eight normal cadaver knees the sulcus angle was generally larger than the patellar facet angle (Fujikawa et al., 1983). The angles were measured from the cartilage geometry on transverse slices taken through the patella and femoral groove. Before the bones were sliced, contact between the patella and femur was measured at various flexion angles using casting

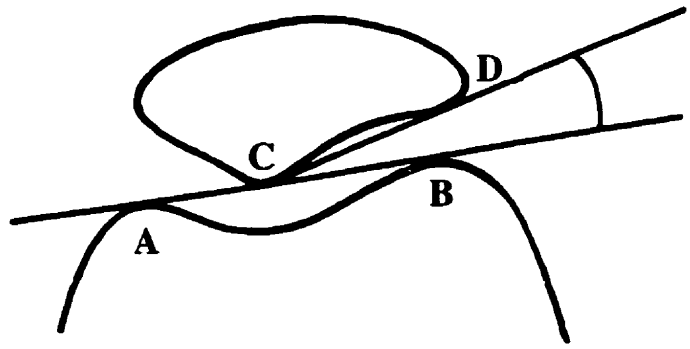

Figure 3.2: The lateral PF angle (∠BCD) was measured between the line connecting the highest points on the femoral condyles (AB) and a line drawn across the two ends of the lateral facet of the patella (CD) (from Bentley and Dowd, 1984).

material. A comparison of the patellar facet and sulcus angles and regions of contact showed that contact occurred in regions where the congruence was high. The PF joint showed high congruence between the distal part of the patella and the proximal part of the femur, between the middle part of each structure, and between the proximal part of the patella and the distal part of the femur.

Each of the above measures was useful in characterizing PF joint geometry. The measures were non-invasive with the use of radiographs, computed tomography (CT), and MRI. They were useful in diagnosing certain knee problems such as subluxation and dislocation and in evaluating treatment. However, these geometric measures had a number of disadvantages. Firstly, they were PF joint specific and could not be generalized to other joints. Secondly, in most studies the angles were calculated at just one joint position and one loading condition. This was not sufficient in characterizing joint congruence because the interaction between the surfaces may change throughout the range of motion of the joint (Hamilton, 1996). The number of joint positions was limited due to concerns regarding radiation exposure. Therefore, due to technical constraints of non-invasive imaging, the full potential of the 2D joint measures as clinical tools may not currently be realized. Thirdly, radiographic techniques typically were based on the measurement of bone. This may not be representative of contact characteristics where the cartilage has

non-uniform thickness, such as the PF joint (Ateshian et al., 1991). Fourthly, the angles were dependent on the accuracy and repeatability of positioning the transverse slice. In addition, the relations between these geometric measures and joint forces and stresses has not been established. Finally, the 3D geometry of the joint surfaces is complex, and it is questionable whether it can be characterized properly by measurements taken in one plane.

3.1.2.2 3D Geometric Measures

The geometry of the joint surfaces plays a large role in joint congruence and contact mechanics. The previously discussed 2D geometric measurements were not sufficient in characterizing the complex geometry of joint surfaces. Numerous methods, ranging in complexity, have been used to obtain the 3D geometry of articulating surfaces:

- plaster molding measured by a coordinate measuring machine (Scherrer and Hillberry, 1979),
- stereophotogrammetry (SPG) (Ateshian et al., 1991),
- MRI (e.g., Ronsky, 1994),
- multi-station digital photogrammetry (MDPG) (Ronsky et al., 1999), and
- laser scanning (Haut et al., 1998).

These methods resulted in a set of data points representing the surface. The surfaces can be reconstructed and mathematically represented using a number of different spline fitting techniques; piecewise bi-cubic surface patches (Scherrer and Hillberry, 1979), least squares B-spline surface fitting technique (Ateshian et al., 1993), and the thin-plate spline (TPS) technique (Lancaster and Salkauskas, 1986) have been used.

Typically, curvature maps have been used to characterize the surface topology (Ateshian et al., 1992; Kwak et al., 1997). Surface curvatures were obtained using differential geometry (Beck et al., 1986). Briefly, an outward normal $\mathbf{n}(u,w)$ was defined at each point $\mathbf{x}(u,w)$ on the surface **S** (Figure 3.3). When a plane was rotated around the normal, a family of curves **C** was generated. The curvatures at $\mathbf{x}(u,w)$ assumed a maximum and minimum value (principal curvatures), along mutually perpendicular directions (principal directions).

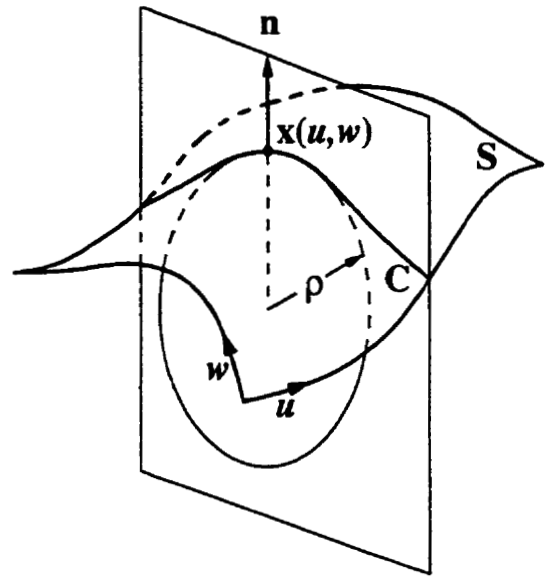

Figure 3.3: An outward normal vector **n** was constructed at every point $\mathbf{x}(u,w)$ on a surface **S**. By rotating the plane a family of curves **C** were generated. Their curvature at $\mathbf{x}(u,w)$ assumed a maximum and minimum value (principal curvatures), along mutually perpendicular directions (principal directions) (from Ateshian et al., 1992).

Plots of the minimum and maximum curvatures identified regions of greatest concavity and greatest convexity, respectively (Ateshian et al., 1992). For example, regions of maximum curvature were used to identify the proximal median ridge and lateral transverse ridge, observed in 97% of the 49 human patella (Kwak et al., 1997). Lines of minimum curvature were used to emphasize the direction of the ridges. Two additional measures of curvature have been reported: Gaussian curvature and RMS curvature. The Gaussian curvature was the product of the principal curvatures:

$$K = \kappa_{min}\kappa_{max}, \tag{1}$$

where K was Gaussian curvature and κ_{min} and κ_{max} denoted minimum and maximum principal curvatures, respectively.

The sign of the Gaussian curvature indicated the shape of the surface in the neighbourhood of that point. If K=0, the surface was cylindrical, if K<0,the surface was sellar or saddle

shaped, and if $K>0$, the surface was ovoid. Gaussian curvature has been used to determine sellar and ovoid regions of the CMC joint surfaces (Ateshian et al., 1992).

RMS curvature was a measure of surface flatness. Although the RMS curvature accounted for both minimum and maximum curvature, it did not provide any information about the direction of curvatures.

$$K_{RMS} = \sqrt{\frac{\kappa_{min}^2 + \kappa_{max}^2}{2}}, \tag{2}$$

where K_{RMS} was RMS curvature and κ_{min} and κ_{max} denoted minimum and maximum principal curvatures, respectively.

A value of $K_{RMS}=0$ indicated a perfectly flat surface in the neighbourhood of that point. K_{RMS} could not assume negative values. RMS curvature was used to determine the most and least curved regions on the surfaces of the CMC joint (Ateshian et al., 1992).

Joint congruence has been estimated by comparing the curvature maps of the two opposing joint surfaces. Similar curvature maps throughout the range of motion indicated a congruent joint. Qualitative analysis showed that the human PF joint surfaces have similar curvatures (Kwak et al., 1997). Relatively consistent curvatures in the anteroposterior direction in the femoral groove indicated that the joint congruence may vary little over a range of motion. For the carpometacarpal (CMC) thumb joint, in the neutral position, the principal directions of curvature on the trapezial and metacarpal surfaces were approximately aligned (Ateshian et al., 1992). From the maps of minimum and maximum curvature, regions of greatest convexity on the metacarpal were aligned with regions of greatest concavity on the trapezium. This suggested that, in a neutral position, the CMC joint was highly congruent.

Typically, the surfaces of the articular cartilage were used to characterize joint geometry. This accounted for non-uniform cartilage thickness and was more representative of joint surface interaction than using subchondral bone geometry. Although measuring the 3D

geometry was time consuming and complex, it provided a more complete description of surface geometry than 2D measures. While comparing the geometry of both articulating surfaces estimated joint congruence, without knowledge of the position and orientation of the joint surfaces, the comparison was strictly qualitative. To quantify surface interaction properly, joint kinematics must be introduced. Since congruence is dependent on the joint position, it is of interest to quantify congruence for a range of motion. It is useful to characterize joint congruence for specific movements that may cause injury (e.g., patellar subluxation or dislocation).

3.1.2.3 Contact Area

Joint contact area measurements have been used to quantify congruence. Recall that high congruence has been associated with increased contact area. Conversely, decreased contact area indicated an incongruent joint position. Contact area measurements depend on the joint surface geometry, the relative positions and orientation of the joint surfaces, as well as joint loading. The following are examples of methods that have been used to measure contact area:

- silicon rubber casting method (Fujikawa et al., 1983),
- micro-indentation transducers (Ahmed and Burke, 1983a; Ahmed et al., 1983b), and
- pressure sensitive film (Fukubayashi and Kurosawa, 1980; Huberti and Hayes, 1984; Huberti and Hayes, 1988; Ronsky et al., 1995).

Experimentally based geometric models have been used to calculate contact area indirectly (Ateshian et al., 1994; Boyd et al., 1999).

Contact area has been used to study surface interaction under a variety of conditions. Contact area has been measured during isometric loading for various flexion angles. Typically, for the human knee PF contact area increased from full extension to 60° to 80° flexion, after which the contact area decreased (Ahmed et al., 1983b). Similar findings were reported in humans using MRI, and in cat PF joints, using pressure sensitive film (Ronsky, 1994; Ronsky et al., 1995). Changes in contact area suggested that joint congruence varied with flexion angle. Since the load was held approximately constant, the changes in congruence were attributed to the changes in contact geometry. Contact

characteristics have been studied during unconstrained extension resulting from stimulation of the quadriceps (Boyd, 1997). A model, based on surface geometry collected using MDPG and kinematic data collected using high speed video, was used. Contact area increased with flexion angle and was laterally positioned throughout the range of motion. It was not known whether lateral tracking was a true result or if it was due to systematic error in the kinematic measurements, or constraints applied to the knee by the experimental set-up. Moreover, it could only be hypothesized whether non-central contact is a characteristic of the normal cat PF joint. A study using pressure sensitive film showed that, in the cats measured, the contact region was predominantly located on the lateral side of the joint (Herzog et al., 1998). However, other studies of contact in the cat (Ronsky et al., 1995) and human PF joints (Ahmed et al., 1983b; Ronsky, 1994) have shown that contact is primarily located in the centre of the joint. It would be of interest to reorient the patella centrally to document resulting changes in congruence, and to determine optimal tracking based on surface geometries.

The effects of changes in muscle function on contact area have been characterized. For the cat, contact patterns were calculated for isometric stimulation of the quadriceps under 60%, 75%, 95%, and 100% of maximum force (Ronsky, 1994). Results showed that the contact area increased with load. Contact area measurements have been used to investigate the effects of abnormal muscle alignment and muscle imbalances (Ahmed et al., 1983b). The effect of varying the tension in the components of the quadriceps was analysed using micro-indentation transducers. Alterations in the vastus lateralis and vastus medialis tension had the most effect on contact mechanics. The different loading conditions affected the location of the contact area as well as its magnitude. Since the load applied to the joint varied, the resulting congruence was due to a change in contact geometry, as well as a change in joint loading. Unless, the load or contact geometry are held constant, it is difficult to determine their relative effect on joint congruence.

The effects of joint alignment on congruence have also been studied. For example, the influence of Q-angle was investigated for a variety of flexion angles and loading conditions on the human PF joint (Huberti and Hayes, 1984). The contact area decreased

as a result of both an increase and decrease in Q-angle, resulting in larger contact pressures. This suggested that perturbing the Q-angle caused a change in patellar kinematics resulting in a less congruent contact position. A number of researchers quantified changes in contact area due to ACL transection/rupture in both human and cat PF joints (Ronsky, 1994; Boyd, 1997; Herzog et al., 1998). Changes in location and magnitude of contact area indicated that ligament transection resulted in changes in kinematics that influence joint congruence. Contact area has also been used to evaluate the effects of passive stabilizers. Huberti and Hayes (1988) used pressure sensitive film in cadaver knees to evaluate capsular reconstructive techniques (medial plication, lateral plication, lateral release, and bilateral release).

Using contact area to characterize joint congruence has a number of advantages. First, the effects of joint geometry, joint kinematics and joint loading are all taken into account. Using contact area analysis, changes in joint contact geometry and joint loading due to motion, different muscle activation patterns, ligament integrity, and joint capsular constraints can be assessed. Although contact area measurements provide an indication of global changes in joint mechanics this method has a number of disadvantages. Firstly, there are limitations associated with the methods used to measure contact area. For example, the casting method, and use of pressure sensitive films, and transducers involve introducing material between the joint surfaces. The net thickness of the micro-indentation transducer used by Ahmed et al. (1983b) was 0.285 mm. The thickness of pressure sensitive film was approximately 0.2 to 0.3 mm. Finite element models suggest that this is enough to alter the interaction of the articular cartilage surfaces (Wu et al., 1998b). Depending on the geometry, material properties, and loading, the introduction of the film was estimated to change the maximum contact pressure by 10-25%. Experimentally based geometric models do not require introducing any material between the joint surfaces. However, since the models are based on unloaded geometries they do not account for changes in cartilage and bone geometry during loading. This method also requires a subjective definition of contact, often based on proximity. Secondly, the contact area is a function of joint loading. For in-vitro or in-situ experiments where loading was induced by

stimulation of the nerves or manually, the loading pattern may not be entirely physiologic. The resulting contact patterns also may be non-physiologic, and this must be taken into account when interpreting the results. In addition, if contact force was not carefully controlled, variations in contact area may be due to a combined effect of changing the contact geometry as well as changing the magnitude and/or direction of loading.

It is useful to study the contribution of loading and geometry independently. For this reason it is useful to compare congruence between contacting positions under constant load. In addition, a number of studies analysed contact area for two conditions (i.e., before and after capsular reconstruction, or before and after ACL transection). It is important to recognize that the biologic system is continuously adapting and remodelling. Therefore, it is of value to understand the effects of kinematics not only under two isolated conditions but throughout a physiologic range of contact positions. This requires prescribing incremental changes to joint kinematics under known load. This type of a sensitivity analysis is very difficult to perform experimentally because of the current inaccuracies and inabilities in controlling joint loads and positions.

Hamilton (1996) established a method to assess the changes in contact area due to perturbing the joint position theoretically. A geometrical model of the subtalar joint in the ankle was created based on MRI data. Both the cartilage and subchondral bone surfaces were represented. An optimization algorithm was used to move the joint virtually into different positions. The objective was to find the positions of maximum congruence. Congruence was defined as the contact area between the two cartilage surfaces under the constraint that the volume of the cartilage overlap, V_o, was constant. Assuming linear elastic cartilage, a constant V_o meant the loading was approximately constant (errors were introduced due to the angulation of the cartilage surfaces). This approach could be used to analyse congruence in a large number of joint positions, under a roughly constant load. The method has a number of disadvantages. The results depended on how contact was defined in terms of surface proximity. The initial volumetric overlap, V_o, was also expected to affect the results. This method did not take into account the deformation of the

cartilage surfaces, and how the compliance of the surfaces affects the contact mechanics. In addition, some of the joint positions tested may be non-physiologic and must be monitored. It was also possible that two positions of the same contact area magnitude but at different locations, could yield different local deformation and stresses due to variations in cartilage thickness, material properties, and local geometry. In addition, since characterizing the joint positions was difficult with this method, establishing a relation between joint kinematics and congruence was problematic. Finally, although this method was useful in performing sensitivity analyses of joint congruence, it was computationally expensive and complex.

3.1.2.4 Congruence Index

Computation of the congruence index was a straight-forward approach used to quantify the relative local geometries for a number of different joint orientations. The measure was initially developed by Lur'e (1964) to characterize convex surfaces. It was applied to analyse the congruence of the CMC joint (Ateshian et al., 1992). The contact geometry was represented by an equivalent system where a new surface, representing the difference in the profiles of the original surfaces, came into contact with a plane (Figure 3.4).

The local congruence of the joint was defined by the principal curvatures of the equivalent surface at the initial point of contact. Briefly, (κ^a_{min}, κ^a_{max}) and (κ^b_{min}, κ^b_{max}) denoted the principal curvatures of surfaces *a* and *b* respectively at the initial point of contact. The angle between the direction of minimum (or maximum) curvature on surface *a* and *b* was denoted by α. The mean curvature on each surface was expressed as

$$H^a = \frac{1}{2}(\kappa^a_{min} + \kappa^a_{max}) \text{ and } H^b = \frac{1}{2}(\kappa^b_{min} + \kappa^b_{max}), \tag{3}$$

and the difference in principal curvatures was defined by

$$G^a = (k^a_{min} - k^a_{max}) \text{ and } G^b = (k^b_{min} - k^b_{max}). \tag{4}$$

The relative principal curvatures of the equivalent surface were obtained from

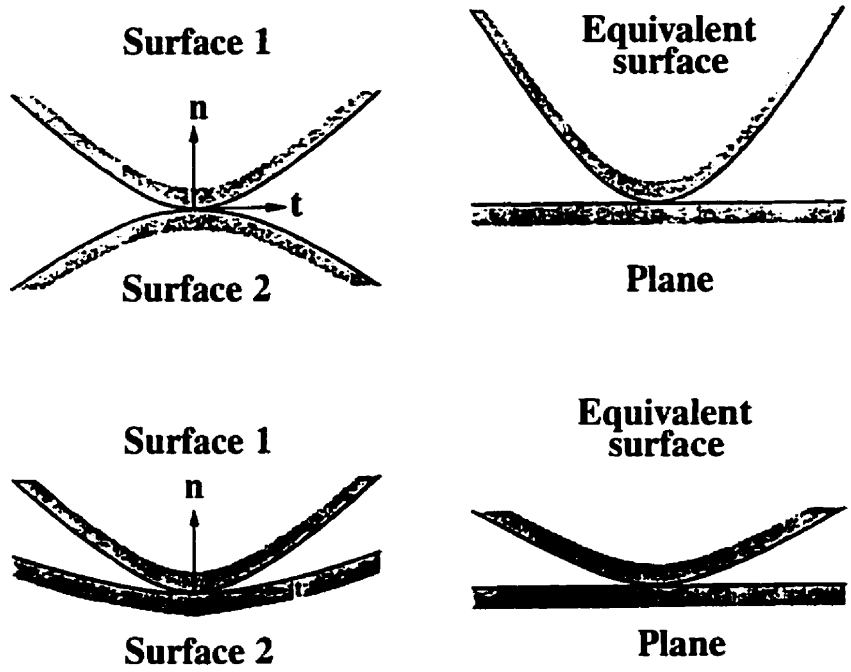

Figure 3.4: Two contacting surfaces were represented by an equivalent system, where surface 2 was subtracted from itself and surface 1. This resulted in a new surface coming into contact with a plane. The subtraction was operated along the coordinate direction **n** only, where **n** represented the normal to the surfaces at the initial point of contact (from Ateshian et al., 1992).

$$k^{e}_{min} = H^{a} + H^{b} - \frac{1}{2}\Delta \text{ and } k^{e}_{max} = H^{a} + H^{b} + \frac{1}{2}\Delta \tag{5}$$

$$\text{where } \Delta^{2} = G^{a^{2}} + G^{b^{2}} + 2G^{a}G^{b}\cos 2\alpha . \tag{6}$$

Finally, the congruence index was calculated as the RMS curvature of the equivalent surface,

$$K^{e}_{rms} = \sqrt{\frac{(\kappa^{e}_{min})^{2} + (\kappa^{e}_{max})^{2}}{2}} . \tag{7}$$

RMS curvature measured the degree of flatness. $K^{e}_{rms} = 0$ indicated two perfectly congruent surfaces. For perfectly congruent surfaces there was no difference in profile and

the equivalent surface was a flat plane. The less congruent the two surfaces, the more curved the equivalent surface, resulting in a higher K^{e}_{rms}. The congruence at any joint position could be calculated, as long as the principal curvatures and their directions were quantified at the initial points of contact of the two original surfaces. The average congruence index was used to quantify the differences between male and female thumb CMC joints (Ateshian et al., 1992). The congruence index was not calculated at certain positions because kinematic data were not collected. The original theory was developed for convex surfaces. For saddle shaped surfaces (e.g., the thumb CMC and PF joints) it was difficult to define a consistent sign convention when labelling which principal curvature is minimum and which is maximum.

There were a number of limitations to using congruence index. Firstly, the undeformed geometry of the cartilage surfaces was used to characterize the congruence. Therefore, the changes in geometry with loading and deformation were not accounted for. It was assumed that the undeformed surface geometries were sufficient indicators of how the surfaces would interact under load. Secondly, congruence index assumed that the joint geometry allowed point contact throughout a range of joint positions. Congruence index was not appropriate for joints with multiple regions of contact, such as in a slightly incongruent hip joint with a deeper socket. Thirdly, the congruence index was based on the surface geometries at the initial points of contact. Therefore, the congruence index quantified the local relative surface geometries around the initial point of contact. It was assumed that the local geometries at the initial points of contact characterized the vicinity around these points, and that this geometry predicted how the joint surfaces interact globally. There may be instances where a joint is locally congruent, but globally, large differences in geometry exist. Irregularities in local geometry were not taken into account. This method was not appropriate if the surface geometry is not smooth (e.g., if surface fissuring or fibrillation is present). Initial work with the cat PF joint suggests that the surface geometry is smooth, and that the geometry at the initial point of contact may be representative of the neighbouring geometry. It is, however, not well understood how well the local geometry characterizes the global congruence of the joint. In addition,

congruence index was a dimensional quantity, affected by the size of the joint. Therefore, it was difficult to compare results between two joints of different sizes. However, for the analysis of one joint in different positions, the measure may be appropriate. The main advantage of the congruence index was that it accounted for the complex geometries of the joint surfaces as well as the joint kinematics. The congruence index could be calculated at any number of joint positions. Therefore, congruence index is ideal for performing sensitivity analyses to quantify the effect of joint position on congruence.

3.1.3 Summary

Joint congruence describes the coincidence of the joint surfaces when they are superimposed. Joint congruence is a function of contact geometry, joint position, compliance of the cartilage and bone, and joint loading. The congruence of joint surfaces plays a large role in joint function and health. The optimal joint congruence to transmit and distribute joint loads and to facilitate joint movement is not well established. While the quantification of relative 3D joint geometries on a global level is a complex problem, which has not been solved in the biomechanics literature, numerous measures have been used to indicate joint congruence. Two-dimensional and 3D geometric measures, as well as contact area and congruence index, have been presented. Two-dimensional geometric measurements were typically taken from transversely oriented slices taken using non-invasive imaging techniques. These measures were useful in diagnosing subluxation and the potential of the patella to dislocate. A measurement taken in one plane, in one joint position, however, was not sufficient in characterizing joint congruence throughout the functional range of motion. In addition, since cartilage has non-uniform thickness, these measurements, typically of bone geometry, did not fully represent the joint surface geometry. Curvature maps described the 3D geometry of joint surfaces. The comparison of curvatures of opposing surfaces was a measure of joint congruence. However, unless the position and the orientation of the joint surfaces are known, the measure is qualitative. To investigate the relation between joint kinematics and joint congruence, a qualitative comparison of joint curvatures is not sufficient. Contact area measurements accounted for joint geometry, loading, as well as joint kinematics. Contact area measurements have

assessed the effects of flexion angle, changing muscle forces and direction, joint alignment (Q-angle), as well as altering the integrity of passive stabilizers (i.e., ligaments and capsular constraints). Most studies were limited to analysing contact area for very few positions. To investigate the relation between joint kinematics and joint congruence it is necessary to calculate congruence throughout a large range of well-defined patellar positions and orientations. This requires prescribing incremental changes to patellar position under known load, which is difficult to do experimentally. Models to perturb the joint theoretically and calculate contact area theoretically are promising, although computationally complex. Congruence index was a comparison of local surface geometries at the initial points of contact, where the initial points of contact are determined by the joint kinematics. The congruence index could be calculated for a large number of joint positions. Since congruence index is ideal for performing sensitivity analyses of congruence to joint position it will be used to indicate joint congruence in this study.

3.1.4 Purpose

The purpose of this component of the research was to investigate the complex relation between patellar kinematics and joint congruence. It was speculated that the position and orientation of the patella play a large role in contact mechanics and influence the joints ability to transmit and distribute force.

The objective was to quantify the congruence index of a cat PF joint

1. as a function of flexion angle (30° to 90°), to investigate the speculation that joint congruence varies throughout the flexion/extension range of motion, and
2. as a function of a range of medial to lateral tracking positions of the patella, to investigate the speculation that joint congruence is highest for central tracking and decreases with medial or lateral tracking.

It was assumed that the local relative geometries characterized by the congruence index indicated the global congruence and interaction between the joint surfaces. It was assumed that a more congruent joint position results in lower cartilage stress. The values of congruence for different joint positions indicated the directional changes in joint stresses.

The range of joint congruence values indicated how sensitive the PF joint was to changes in medial/lateral joint alignment. This research will increase understanding of the effects of muscle imbalances and ACL injuries.

A geometric model of a cat PF joint was used (Boyd, 1997). As an intermediate step, the RMS curvature of the PF cartilage surfaces were quantified. An analysis of the geometry of the surfaces was useful in interpreting congruence index results.

3.2 METHODS

3.2.1 3D Geometric Model

The congruence index was calculated for a 3D geometric model of the PF joint of a mature outbred cat (4.0 kg). Collection of experimental data and formulation of the geometric model were completed by Boyd (1997). Briefly, a cat was anaesthetized and placed on its back in a hammock. The left hind femur was fixed in a stereotaxic frame, with the tibia free to move. Bone pins with four kinematic markers each were installed on the tibia, femur, and patella (Figure 3.5). A video motion analysis system consisting of four

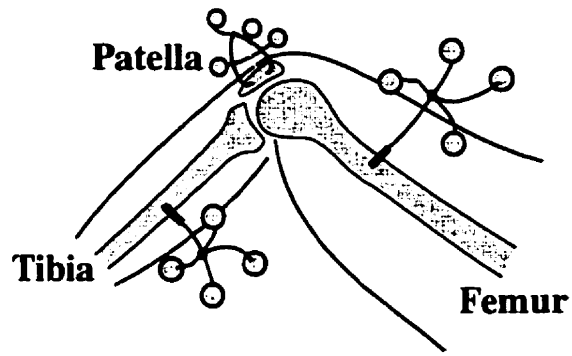

Figure 3.5: 3D kinematics of the knee joint were collected in the global coordinate system (GCS) using a video motion analysis system and bone pins (from Boyd, 1997 with permission).

cameras (240 Hz) measured kinematics in unconstrained extension (Motion Analysis Corporation, Santa Rosa, CA). Extension of the tibia through a range of motion of 110° to 30° (0°= full knee extension) was induced by stimulation of the quadriceps. A low stimulation voltage (20% of maximal stimulation) was applied to an electrode surgically implanted on the femoral nerve. Video data for the kinematic markers were converted to the 3D coordinates with commercially available software (EVA, Motion Analysis Corporation, Santa Rosa, CA). The kinematic data were smoothed using the GCVSPL routine (Woltring, 1986) in the quintic spline mode with an equivalent smoothing

frequency of 10 Hz. The smoothing frequency was chosen based on subjective evaluation of the fit between the smoothed data and the raw data. It was estimated that the kinematic error was on the order of 60 μm (Ronsky et al., 1999).

Subsequently, the cartilage and subchondral bone surfaces of the distal femoral groove and the patella were measured. First the knee joint was dissected, and the articular surfaces were exposed. The new optical technique, multi-station digital photogrammetry (MDPG) was used (Ronsky et al., 1999). The femur and patella were, respectively, mounted in a specimen ring consisting of eight equally spaced posts. The eight posts provided reference points for the surface coordinate system (Figure 3.6). A uniform rectangular grid was projected on the specimen surface, to provide reference marks (Huiskes et al., 1985).

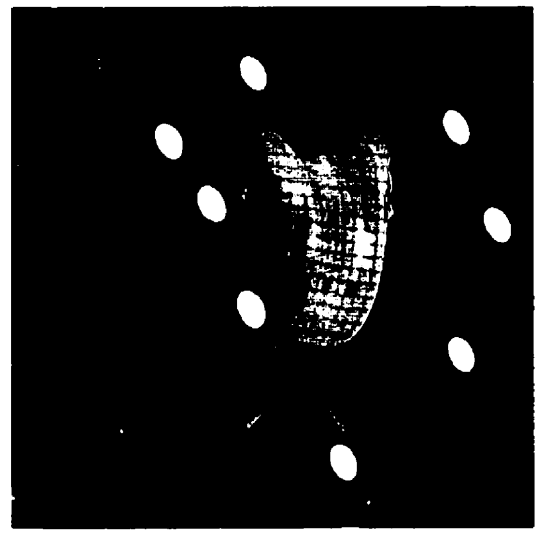

Figure 3.6: A sample photographic image of the distal femoral cartilage surface and the specimen ring (from Boyd, 1997 with permission).

A Kodak DCS 420 digital camera (Eastman Kodak Company, Rochester, NY) fitted with a macro-focusing zoom lens (Nikon, Nippon Kogaku KK, Japan) was used. Six photographs, equally spaced in a radial pattern 300 mm from the specimen, were taken. The kinematic markers were visible in the MDPG photographs so that the surface

coordinate system (SCS) could be transformed back to the global coordinate system (GCS) to combine both the kinematic and surface data (Boyd, 1997). After the cartilage surfaces were photographed, the patella and distal femur, still mounted in their respective specimen rings, were immersed in a solution of bleach for three hours to dissolve the cartilage (Ateshian et al., 1991). The same procedure was repeated to photograph the subchondral bone surfaces.

Two dimensional coordinates of the control posts and the grid intersections were determined using a semi-automatic digitizing program based on edge detection and pattern fitting techniques (Ronsky et al., 1999). A bundle adjustment was used to calculate the 3D surface coordinates. The result was a set of data points representing each surface. The photogrammetric reconstruction error was estimated as 25 μm, using the mean measurement precision determined by the bundle adjustment (Ronsky et al., 1999).

Once the surface data were collected, the mathematical expressions representing each surface were obtained, using the thin-plate spline (TPS) technique (Lancaster and Salkauskas, 1986; Boyd et al., 1999). The height of the surface was described by the surface function

$$S(x, y) = \sum_{i=1}^{n} c_i f_i(x_i, y_i) + c_{n+1} + c_{n+2}x + c_{n+3}y, \tag{8}$$

where c_i are constants, and the functions f_i are the translates of the radial basis function

$$f_i(x, y) = r_i^2 \ln(r_i), \tag{9}$$

$$\text{where } r_i^2 = (x - x_i)^2 - (y - y_i)^2. \tag{10}$$

The measured data points were used to solve for the constants that describe the surface mathematically. Smoothing was introduced by replacing the interpolation condition by a least squares criterion (Boyd et al.,1999). A smoothing parameter of λ=1.7 was chosen, for which the average surface fitting error was equal to the RMS measurement precision.

To increase the resolution of the results the surfaces were resampled at points arranged in a grid pattern with a spacing of 0.25 mm. Finally, the geometric model was created by reorienting the surfaces from the SCS to the GCS using the kinematic data (Boyd, 1997).

3.2.2 Curvature Analysis

Analysis of the curvatures of the patellar and femoral cartilage surfaces provided information on the geometry of the surfaces. This information was useful in interpreting the congruence index results. The principal curvatures were evaluated at all the resampled points using differential geometry (Beck et al., 1986). Determination of the principal curvatures as well as the surface normals required calculation of the first and second partial derivatives of the TPS surface function (Boyd et al., 1999). Briefly, the first partial derivatives were calculated as follows:

$$S_x = \frac{\partial}{\partial x} S(x, y) = \left[f_{1_x} \; f_{2_x} \; f_{3_x} \; \cdots \; f_{n_x} \; 0 \; 1 \; 0 \right] c^T, \text{ and similarly } S_y, \tag{11}$$

where $f_{i_x} = \frac{\partial f}{\partial x} = (x - x_i)\ln(r_i^2) + (x - x_i)$, and similarly f_{i_y}.

The second partial derivatives were

$$S_{xx} = \frac{\partial^2}{\partial x^2} S(x, y) = \left[f_{1_{xx}} \; f_{2_{xx}} \; f_{3_{xx}} \; \cdots \; f_{n_{xx}} \; 0 \; 0 \; 0 \right] c^T, \text{ and similarly } S_{yy} \tag{12}$$

$$S_{xy} = \frac{\partial^2}{\partial x \partial y} S(x, y) = \left[f_{1_{xy}} \; f_{2_{xy}} \; f_{3_{xy}} \; \cdots \; f_{n_{xy}} \; 0 \; 0 \; 0 \right] c^T, \tag{13}$$

where $f_{i_{xx}} = \frac{\partial^2 f}{\partial x^2} = \frac{2(x - x_i)^2}{r_i^2} + \ln(r_i^2) + 1$, and similarly $f_{i_{yy}}$, and

$$f_{i_{xy}} = \frac{\partial^2 f}{\partial x \partial y} = \frac{2(x - x_i)(y - y_i)}{r_i^2}.$$

The principal curvatures (κ) and their orientation (h) were determined at every resampled point on each surface by solving the roots of the following two equations (Beck et al., 1986):

$$(EG - F^2)\kappa^2 - (EN + GL - 2FM)\kappa + (LN - M^2) = 0 \quad (14)$$

$$(FN - GM)h^2 - (EN - GL)h + (EM - FL) = 0 \quad (15)$$

where $E = S_x \bullet S_x$ $\quad L = S_{xx} \bullet \mathrm{n}$

$F = S_x \bullet S_y$ $\quad M = S_{xy} \bullet \mathrm{n}$

$G = S_y \bullet S_y$ $\quad N = S_{yy} \bullet \mathrm{n}$

where the surface normal was $\mathrm{n} = \left[S_x \; S_y \; -1\right]$ and was normalized by dividing by

$$\sqrt{(S_x)^2 + (S_y)^2 + (-1)^2}.$$

In this study, RMS curvatures were reported (Eq. 2). RMS curvature provides a measure of surface flatness, accounting for both minimum and maximum principal curvatures.

The RMS curvatures in the regions of contact throughout unconstrained extension were investigated. Using the geometric model, the contact area was quantified at 13 discrete flexion angles, between 30° and 90° at 5° increments (Boyd, 1997). Briefly, the contact area was defined as regions of overlap (i.e., a proximity less than 0 mm). The proximity was calculated as the distance along the surface normal projected from a resampled point on the patellar cartilage surface to its intersection with the femoral cartilage surface. The proximal and distal limits of contact throughout unconstrained extension were determined. The flatness of the two opposing surfaces in the regions of contact was compared. The comparison provided a qualitative analysis of joint congruence and the geometric similarity of the two opposing cartilage surfaces.

3.2.3 Congruence Index

Using the geometric model, the effect of changing the position and orientation of the patella within the femoral groove on joint congruence was investigated. To quantify joint congruence the congruence index was calculated, because it was a straight-forward measure of contact geometry, and could be easily calculated for a large number of joint positions. In this section, the method used to calculate congruence index will be conceptually introduced. Then, the manner in which this method was applied to investigate PF congruence as a function of flexion angle and patellar alignment, will be presented.

3.2.3.1 Congruence Index Calculation

Congruence index was calculated based on a method adapted from Ateshian et al. (1992). Recall that two surfaces could be represented by an equivalent system, where a new surface, representing the difference in profile of the two original surfaces, came into contact with a plane (Section 3.1.2.4). The congruence index was defined as the RMS curvature of the equivalent surface at the point of initial contact with the plane. Ateshian et al. (1992) calculated the congruence index using the magnitude and direction of the principal curvatures of the surfaces at the initial point of contact. However, for saddle shaped surfaces it was difficult to define a consistent sign convention when labelling maximum and minimum principal curvature. An equivalent method was devised that avoided the sign convention issue. The equivalent method, involved calculating the congruence index directly from the equation representing the equivalent surface. The equation of the equivalent surface was derived by subtracting the Taylor series expansion of the femoral surface from the Taylor series expansion of the patellar surface. The subtraction was operated along the direction of the surface normal, at the contact point. This involved reorienting the surfaces so that there was point contact and establishing a new coordinate system (*uvw*). First, the initial points of contact were chosen. Next, the patella was translated until the patellar and femoral initial points of contact coincided. Then the patella was rotated until the 3D surface normals at the points of contact were aligned. A coordinate system (*uvw*) was established, where the coordinate axis *w* was

aligned with the surface normals at the point of contact, and the origin coincided with the point of contact (Figure 3.7).

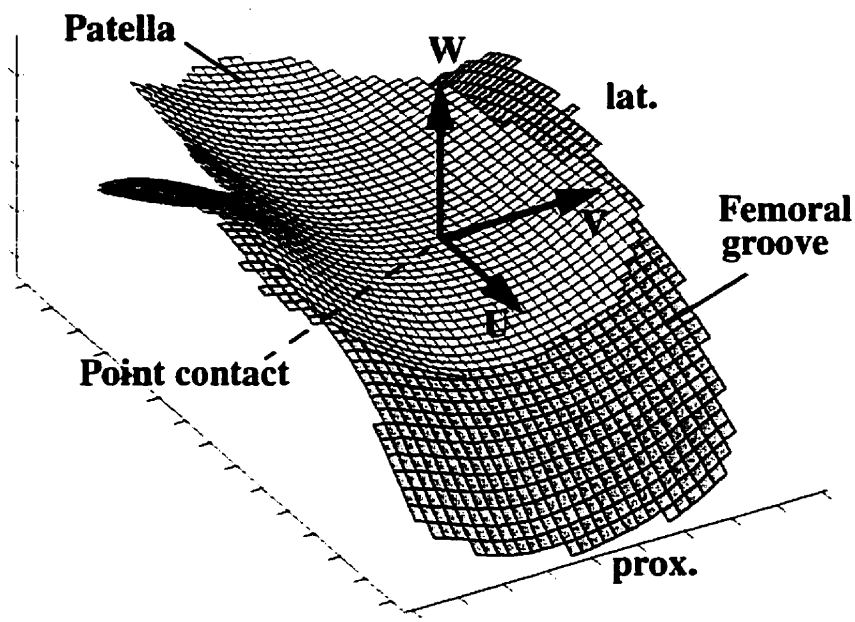

Figure 3.7:A sample orientation of the patellar and femoral cartilage surfaces in point contact and the *uvw* coordinate system. The subtraction is operated along the direction of the *w* axis.

The Taylor series equation of the patellar and femoral surfaces are $F(u,v)$ and $G(u,v)$, respectively.

$$F(u,v) = F(u,v) + F_u(u,v)u + F_v(u,v)v + \frac{1}{2}F_{uu}(u,v)u^2 + F_{uv}(u,v)uv + \frac{1}{2}F_{vv}(u,v)v^2 \quad (16)$$

$$G(u,v) = G(u,v) + G_u(u,v)u + G_v(u,v)v + \frac{1}{2}G_{uu}(u,v)u^2 + G_{uv}(u,v)uv + \frac{1}{2}G_{vv}(u,v)v^2 \quad (17)$$

At the points of contact where the coordinates are (u=0,v=0)

$$F(0,0) = F(0,0) + F_u(0,0)u + F_v(0,0)v + \frac{1}{2}F_{uu}(0,0)u^2 + F_{uv}(0,0)uv + \frac{1}{2}F_{vv}(0,0)v^2 \text{ and} \quad (18)$$

$$G(0,0) = G(0,0) + G_u(0,0)u + G_v(0,0)v + \frac{1}{2}G_{uu}(0,0)u^2 + G_{uv}(0,0)uv + \frac{1}{2}G_{vv}(0,0)v^2. \quad (19)$$

The partial derivatives in Eq. 18 and Eq. 19 were calculated with respect to u and v. However, the partial derivatives have already been calculated with respect to x and y, using the TPS technique (Eq. 11, Eq. 12, and Eq. 13). The chain rule and the rotation matrices, $\left[R\right]^{\text{patella}}_{xyz \rightarrow uvw}$ and $\left[R\right]^{\text{femur}}_{xyz \rightarrow uvw}$, and translation vectors, $\left[D\right]$, were used to transform the partial derivatives from the xyz system to the uvw coordinate system. For the patella

$$\begin{bmatrix} u \\ v \\ w = F(u, v) \end{bmatrix} = \begin{bmatrix} R(1,1) & R(1,2) & R(1,3) \\ R(2,1) & R(2,2) & R(2,3) \\ R(3,1) & R(3,2) & R(3,3) \end{bmatrix}^{\text{patella}}_{xyz \rightarrow uvw} \begin{bmatrix} x \\ y \\ z = S(x, y) \end{bmatrix} + \begin{bmatrix} D(1) \\ D(2) \\ D(3) \end{bmatrix} \tag{20}$$

Therefore u, v, and w were functions of x and y.

$$u = R(1,1)x + R(1,2)y + R(1,3)S(x, y) \tag{21}$$

$$v = R(2,1)x + R(2,2)y + R(2,3)S(x, y) \tag{22}$$

$$w = F(u, v) = R(3,1)x + R(3,2)y + R(3,3)S(x, y) \tag{23}$$

Using the chain rule

$$\frac{\partial w}{\partial x} = \frac{\partial w}{\partial u} \cdot \frac{\partial u}{\partial x} + \frac{\partial w}{\partial v} \cdot \frac{\partial v}{\partial x}, \text{ and similarly } \frac{\partial w}{\partial y}. \tag{24}$$

Rearranging, the first partial derivatives with respect to u and v were given by

$$\begin{bmatrix} F_u(u, v) \\ F_v(u, v) \end{bmatrix} = \begin{bmatrix} \frac{\partial u}{\partial x} & \frac{\partial v}{\partial x} \\ \frac{\partial u}{\partial y} & \frac{\partial v}{\partial y} \end{bmatrix}^{-1} \begin{bmatrix} \frac{\partial w}{\partial x} \\ \frac{\partial w}{\partial y} \end{bmatrix}, \tag{25}$$

where all the elements on the right hand side were evaluated by differentiating Eq. 21, Eq. 22, and Eq. 23 with respect to x and y. Differentiating Eq. 24 gave

$$\frac{\partial^2 w}{\partial x^2} = \left(\frac{\partial^2 w}{\partial u^2} \cdot \frac{\partial u}{\partial x} + \frac{\partial^2 w}{\partial u \partial v} \cdot \frac{\partial v}{\partial x}\right) \cdot \frac{\partial u}{\partial x} + \frac{\partial w}{\partial u} \cdot \frac{\partial^2 u}{\partial x^2} + \left(\frac{\partial^2 w}{\partial u \partial v} \cdot \frac{\partial u}{\partial x} + \frac{\partial^2 w}{\partial v^2} \cdot \frac{\partial v}{\partial x}\right) \cdot \frac{\partial v}{\partial x} + \frac{\partial w}{\partial v} \cdot \frac{\partial^2 v}{\partial x^2} \tag{26}$$

Similarly $\frac{\partial^2 w}{\partial y^2}$ and $\frac{\partial^2 w}{\partial x \partial y}$ were obtained. This resulted in a system of 3 equations and 3 unknowns, and was rearranged to calculate the second partial derivatives with respect to u and v.

$$\begin{bmatrix} F_{uu}(u,v) \\ F_{uv}(u,v) \\ F_{vv}(u,v) \end{bmatrix} = \begin{bmatrix} \frac{\partial^2 w}{\partial u^2} \\ \frac{\partial^2 w}{\partial u \partial v} \\ \frac{\partial^2 w}{\partial v^2} \end{bmatrix} = \begin{bmatrix} \left(\frac{\partial u}{\partial x}\right)^2 & 2\left(\frac{\partial u}{\partial x}\cdot\frac{\partial v}{\partial x}\right) & \left(\frac{\partial v}{\partial x}\right)^2 \\ \left(\frac{\partial u}{\partial y}\right)^2 & 2\left(\frac{\partial u}{\partial y}\cdot\frac{\partial v}{\partial y}\right) & \left(\frac{\partial v}{\partial y}\right)^2 \\ \frac{\partial u}{\partial x}\cdot\frac{\partial u}{\partial y} & \left(\frac{\partial v}{\partial y}\cdot\frac{\partial u}{\partial x}+\frac{\partial v}{\partial x}\cdot\frac{\partial u}{\partial y}\right) & \frac{\partial v}{\partial x}\cdot\frac{\partial v}{\partial y} \end{bmatrix}^{-1} \begin{bmatrix} \frac{\partial^2 w}{\partial x^2}-\frac{\partial w}{\partial u}\cdot\frac{\partial^2 u}{\partial x^2}-\frac{\partial w}{\partial v}\cdot\frac{\partial^2 v}{\partial x^2} \\ \frac{\partial^2 w}{\partial y^2}-\frac{\partial w}{\partial u}\cdot\frac{\partial^2 u}{\partial y^2}-\frac{\partial w}{\partial v}\cdot\frac{\partial^2 v}{\partial y^2} \\ \frac{\partial^2 w}{\partial x \partial y}-\frac{\partial w}{\partial u}\cdot\frac{\partial^2 u}{\partial x \partial y}-\frac{\partial w}{\partial v}\cdot\frac{\partial^2 v}{\partial x \partial y} \end{bmatrix} \quad (27)$$

Similar equations were obtained for the femoral surface. The Taylor series expansion of the equivalent surface $H(u,v)$ was obtained by subtracting Eq. 19 from Eq. 18. Since the two surfaces coincided and the surface normals were aligned at the initial points of contact, $H(u,v)$ simplified to the following expression

$$H(u,v) = \frac{1}{2}(F_{uu}(0,0) - G_{uu}(0,0))u^2 + (F_{uv}(0,0) - G_{uv}(0,0))uv + \frac{1}{2}(F_{vv}(0,0) - G_{vv}(0,0))v^2. \quad (28)$$

The relative principal curvatures of the equivalent surface were calculated using differential geometry. Subsequently, congruence index was calculated as the RMS curvature of the equivalent surface (Eq. 7). Congruence index could assume values from 0 to ∞. A congruence index of 0 indicated perfectly congruent surfaces. The smaller the value of the congruence index, the more congruent the two surfaces. The congruence index was a 3D measure that took into account the 3D geometries at the point of contact. It was assumed that since the surfaces are smooth and continuous, the Taylor series expansion at the initial point of contact adequately characterized the surfaces in the neighbourhood of the contact point.

3.2.3.2 Congruence Index Application

Thirteen discrete flexion angles, between 30° and 90°, representing the full range of motion, were analysed (0° represents full extension). For each flexion angle, the patellar orientation was incrementally perturbed to produce central tracking and a range of medial

and lateral tracking alignments.

Using the geometric model, for each flexion angle, a transverse plane was established through the centroid of the contact area (Figure 3.8). The centroid of the contact area was estimated by reorienting the patella parallel to the *xy*-plane and calculating the centroid of the area projected on the x-y plane.

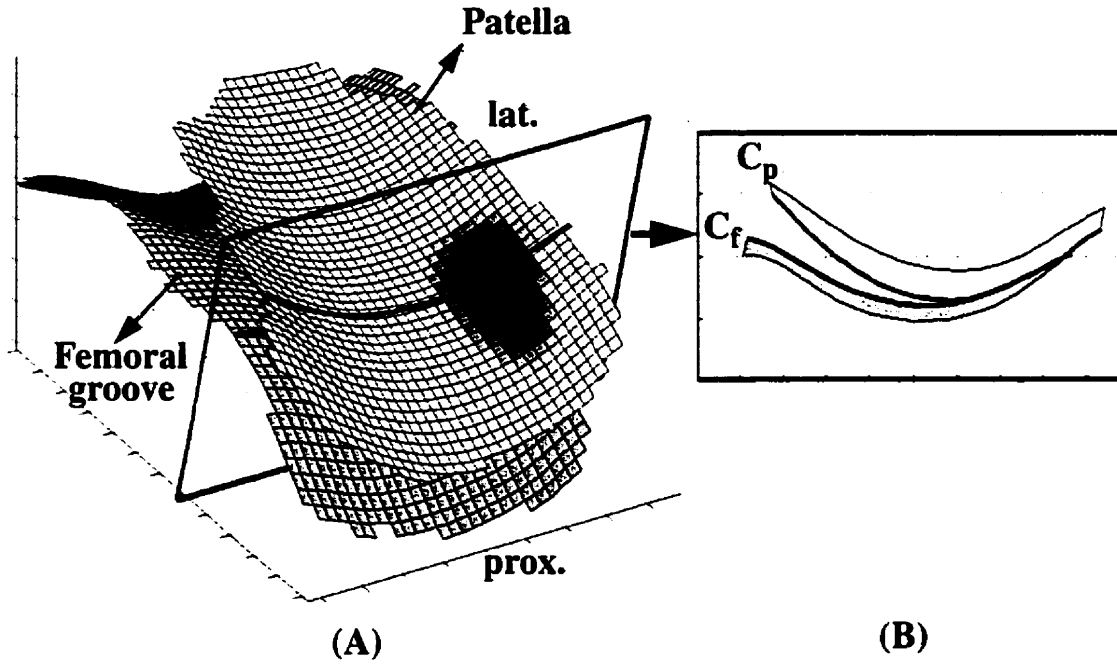

Figure 3.8: The patellar and femoral cartilage surfaces at 70° of flexion. A) The dark area indicates the contact area. The transverse plane is taken through the centroid of the contact area, aligned with the surface normal of the patellar cartilage at the centroid, and a vector running medially. B) The transverse plane intersects the cartilage surfaces along curves C_p and C_f. All perturbations of the patella involved initial points of contact located on curves C_p and C_f.

The orientation of the transverse plane was determined by two vectors; the surface normal of the patellar cartilage at the centroid of the contact area, and a vector running laterally. The transverse plane intersected the patellar and femoral cartilage surfaces along curves C_p and C_f, respectively. To establish the patellar orientation corresponding to central

tracking, the 2D curvatures of each curve were analysed. The points of maximum curvature along C_p and C_f were used as the initial points of contact for central tracking. The patella and femur were subsequently oriented in the *uvw* coordinate system so the initial points of contact coincided with the origin and the 3D surface normals were aligned with the *w* axis (Figure 3.9). Note that the 3D surface normals, generally, did not lie within the transverse plane. For the central tracking orientation, the congruence index was calculated using the method outlined in Section 3.2.3.1.

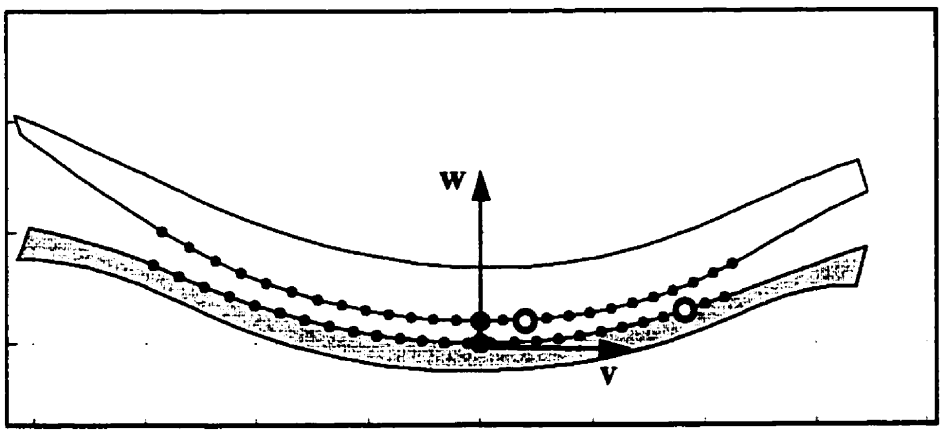

Figure 3.9: The orientation of the patella and femur during central tracking at 70° of flexion. The black dots (resampled points) indicate potential initial points of contact. ● indicates the initial points of contact for central tracking. **O** indicates an example of the contact points during lateral tracking.

To simulate changing patellar tracking alignment, the patella was incrementally reoriented medially and laterally, for each of the thirteen flexion angles. This involved using the TPS technique to resample the cartilage surfaces every 0.2 mm along each curve (i.e., C_p and C_f). The patella and femur were subsequently reoriented so that each of the resampled points on curve C_p came into initial contact with each of the resampled points on curve C_f, and the 3D surface normals were aligned. Due to edge effects, resampled points within 1 mm from the edge of the data set were not used. One mm was the distance between two consecutive digitized data points used to measure the surfaces. Tests with cylinders of various radii indicated that up to 10% error in curvatures could occur within one original

datum point from the edges of the data set. As well, physiologically the initial points of contact would not be expected to be located so far medially and laterally. Only those positions exhibiting point contact were analysed. To determine whether there was point contact, the overlap of the cartilage surfaces was calculated using differential geometry. If the overlap was less than 25 μm, the orientation was classified as a valid point contact orientation. A value of 25 μm was chosen because it was equivalent to the estimated error in the surface geometry. Thus, overlap of this magnitude could be due to the experimental error. For all the positions that exhibited point contact the congruence index was calculated using the method outlined in Section 3.2.3.1. Initially, a second constraint was used to determine whether the orientation was physiologically valid. The medial-lateral distance, d, between the resampled point on the patella and femur in the central tracking orientation was determined (Figure 3.10).

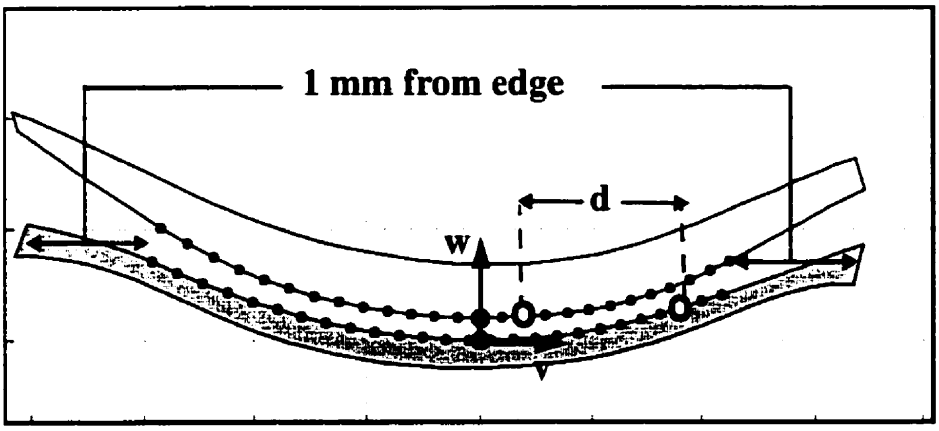

Figure 3.10: Orientation of the patellar and femoral cartilage surfaces for central tracking at 70° of flexion. The black dots indicate resampled points. **O** indicates two potential initial points of contact. Resampled points within 1 mm from the edges were not used. The initial criterion that the distance between the points, d, must be less that half the width of the joint for these points to be valid was not necessary.

If the distance was greater than half the width of the joint, the resulting orientation was classified as non-physiologic and was not used in the analysis. For example, this constraint prevented the far medial side of the patella from coming into initial contact with the far

lateral side of the patella. However, all the positions for which d was greater than the width of the joint did not exhibit point contact. Therefore, the constraint of point contact was sufficient.

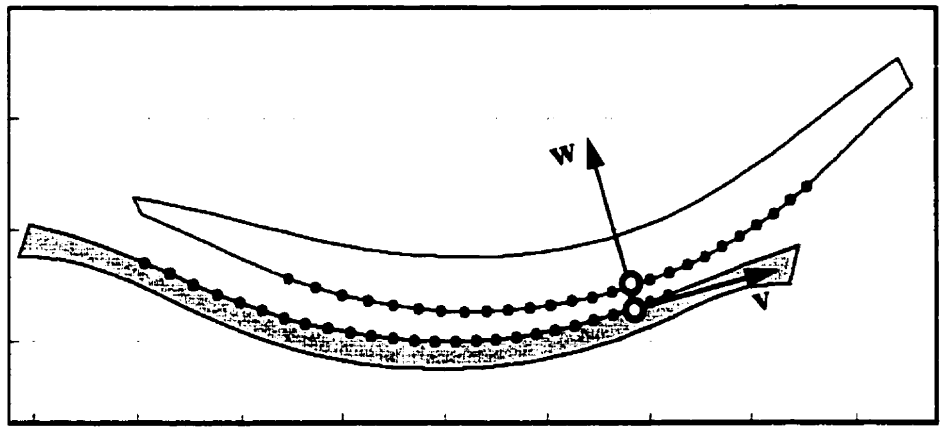

Figure 3.11: An example of a valid lateral tracking orientation of the patellar and femoral cartilage surfaces at 70° of flexion.

This resulted in a set of congruence indices for each angle. The congruence index data were highly skewed, with most data points close to zero. The first and ninety-fifth percentiles of the data were used to characterize the range of probable congruence indices due to medial-lateral perturbations. Therefore, 94% of all the valid positions measured, resulted in a congruence index within the characteristic range. The first and ninety-fifth percentiles were chosen because very low congruence indices (i.e., close to zero) were expected, where as high congruence indices were not. The above was repeated for each of the thirteen flexion angles.

To determine the effect of flexion angle on joint congruence, the congruence index corresponding to central tracking was compared for each flexion angle. The characteristic range of congruence indices resulting from changing the medial/lateral positions of the patella was compared for each flexion angle. The range indicated how sensitive PF joint congruence was to patellar position. Finally, to determine the effect of smoothing during

the TPS technique, smoothing factors between 1.0 and 3.0 were analysed, and the mean difference in congruence index for central tracking at each flexion angle was calculated. Smoothing factors under 1.0 were not used because oversmoothing resulted, based on subjective evaluation of the fit between the raw MDPG data and the resampled surface.

3.3 RESULTS

The RMS curvatures of the patella and femur were calculated (Figure 3.12 and Figure 3.13). For flexion to extension the contact region shifted from distal to proximal on the femur, and proximal to distal on the patella. The mean RMS curvature in the proximal-distal central ridge of the patella was 0.126 mm^{-1} (S.D.=0.01 mm^{-1}). The RMS curvature increased to between 0.16 and 0.20 mm^{-1} in the medial and lateral directions away from the central ridge. The RMS curvature of the femur in the central groove was 0.154 mm^{-1} (S.D.=0.02 mm^{-1}). The RMS curvature decreased to between 0.08 and 0.1 mm^{-1} in the medial and lateral directions away from the central groove.

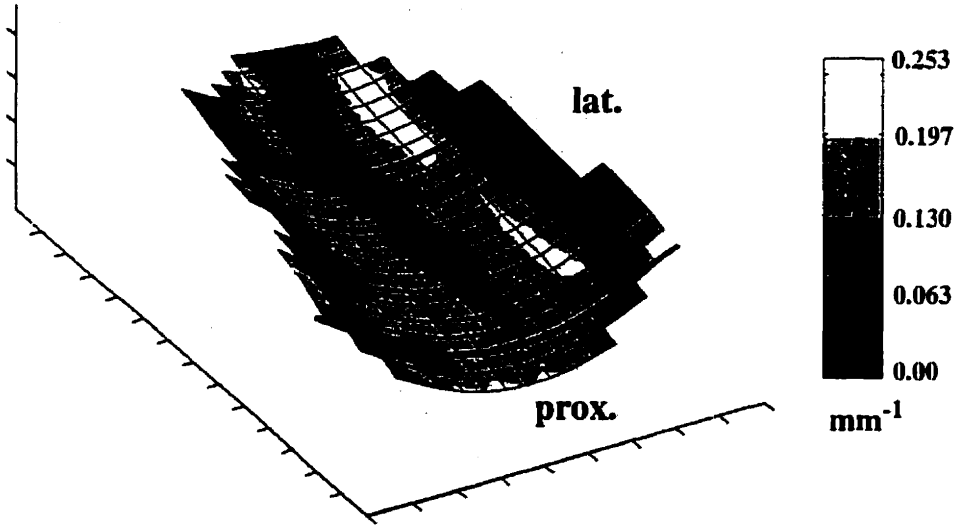

Figure 3.12: The RMS curvature map of the patella. The dark lines indicate the proximal and distal limits of contact during the unconstrained extension. The patella is viewed from the subchondral bone view.

The position of the patella was perturbed within a transverse slice. The location where the transverse slices intersected the patellar and femoral cartilage surfaces indicates the migration of the centroid of the contact area (Figure 3.14 and Figure 3.15). For flexion to extension the transverse plane shifted from distal to proximal on the femur, and proximal to distal on the patella.

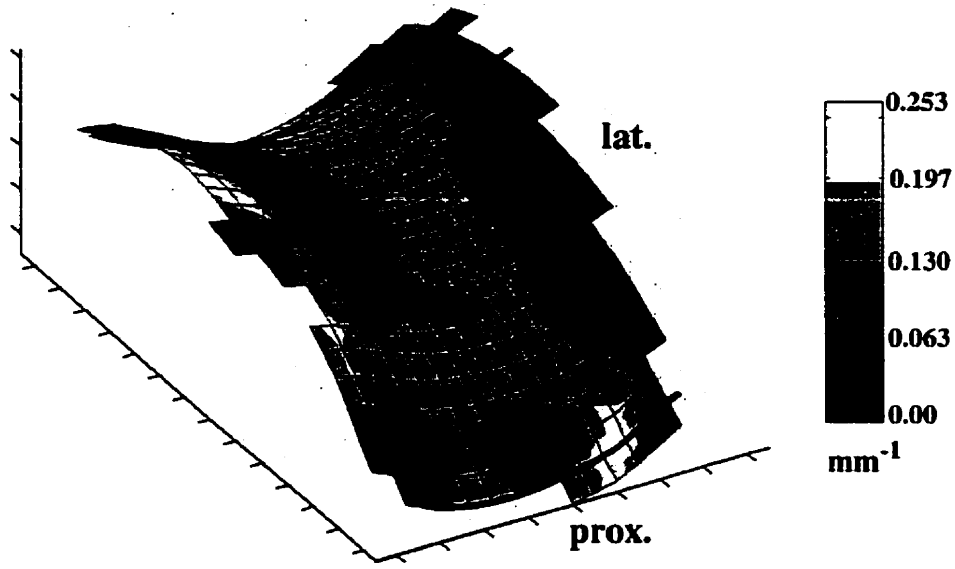

Figure 3.13: The RMS curvature map of the femoral groove. The dark lines indicate the proximal and distal limits of contact during the unconstrained extension.

The congruence index corresponding to central tracking was calculated for 13 discrete flexion angles (Figure 3.16). The average congruence index corresponding to central tracking was 0.058 mm^{-1}. Between 62° and 90° of flexion the congruence index was below average. The congruence index decreased between 40° and 75° and increased slightly from 75° to 90°.

The congruence index was sensitive to medial-lateral perturbations of the patella. Depending on the flexion angle, medial and lateral tracking resulted in up to a twenty fold increase in congruence index. To indicate the spread of the data, the congruence index calculated for each patellar position tested was plotted within the bin representing the flexion angle (Figure 3.17). The values had a higher density around the congruence index corresponding to central tracking.

All smoothing factors from λ=1.0 to 3.0 yielded the same trends for flexion angles between 30° and 90°, with a maximum difference in congruence index of 0.05 mm^{-1}.

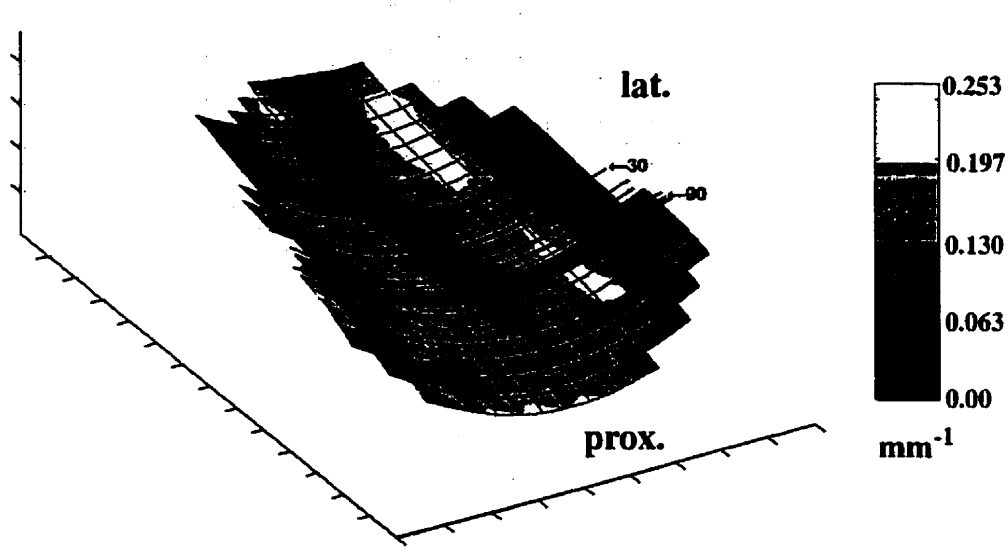

Figure 3.14: The variation in the location of the transverse plane on the surface of the patellar cartilage for flexion angles between 30 and 90 degrees.

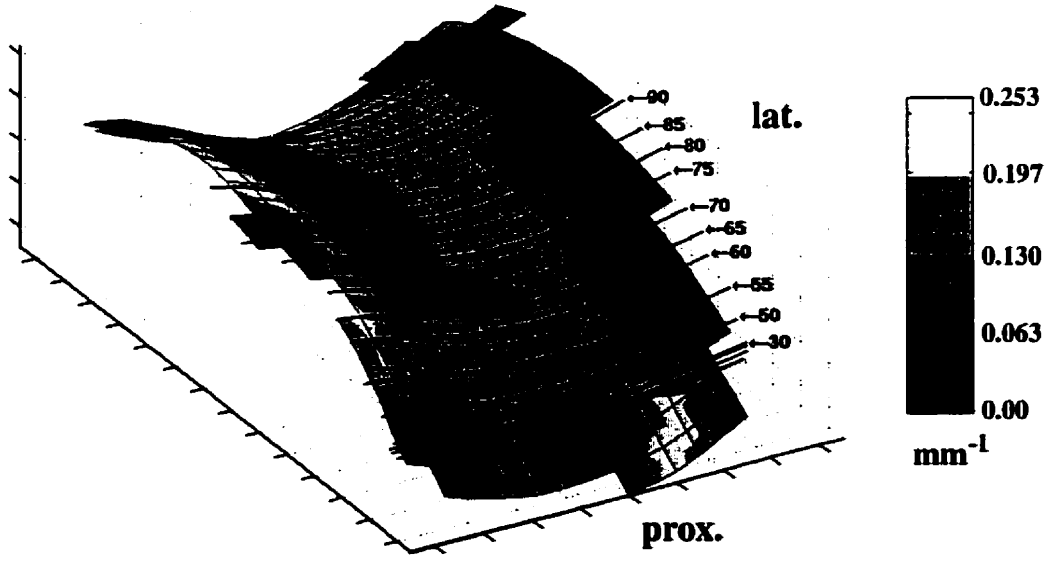

Figure 3.15: Variation in the location of the transverse plane on the surface of the femoral cartilage for flexion angles between 30 and 90 degrees.

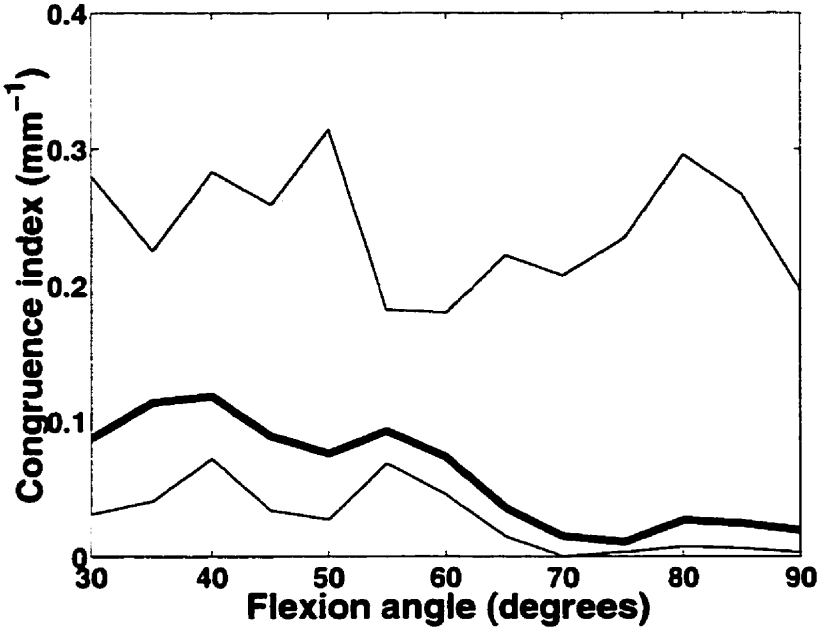

Figure 3.16: Congruence index corresponding to central tracking (solid dark line). Medial and lateral perturbations in alignment resulted in large variations in congruence index (grey band). The grey band represents the first and ninety-fifth percentiles of the data set for each flexion angle.

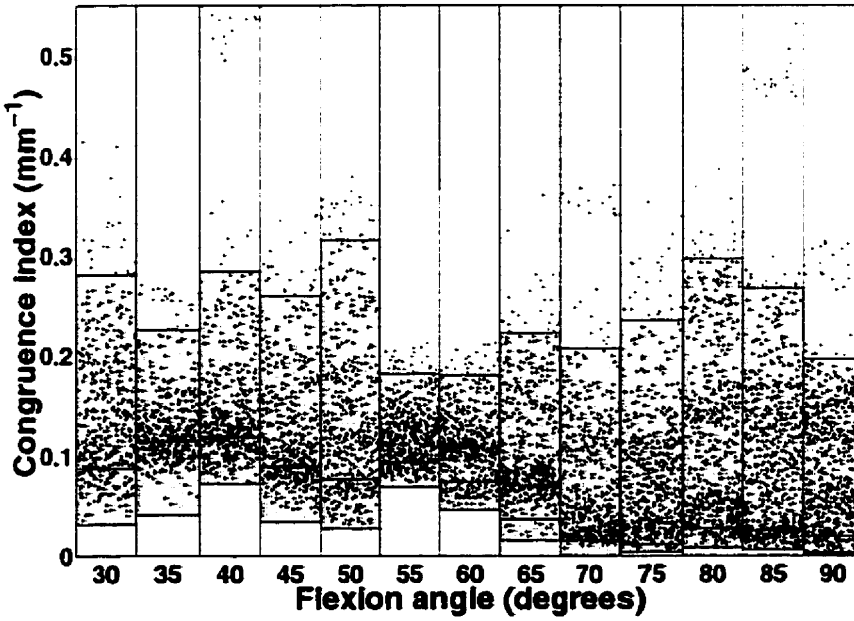

Figure 3.17: Within each bin, the points represent the congruence index calculated for each patellar position tested. Note that the congruence indices are clustered around the index representing the central tracking position.

3.4 DISCUSSION

The effects of incremental changes in patellar alignment on joint congruence were analysed using a geometric model. The model was based on experimentally collected surface and kinematic data from the PF joint of one cat specimen. Since, the geometry and kinematics of only one specimen were used, these results represent a case study. Therefore, conclusions regarding the relation between joint congruence and patellar alignment, cannot be generalized. Further studies involving a larger sample size would be required to establish these relations definitively. Consequently, the following discussion is limited to exploring various aspects of joint geometry and joint alignment, and to speculating about the functional implications of these aspects.

As expected, this particular PF joint was not perfectly congruent. The curvature analysis showed that the RMS curvatures of the patella and femur were not identical. In the central region the mean curvature of the femur was approximately 20% greater than the mean curvature of the patella. However, the similarity between the magnitude of the RMS curvatures of the patella and femur indicated a reasonably congruent joint. The congruence index values corresponding to central tracking were less than 0.05 mm^{-1} for much of the flexion-extension range. However, classification of what constitutes a congruent joint has not been well established. For comparison, the average congruence index for the thumb CMC joint has been reported as 0.064 and 0.129 mm^{-1}, for males and females respectively (Ateshian et al., 1992). The thumb CMC joint is typically classified as a congruent joint. Therefore, this PF joint may be classified as congruent.

The first speculation investigated in this study was that congruence is a function of flexion angle. For this particular joint, local congruence corresponding to central tracking was a function of flexion angle. Analysis of the congruence index during central tracking confirmed that congruence was lowest (i.e., high congruence index) at low flexion angles, increased from 40° to 75°, and decreased slightly from 75° to 90° of flexion. (Recall, that a decrease in joint congruence corresponds to an increase in congruence index). Similar findings have been reported based on contact area magnitude (Ronsky, 1994). Under

constant load, the contact area increased with increasing flexion angle until 75°, and then decreased slightly. Previous studies have shown that the PF contact force increased with knee flexion (Hasler and Herzog, 1998a). It is speculated that the increase in local joint congruence with flexion may allow for a corresponding increase in contact area. This may help the joint maintain a constant stress distribution throughout the range of motion. This is supported by studies that have shown that contact area increases with load (Ronsky, 1994).

The change in local joint congruence indicates a change in contact geometry with extension. During extension, the joint contact region shifted from the distal to the proximal region of the femur, and from the proximal to distal region of the patella, as was indicated by the location of the centroid of the contact area. Similar patterns have been reported for humans using micro-indentation transducers and pressure sensitive film (Ahmed et al., 1983; Huberti and Hayes, 1984). Aside from a flat region on the proximal portion of the femoral groove, the RMS curvatures of the patella and femur varied little in the proximal-distal direction. Consistent principal curvatures in the proximal-distal direction in the femoral groove were reported for humans (Kwak et al., 1997). During 30° to 45° of flexion, contact occurred on the flat proximal region of the femur, causing the decrease in joint congruence.

The local congruence corresponding to central tracking was higher than average between 62° and 90° of flexion. For flexion angles less than 62° the congruence was below average. Previous kinematic studies indicated that during normal walking the cat knee operates within 55° to 80° of flexion (Hasler et al., 1998b). The overlap of these ranges suggests that during normal walking, joint contact occurs at regions of high congruence. Speculating that high congruence is associated with lower stresses and more efficient load transmission, this may indicate that the joint is designed to operate optimally within a certain range.

The second speculation investigated in this study was that joint congruence varies with patellar orientation. The large range of congruence index values resulting from perturbing

the patella in the medial-lateral plane indicates that the local congruence was sensitive to patellar position. The joint was able to accommodate small perturbations in alignment around central tracking. However, large changes in alignment caused up to a twenty fold increase in the congruence index. The maximum congruence index between 0.2 and 0.35 mm^{-1} occurred when the patella tracked high on its lateral side. This was caused by a band of high RMS curvature running in the proximal-distal direction on the lateral patella (Figure 3.14). Further research must be done to determine whether this is a trend or unique to this specimen. As the curvatures on the medial side of the patella were more consistent, this joint could better accommodate medial translations of the patella without resulting in large changes in congruency and, potentially, cartilage stresses.

Results showed that the congruence index due to central tracking corresponded well with maximum congruence. The best correlation was between 55° and 90° of flexion, with a mean difference of 0.012 mm^{-1}. Although it has not been well established, it was speculated that high local congruence may yield lower stresses and a more uniform load distribution. This suggests that central tracking may be optimal in terms of minimizing cartilage stresses. Closer to extension, the difference between central tracking and maximum congruence increased, suggesting that some other criteria may play a role in optimizing joint contact, near extension. These results, however, are not conclusive. Further work must be done to determine how local congruence at the initial points of contact relate to the global interaction of the joint surfaces and the resulting stress distributions. Moreover, it is still unclear how global joint congruence affects joint function and health. It is suspected that the thickness of the layers of cartilage as well as the material properties and deformability of cartilage may have a role in optimizing cartilage stresses, and this was not accounted for in this study.

One of the main limitations of this study was the accuracy of the experimental inputs to the geometric model. The two inputs were surface geometry and joint kinematics. The curvature characteristics and congruence were evaluated for the TPS mathematical surface. Therefore, the reliability of the results depends on the accuracy of the MDPG system and the quality of the surface fit. The accuracy of the MDPG system was estimated

at 25 μm. The accuracy of the TPS was previously tested with 3D data points generated for cylinders of radii varying from 1 to 500 mm. It was found that errors greater that 10% resulted within a region of one original data point along each edge of the data set. Due to the edge effects, resampled points within one original data point from the edge were excluded in the congruence analysis. The congruence index was insensitive to changes in smoothing factor between 1.0 and 3.0. The accuracy of the measured kinematics during unconstrained extension affected the centroid of the contact area and the location of the transverse slice for each flexion angle. Due to the number of slices taken, and the approximately constant RMS curvatures in the anteroposterior direction, the slices analysed were taken as a reasonable approximation of patellar tracking during extension.

Although, the congruence index was ideal for performing a sensitivity analysis to patellar kinematics, several limitations were associated with this measure. Firstly, the congruence index was based on the relative surface geometries of the undeformed cartilage surfaces. It was assumed that the comparison of the undeformed surface geometries was sufficient to differentiate congruent versus incongruent contact interactions. Due to the biphasic properties of articular cartilage as the joint is loaded the articular cartilage deforms and joint congruence changes in a non-linear manner. Theoretical analyses have suggested that an unloaded incongruent joint may yield a more equal distribution of lower stresses than an initially perfectly congruent joint. It is, therefore, suggested that future investigation of the changes in joint congruence for a range of loading and cartilage deformation would further insight on the effects of joint surface geometry. Secondly, joint congruence index was based on the relative surface geometries at the initial point of contact. Therefore, the congruence index was a measure of the local congruence. It was assumed that the Taylor series expansion described the surfaces in a large enough region around the contact points to indicate surface interaction sufficiently. This assumes that the cartilage surfaces are smooth and continuous. If the rate of change of curvatures is large, the Taylor series will only describe a very small region around the contact point, and subsequently local congruence will not indicate global surface interaction. In addition, as loading increases, due to the relative congruence of the joint surfaces and the biphasic properties of cartilage,

it is expected that the cartilage deforms and the contact area increases rapidly. It is, therefore, suggested that a measure of global joint congruence would provide further insight on joint surface interaction and joint mechanics. However, the quantification of global congruence of two complex surfaces is not trivial, and has not been presented in the biomechanics literature. Thirdly, the congruence index can only be analysed for positions of point contact. Certain joints exhibit incongruence under no load, for example, a hip joint with an oversized head in a deep socket (Eckstein et al., 1994). For this joint the undeformed shapes result in two contact regions located towards the joint margins rather than a single contact region. These types of joints cannot be analysed using the method presented. The PF surfaces of this particular joint accommodated point contact throughout a wide range of positions. Further research with a larger sample size is necessary to determine whether PF joints commonly exhibit point or bicentric contact. In addition, congruence index does not account for cartilage thickness, the compliance of the cartilage and bone, and joint loading.

The geometry and kinematics of a cat PF joint were used in this study. To what extent do the results relate to human joints? There are differences in geometry between the human and cat PF joint (Kwak et al., 1997). The human patella has been shown to have a more multi-faceted complex geometry. As well the human femoral groove is not as long or shallow. There are also differences in material properties between species (Athanasiou et al., 1991). However, the function of the PF joint is the same in both species. In relation to body weight both joints are subjected to similar loading conditions. As well, the joint structures (i.e., passive and active constraints) are very similar in both species. It is reasonable to suggest that the effect of ligaments and muscles on the function of the joint is similar in both species. Although there are differences between the species, it has been proposed that similar mechanisms for load transmission and distribution act in both humans and cats.

This research indicates that, in the PF joint studied, the local joint congruence was sensitive to flexion angle and to changes in kinematics, such as might be caused by ligament laxity, injury, or muscle imbalances. Lateral shifts in patellar tracking increased

the congruence index up to twenty fold. However, the effects of the calculated changes in joint congruence on transmission and distribution of stresses are not well established. It was speculated that low joint congruence would lead to a decrease in contact area and an increase in contact stress. However, theoretical analyses have shown that slightly incongruous joints with bicentric contact provided a more equal distribution of lower cartilage stresses than a perfectly congruent joint. Moreover, the correlation between stresses and cartilage health is not well established. It has been suggested that there is a window of optimal loading to promote cartilage health. However, the window of optimal loading is not well defined and it is not known whether perturbing the patellar position is sufficient to cause loading outside this window. It has also been suggested that a certain amount of incongruence may be necessary for pooling and movement of synovial fluid affecting cartilage health. Further work must, therefore, be done to investigate the effect of congruence on joint function and health, to determine the optimal joint congruence.

Due to the limitations of the congruence index, in the second part of this thesis a plane strain finite element model incorporating the biphasic theory of cartilage and joint specific geometry was created. The model introduced compliance of cartilage and bone, as well as geometry of the subchondral bone surfaces, which were not included in the calculation of congruence index. The model was used to quantify the distribution of stresses as a function of joint congruence and patellar orientation. The model allowed the investigation of the relationship between local joint congruence and cartilage stresses.

This preliminary work, suggests that patellar alignment alters contact mechanics, which may be linked to joint function and cartilage health. It is proposed that patellar alignment may be an important consideration in rehabilitation and treatment programs, as well as for surgical interventions, and reconstructive procedures. Further research to aid our understanding of joint congruence and its effect on the mechanical function of the joint is vital in furthering insight on joint mechanics and the effects of joint injuries and disease on cartilage.

4.0 PATELLOFEMORAL CARTILAGE STRESS ANALYSIS

4.1 LITERATURE REVIEW

The forces and stresses acting on or within articular cartilage are thought to have a large effect on the tissue's health and function (Radin et al., 1978; Moskowitz, 1992; Shrive and Frank, 1994). Loading directly affects the nutrition of the matrix and chondrocytes. Loading stimulates pore fluid movement within the matrix that carries essential nutrients to the chondrocytes (Newman, 1998). The mechanical loading environment may also affect the cellular function of the chondrocytes (Wong et al., 1997). It is generally accepted that there is a window of optimal loading to maintain normal healthy cartilage. Loading outside this window has been implicated in cartilage degeneration and joint disease; for example chondromalacia, patellofemoral pain syndrome and osteoarthritis (Huberti and Hayes, 1984; Howell et al., 1992; Insall et al., 1972). In animal injury models, both excessive joint loading (Dekel and Weissman, 1978) and insufficient joint loading (Palmoski et al., 1980) have been associated with cartilage degeneration. Understanding the changes in mechanical loading in a normal and abnormal joint may provide information on the mechanism of cartilage degeneration and disease, leading to better treatment and prevention.

4.1.1 Quantification of Forces and Stresses

Numerous ways to quantify joint forces and stresses have been reported in the literature, including experimental, analytical, and numerical methods. The following sections will present an overview of these methods; the advantages and disadvantages of each method will be discussed.

4.1.1.1 Experimental

Experimental techniques to measure joint contact forces are primarily invasive, in-vitro techniques. Miniature piezoresistive contact pressure transducers have been implanted at various locations on the surface of joints (Brown and Muratori, 1979). This method allowed dynamic measurement of contact stress at discrete locations during joint loading throughout a range of motion. Transducers have been used to measure time-dependent

contact stresses in the PF joint with static and cyclic loading (Ferguson et al., 1979). Piezoresistive transducers were also used to study contact stresses in the hip (Brown and Shaw, 1983) and on the femoral chondyles (Brown and Shaw, 1984) during locomotion. A disadvantage of this method was that contact stress was only measured at discrete locations in the joint. Therefore, this method did not provide information on the overall pressure distribution in the joint. In addition, the introduction of the transducer may have disturbed the joint and altered its contact characteristics.

Pressure sensitive film has been used to measure peak contact pressures, by inserting the film between the contacting articular surfaces (Fukubayashi and Kurosawa, 1980). The film consisted of polyester sheets embedded with dye capsules which, when pressed together, produced a red stain. The intensity of the stain was non-linearly dependent on the applied pressure. Pressure sensitive film was used to analyse the effect of Q-angle on PF contact pressures (Huberti and Hayes, 1984) and to measure PF contact pressures during impact loading of the knee (Atkinson et al., 1998). Pressure sensitive film was used in conjunction with high speed video, and implantable force transducers, to measure in-situ joint mechanics as a function of flexion angle, joint loading, and ACL integrity (Ronsky et al., 1995). With the pressure sensitive film both the peak pressure distribution and the contact area could be measured concurrently. Integrating the pressure distribution provided a rough estimate of the peak contact force. An unlimited number of measurements may be performed under different conditions. However, there were a number of limitations to using pressure sensitive film. Since only the peak pressures were recorded, the time-dependent stress response could not be studied. In addition, the film, which was approximately 0.2 to 0.3 mm thick, altered the interaction of the articular surfaces. Finite element models suggested that the introduction of the film may alter contact stress by between 10 to 26%, depending on the loading, geometry of the surfaces, and the mechanical properties of the cartilage (Wu et al., 1998b). The film was also difficult to calibrate and was sensitive to shear and friction stress, sliding, crinkling, and handling. The measurement precision of the film was approximately 10% (Ronsky et al., 1995). With pressure sensitive film the stress distribution throughout the depth of the

tissue could not be determined.

A micro-indentation transducer was used to study the pressure distribution on the surfaces of the tibia and the retropatellar surface (Ahmed and Burke, 1983a; Ahmed et al., 1983b). The principle was similar to pressure sensitive film. A multi-layered sheet was inserted between the joint surfaces. One layer served as an indenter, while the other acted as a plastic material. The contact pressure distribution was interpreted from the corresponding micro-indentation pattern. The advantages and disadvantages of this method were similar to those of the pressure sensitive film.

In summary, although experimental techniques were useful in quantifying contact pressure distributions, they had many limitations. Experimental techniques were highly invasive, difficult to calibrate, and may alter joint stresses. Finally, these techniques could not be used to determine the distribution of stress throughout the depth of the cartilage.

4.1.1.2 Analytic Models

Two-dimensional and 3D mathematical models have been used to predict joint contact forces (Wismans et al., 1980; van Eijden et al., 1986; Hirokawa, 1991). The models were based on simplified joint geometry and assumptions of the magnitude and direction of the muscle and ligament forces. More simple models assumed that the articular cartilage surfaces were rigid, resulting in point contact (e.g., Wismans et al., 1980; van Eijden et al., 1986; Hirokawa, 1991). For example, a 2D point contact model was used to quantify PF contact forces before and after ACL transection (Hasler and Herzog, 1998a). Analysis was limited to contact forces and kinematic variables, as contact areas and stresses could not be studied with these models.

More realistic representations of the cartilage layers were developed using elastic compression spring elements (Essinger et al., 1989) and rigid body springs (An et al., 1990). These models were used to predict contact area and contact stress. However, stresses throughout the depth of the cartilage could not be calculated using this approach.

Numerous analytical models have been used to calculate the distribution of stress throughout the depth of the cartilage. Hertz theory was used to model joints analytically as contacting elastic spheres (Eberhardt et al., 1990). A biphasic model was used to calculate stress analytically in a loaded cartilage layer (Mow et al., 1980). These models were restricted to simple geometries because of the difficulty in deriving analytic solutions. For stress analysis of joints incorporating complex geometry and physiologic load, numerical methods were more appropriate due to their efficiency and flexibility.

There were a number of advantages to using models as compared to experimental methods. The effect of varying input parameters, such as geometry (e.g., Huber-Betzer et al., 1990; Eckstein et al., 1994) and material properties (e.g., Huber-Betzer et al., 1990), could be investigated. This was not possible in an experimental set-up. The contribution of isolated structures to the overall function of the joint could be identified. The joint could be tested at the limits of physiologic performance to study injury mechanisms. Models could be useful in evaluating surgical treatment and rehabilitation programs. However, due to the complexities of the joints, simplifying assumptions had to be made, which limited the validity of the model. Evaluation and validation of the models with experimental data was very important.

4.1.1.3 Numerical - Finite Element Models

Numerical procedures have been used when the models have been too complicated to be solved by analytical methods. Numerous different numerical procedures exist. In this section a brief overview of one numerical method; the finite element method will be discussed. The finite element method models a structure by breaking it up into a collection of smaller parts (elements). Each element has a simple geometry and is easier to analyse than the actual structure. The complicated solution is approximated by a model consisting of piece-wise continuous simple solutions.

The inputs to the finite element model are: element properties, material properties, geometry, boundary conditions, contact modelling, and loading. Understanding how the inputs and assumptions affect the validity of the model is vital.

In the following sections a number of key issues surrounding finite element modelling of joints are presented. The goals of the review are to:

- present the issues and complexities involved in modelling biological tissues,
- present the simplifying assumptions that have been made,
- discuss how these assumptions affect the results and validity of the models, and
- familiarize the reader with past work, in terms of models and research questions.

The review is divided into the following sections: element properties, material properties, geometry, and boundary conditions. Finally, a brief review of the experimental and theoretical techniques used to investigate the effects of congruence and changes in kinematics on joint stresses is presented.

4.1.2 Element Properties for Modelling Cartilage

Articular cartilage is a viscoelastic material consisting of chondrocytes (5%) embedded in an extracellular matrix. The extracellular matrix, consisting mostly of proteoglycans and collagen, makes up 20-40% of the wet weight of cartilage. The other 60-80% is made up of tissue fluid. Due to its structure, modelling cartilage is complex. A number of ways to simplify the problem have been developed. The assumptions and implications of each will be discussed.

4.1.2.1 Elastic

A single phase elastic model was the most basic way to model cartilage. The cartilage was assumed to be an isotropic linearly elastic solid, and the material coefficients were chosen to account for both the solid and fluid phase. However, since fluid flow effects were not included, the time dependent behaviour of cartilage was not modelled. This approach was only valid for certain loading conditions: (1) at the instant of loading, when no fluid flows, and (2) at equilibrium, when all fluid flow has ceased.

This approach to modelling cartilage as a single phase elastic solid was used in analyses of whole articulating joints. For example, elastic assumptions were used to model the hip to investigate the effects of changing material properties associated with osteoarthritis (Brown and DiGioia, 1984). It was assumed that at equilibrium, the material behaviour

was similar to that predicted by biphasic models. Heegaard et al. (1995) presented a 3D kinematic and contact analysis of the PF joint, in which cartilage was also modelled as an elastic solid. Cartilage was believed to behave as a single phase incompressible linearly elastic solid as the strain rate of the loading approached infinity (Brown and Singerman, 1986). Therefore, single-phase models have been used to study the effect of impact loading (Haut et al., 1995; Atkinson et al. 1998; Newberry et al., 1998). These models were valid if the strain rate was larger than that required to cause divergence from the biphasic model. The strain rate that causes divergence from the biphasic model was not well documented and depended on loading, surface geometries, and the material properties of the cartilage. An impulsively loaded rabbit knee was studied using an elastic model (Anderson et al., 1990). The impact time scale was 20-200 ms, with a strain rate of ($0.5\ s^{-1}$). The local stresses due to displaced articular fractures in the tibiofemoral joint were analysed (Huber-Betzer et al., 1990). Due to the high strain rates characteristic of normal locomotion, an elastic model was deemed valid. Finally, some elastic models incorporated the inherent heterogeneity found in cartilage by modelling layers of cartilage, each with different properties. For example, Galbraith and Bryant (1989) modelled 3 isotropic, homogeneous, elastic layers.

In summary, the validity of elastic assumptions depended on the loading conditions. Elastic models were limited to the study of equilibrium conditions or impact loading. Such models were incapable of modelling time-dependent behaviour and could only be used to estimate the overall cartilage stress. The elastic single-phase approach did not provide any information about the interaction between the solid and fluid phases. To address some of these limitations, biphasic models have been developed.

4.1.2.2 Linear and Non-Linear Biphasic Theory

The biphasic theory was developed to incorporate the effects of the fluid flow on cartilage behaviour (Mow et al., 1980). The cartilage was modelled as two immiscible phases; a solid phase, representing the collagen, proteoglycan matrix, and chondrocytes, and a fluid phase, representing the interstitial fluid. The solid was assumed to be homogeneous,

isotropic, permeable, and linearly elastic. The fluid was assumed to be non-viscous. Although both phases were incompressible, the tissue as a whole was compressible through exudation of water. For the linear biphasic theory all of the material properties, such as volumetric fraction of constituents, elastic moduli, and permeability, were assumed to be constant. For such a mixture, the governing equations were derived from mass continuity, constitutive, and equilibrium equations (Mow et al., 1980). Many simple geometry experiments have been modelled using the biphasic theory: unconfined compression (Armstrong et al. 1984), confined compression (Mow et al., 1980), and indentation (Mak et al., 1987) (Figure 4.1). These models have been used to study the interaction between the solid and fluid phase during creep and stress relaxation. Discrepancies between theoretical and experimental data early in the time response were noted (Mow et al., 1989; Brown and Singerman, 1986). A possible cause of the discrepancies was that permeability was held constant. Physiologically, the permeability depends on the tissue strain (Lai et al., 1980). As the compressive strain increases, the size of the pores decrease. This results in an increase in drag force on the pore fluid causing the permeability of the cartilage to decrease. Strain-dependent permeability was introduced in the non-linear biphasic theory (Lai et al., 1981).

Both advantages and disadvantages were associated with biphasic theories. The main advantage was that the biphasic theories allowed the quantification of the load carried by the solid and fluid phases. Therefore, the interaction between the two components could be investigated. This led to a better understanding of the structure and function of cartilage. During cartilage failure it was the solid phase that failed. Therefore, knowledge of the load carried by the solid was vital in determining the mechanism and criteria for failure. However, both the linear and non-linear biphasic theory assumed infinitesimal strain (both phases were incompressible). This assumption was only valid for loading conditions resulting in small strain and strain rates. The maximum strain or strain rate that could be used to model cartilage validly using the biphasic model was not well defined in the literature, and was dependent on loading, surface geometries, and the material properties of cartilage. Another disadvantage of the biphasic theory was the added

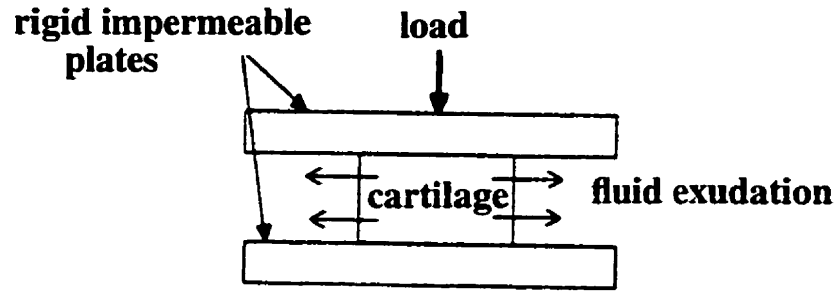

(A)

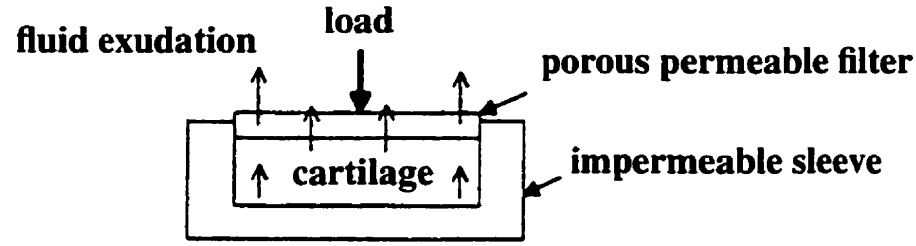

(B)

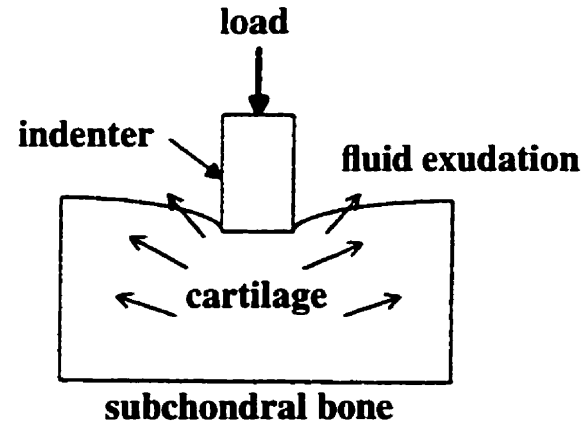

(C)

Figure 4.1:A) Unconfined compression test geometry. A specimen of cartilage was compressed between two platens. B) Confined compression test geometry. No radial displacement of the specimen was allowed. C) Indentation test geometry (from Goldsmith et al., 1996).

complexity of determining the material coefficients necessary to describe the fluid and solid behaviour. The difficulty of characterizing the material properties introduced uncertainty in the model results.

4.1.2.3 Finite Deformation Biphasic Theory

Physiologic loading, such as walking or running, involves high strain and fast loading rates. It has been speculated that large cartilage deformation results (Huber-Betzer et al., 1990). The finite deformation biphasic model accounted for high levels of strain by incorporating material non-linearities such as non-linear elastic modulus for the solid, non-linear strain dependent permeability, and variable solid to fluid ratio (Suh et al., 1991). A disadvantage of the finite deformation theory was the difficulty and complexity in estimating the material coefficients that appropriately described the non-linear behaviour of cartilage (Ateshian et al., 1997). To date, there is no method to estimate the material coefficients needed to describe non-linear cartilage behaviour accurately during large strain.

4.1.2.4 A Comparison of Biphasic Models

Linear, non-linear, and finite deformation theories have been compared using models of confined compression tests (Figure 4.1) (Suh et al., 1991). Under low strain (ε_o=0.05, in a ramp time of t_o=500 seconds), all models predicted a similar response, with the linear biphasic theory predicting slightly less compressive strain and reaction force. For large strain (ε_o=0.15, t_o=350 seconds), the effects of the non-linearities were more dramatic. The linear biphasic model predicted a peak strain of 18.8%, the non-linear biphasic model predicted 54.3% and the finite deformation model predicted 34.8%. The results suggested that non-linear elasticity for the solid phase must be incorporated to control the exaggerated effect of non-linear permeability. This became more evident at high strain rates (ε_o=0.05, t_o=50 seconds). The non-linear biphasic model predicted compressive strains in excess of 100%, which is not possible. The finite deformation model predicted strains of 44%. It was concluded that non-linearities incorporated in the finite deformation theory are important at higher levels of strain and strain rates.

Linear and finite deformation theories have been compared using an indentation model (Suh and Spilker, 1994). The finite deformation model predicted a larger reaction force, and an increase in pore fluid pressures (ε_0=0.1, in a ramp time of t_0=50 seconds). The effect became more pronounced when the compression rate was increased (ε_0=0.1, in a ramp time of t_0=2 seconds). The reaction force exceeded that of the linear model by up to 38% depending on the porosity of the indenter used.

The results of the above studies suggested that for large local deformations the finite deformation biphasic model may be required. The linear biphasic theory may be considered reasonably accurate if the local strains are within 25% (Spilker et al., 1992). Strain and strain rates were discussed in terms of compression and indentation tests, in which the planar geometries result in large local deformations. It was not shown how much of an effect the theories would have on a geometrically accurate joint, where congruence is speculated to result in smaller local deformations. Furthermore, neither study referenced how the material properties of the different models were derived. It is speculated that the material properties would have a large effect on the results of the models.

In summary, cartilage is a complex material which is challenging to model. There have been numerous ways to model cartilage, each involving simplifying assumptions. These assumptions limited the validity of the models. It has been shown that the validity of the theories depended on the loading conditions modelled.

4.1.2.5 Poroelastic Theory (ABAQUS)

There were two theories commonly used to describe soft tissue as a biphasic material; the mixture theory (Mow et al., 1980) (previously described), and the poroelastic theory. The poroelastic theory was developed for analysing wet soils (Biot, 1941) and applied to study soft tissue (e.g., van der Voet, 1992). The mixture theory was more general, but when applied to the compression of soft tissues the two theories were equivalent (Simon, 1992). Van der Voet (1992) analysed indentation models using soils consolidation procedure in the commercially available package ABAQUS. Results compared favourably to those

obtained by the mixture theory. Solutions obtained with ABAQUS were compared with analytic solutions for three tests: an unconfined indentation test, a test with the contact of a spherical cartilage surface with a rigid plate, and an axisymmetric joint contact test (Wu et al., 1998a). It was concluded that the soils consolidation procedure in ABAQUS was appropriate for modelling cartilage as a biphasic material.

In this thesis the poroelastic theory of soils consolidation in ABAQUS will be used to model cartilage. Briefly, in ABAQUS the element stiffness equations were based on Terzaghi's effective stress principle, while fluid flow was described by Darcy's law. Using the principle of virtual work and accounting for continuity of the fluid phase, the following equation was obtained (ABAQUS, 1994a):

$$\begin{bmatrix} [K] & -[C] \\ -[C]^T & -\Delta t[H] \end{bmatrix} \begin{Bmatrix} \{u\} \\ \{p\} \end{Bmatrix} = \begin{Bmatrix} \{F\} \\ \{R\} \end{Bmatrix} \tag{29}$$

where $[K]$ was the stiffness matrix, $[H]$ was the permeability matrix, and $[C]$ was the matrix that coupled the fluid flow and equilibrium equations. $\{F\}$ contained the nodal forces while $\{R\}$ represented the fluid flows. The coupled system of equations was solved iteratively for increments of the unknown solid displacements, $\{u\}$, and pore pressures, $\{p\}$, at a given time. A backward difference operator was used for progressing through the time history of the simulation (ABAQUS, 1994b).

4.1.3 Material Properties for Modelling Cartilage

One of the most important aspects of finite element modelling in biomechanics is defining the material properties (Simon, 1992). Determination of the material properties of cartilage is complex. Cartilage is an inhomogeneous, anisotropic biphasic material. The most frequently used methods to determine the material properties required to model cartilage will be discussed.

Experimentally, conventional mechanical tests have been applied: uniaxial compression (McCutchen, 1962), uniaxial strain (Edwards, 1967), uniaxial tension (Kempson et al.,

1968), and bulk indentation tests (Kempson et al., 1971). McCutchen (1962) estimated two time-dependent values for Young's modulus: for short term response E=11.1 MPa, and for long term response E=0.58 MPa. Kempson et al. (1971) used a "2 second creep modulus" to estimate the instantaneous properties of normal and diseased human femoral heads at a number of positions on the surface. Even in the normal joints a range of 1 to over 10 MPa were reported. Material properties were found to vary with location of the test site, depth and with the specific experimental method used. These tests were useful in qualitative analysis of the structure and function of cartilage. However, with the exception of the indentation test, they were limited to analysing standardized samples and were not suitable for analysing intact cartilage.

Analytic approaches were developed to investigate cartilage indentation. Cartilage indentation simulated in-situ conditions more closely than other mechanical tests (Suh and Spilker, 1994). Material properties were derived which allowed a good fit between experimental and analytic results. Zarek and Edwards (1963) used a Hertz solution for the contact of elastic spheres. The model showed poor agreement between analytical and experimental results, due to inaccurate constitutive relations. These problems were partially overcome in later models also based on incompressible, elastic material assumptions (Hayes et al., 1972). The results were limited to describing the instantaneous and equilibrium response at small applied loads.

Theoretical analysis of the indentation experiment was extended to include the biphasic nature of cartilage. The constitutive relations developed in the linear biphasic theory were used to establish master solutions for all values of Poisson's ratio (Mow et al., 1980; Mak et al., 1987; Mow et al., 1989). Creep indentation experiments were then performed under small loads on the intact joint. The resulting experimental curve was fit to the master solutions to determine the material properties. Three intrinsic material properties were used to describe the compressive behaviour of cartilage: the aggregate modulus (H_A), Poisson's ratio (ν_s), and permeability (k). Poisson's ratio determined the shape of the curve, while permeability determined the rate of creep, expressed as a shift factor, S.

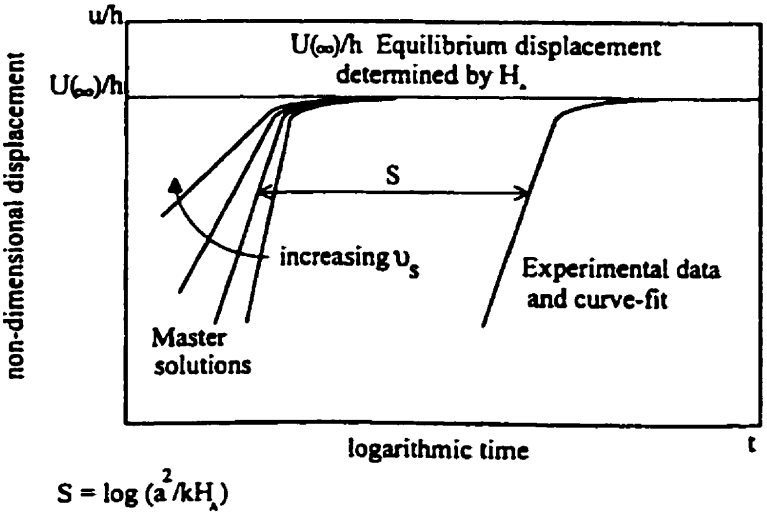

Figure 4.2: Curve fitting experimental results to master solutions to determine material properties (from Mow et al., 1989).

Note that the aggregate modulus was related to Young's modulus (E_s) by the following relation:

$$H_A = \frac{E_s(1-\nu_s)}{(1+\nu_s)(1-2\nu_s)} \tag{30}$$

In some papers where the material properties were quoted in terms of Lame's constants, the following relations applied:

$$H_A = \lambda_s + 2\mu_s \tag{31}$$

$$E_s = \frac{\mu(3\lambda_s + 2\mu_s)}{\lambda_s + \mu_s} \tag{32}$$

$$\nu_s = \frac{\lambda_s}{2(\lambda_s + \mu_s)} \tag{33}$$

where μ_s and λ_s were Lame's coefficients of the solid matrix. Curve-fitting methods have been applied to estimate the material properties of the human femoral head at three

locations; the lateral and medial condyles and the patellar groove (Mow et al., 1989). It was found that the femoral groove had a significantly lower Poisson's ratio (0.25 compared to an average of 0.39 of the condyles), lower aggregate modulus (0.47 compared to 0.89 MPa), and higher permeability (1.42×10^{-15} compared to 0.45×10^{-15} m^4/Ns). It was speculated that site-specific material properties may be a function of the joint congruity and loading environment. Similar techniques were used to study the distal femoral cartilage in different species (bovine, canine, human, monkey, and rabbit) (Athanasiou et al., 1991). Significant differences existed in some material properties among species and test sites. Typically, the femoral groove had the lowest aggregate modulus, highest permeability, and lowest Poisson's ratio. It was speculated that the material properties allowed the cartilage in the femoral groove to compress quickly to create a congruent PF joint articulation. For any given location, no significant difference was found between the aggregate modulus among species. However, the permeability and Poisson's ratio were found to vary significantly among species. Similar curve-fitting procedures were performed to estimate the material coefficients from unconfined compression tests of the chondroepiphysis of human fetal femoral heads (Brown and Singerman, 1986). Poor fit between the experimental data and master solutions was noted. The best fit aggregate modulus was 0.699 MPa with a S.D. of 0.346 MPa. The best fit permeability was 2.51×10^{-15} MPa with a S.D. of 1.59×10^{-15}. In all tests the corresponding value of Poisson's ratio was 0.0. The accuracy of the linear biphasic theory to fit the experimental data appeared to depend on the specific experiment performed.

The finite deformation theory required 5 material coefficients to describe cartilage behaviour under large strains. These coefficients were the aggregate modulus under zero strain (H_{Ao}), a non-dimensional coefficient (v) that reduced to the Poisson's ratio of the solid phase under infinitesimal strain, a compressive-stiffening coefficient (β), permeability at zero strain (k_o), and finally a non-dimensional permeability coefficient (M), which weighted the exponential function dependence of permeability on strain. Ateshian et al. (1997) performed two confined compression tests to estimate the material coefficients: a stress relaxation and a creep test. A confined compression test was used to

reduce the constitutive equations to their one dimensional form where Poisson's ratio did not affect the solution. The remaining four material coefficients were estimated by curve fitting the experimental and theoretical master solutions. The material properties estimated from the stress relaxation test were unable to predict the experimental creep response accurately. In addition, the material properties (k_o and M) estimated from a stress relaxation test were statistically different from those estimated using the experimental creep data. Ateshian et al., (1997) concluded that either the constitutive equations were not appropriate or the indirect determination of permeability coefficients from creep or stress-relaxation experiments did not yield precise values of those coefficients. To date there is no method to estimate the material coefficients needed to describe non-linear cartilage behaviour accurately during large strain.

In summary, there was a number of experimental and theoretical methods used to estimate the material properties of cartilage. The variation in the material properties used for modelling was very large, as indicated in Table 4.1. Variations in material properties have been attributed to

- natural variation of tissue structure and composition,
- variation between species,
- variation in specific testing protocol,
- methods of storing cartilage, and
- theoretical approach used (i.e., lack of appropriate constitutive equation).

The majority of the methods were subjective, in that the material properties were chosen to give a good fit with theoretical models. As yet, there is no method to determine the material properties independently. Given the uncertainty of the material properties, it is suggested that sensitivity analyses be performed to understand the effect of the assumed properties on the finite element model results.

Table 4.1: Material properties commonly used to model cartilage.

Model type	Reference	Young's modulus (MPa)	Poisson's ratio	Permeability $x10^{15}$ m^4/Ns
Single-phase elastic	Galbraith and Bryant (1989)	12	0.45	n/a
	Huber-Betzer et al. (1990)	20	0.47	n/a
	Anderson et al. (1990)	35	0.45	n/a
	Heegard et al. (1995)	2.0	0.47	n/a
	Atkinson et al. (1998)	20	0.49	n/a
Biphasic	Mow et al. (1980)	H_{Ao}=0.7	--	7.6
	Brown and Singerman (1986)	0.699	0.0	2.51
	van der Voet (1992)	0.467	0.1667	7.5
	Mow et al. (1989)	0.45 (condylar) 0.40 (groove)	0.39 0.24	0.44 1.42
	Athanasiou et al. (1991)†	Ha=0.64 (condylar) Ha=0.47 (groove)	0.27 0.17	1.28 2.50
	Spilker et al. (1992)	0.54	0.08	4.0
	Schinagl et al. (1997)	0.079 (surface) 2.10 (deep layer)	--	--
	Setton et al. (1994)	0.55	0.07	2.4
	Mukherjee and Wayne (1998a)	0.64 (depression) 0.32 (condylar)	0.13	1.17
finite deform-ation	Suh et al. (1994)	E_0=0.44 ß= --	0.02	k_0=26.5 M=10
	Ateshian et al. (1997)	H_{Ao}=0.4 ß=0.35	--	k_0=2.2-2.7 M=0.4-2.2

†These are average values of a number of species

4.1.4 Model Geometry

In addition to the element and material property assumptions, joint geometry is another important input to the finite element model of cartilage. Articular joint surfaces have complex 3D geometry. The curvatures of the articular surfaces vary in the sagittal and transverse planes (Kwak et al., 1997), as does the thickness of the cartilage layer (Ateshian et al., 1991). A rationale for how to represent the complex joint geometry most appropriately depends on several factors, including the specific research question proposed, limitations due to theoretical complexities, and the experimental data available. The goal of this section is to summarize the types of model geometries that have been reported in the literature. The models will be classified by the degree of geometric complexity.

4.1.4.1 Simple Geometry

The simplest geometries were those of the confined and unconfined compression, and indentation tests (Mow et al., 1980, Armstrong et al., 1984). For the compression tests the cartilage was represented as a standardized cylindrical plug. Indentation models typically assumed that the cartilage had planar geometry and uniform thickness. Indentation models were useful as the indentation experiments could be performed on intact cartilage thus the loading was more representative. Due to the simple geometry, more controlled experiments could be performed. Comparing the model and experimental results allowed evaluation of the theoretical assumptions and boundary conditions used, as well as determination of the material coefficients of the cartilage. These simpler models typically incorporated the biphasic and finite deformation theory and were useful in analysing the interaction between the fluid and solid phases (Mak et al., 1987; Spilker et al., 1992); Mow et al., 1989). Stress-relaxation and creep tests have also been modelled to investigate the load-dependent nature of cartilage. Therefore, these models were useful in model evaluation and provided insight into cartilage behaviour. However, the simple geometries did not represent the complex surface geometries of the opposing joint surfaces. Therefore, the models did not represent the surface interactions during in-vivo loading where the contact area was a function of load, joint surface geometries, and joint

orientation. These models were insufficient to investigate the influence of joint congruence on cartilage stresses.

4.1.4.2 Non-specific Joint Geometry

Circular arcs, spheres, and ellipses have been used to characterize joint geometry. Typically, the models were not joint specific, but represented general joint surface interaction. Incorporating curvature of the joint surfaces provided a more realistic representation of the joint and load transmission. The influence of geometry on the stress distribution of joints has been investigated (Eckstein et al., 1994). The joint surfaces were modelled as spherical or semielliptical. Five configurations with different elliptic radii, representing different degrees of joint congruence, were used. The geometry and congruence of the joint had a large influence on the stress distributions, as much as doubling the peak von Mises stresses. Although the cartilage layer was not modelled, this study demonstrated the importance of the joint geometry in optimizing transmission of joint forces. The PF joint was modelled using concentric half spheres (Herzog et al., 1998). Values of the radii and uniform thickness of cartilage were experimentally derived. Using the biphasic model, the contact radius and peak pressures were predicted and compared to values derived using pressure sensitive film. Plane strain models have been used to represent the joints (Huber-Betzer et al., 1990; van der Voet, 1992). Plane strain assumed that the out-of-plane strain was zero. It was equivalent to analysing a thin slice through a joint, in which the out-of-plane geometry was assumed constant. A plane strain elastic model of the tibiofemoral joint was used to analyse the effects of changing surface curvatures, cartilage thickness, and introducing a surface discontinuity (Huber-Betzer et al., 1990). The surfaces were approximated by circular arcs with constant cartilage thickness. It was found that changing the global geometry of the joint resulted in changes in both contact area and pressure.

These non-specific joint models have been useful in estimating the stresses in a joint, and investigating the effects of joint surface geometries on cartilage and bone stresses. Although, valuable in identifying general trends, simplified non-specific geometry did not

completely characterize in-vivo surface interactions. To investigate the influence of joint orientation on joint stresses more complex and specific geometry was required.

4.1.4.3 Complex Geometry

To represent in-vivo surface interactions more accurately, numerous models have incorporated complex joint surface geometry. The porcine tibiofemoral joint was studied using a plane strain model which incorporated the 2D geometry of a transverse slice (Mukherjee and Wayne, 1998b). The slice geometry was derived by digitizing roentgenograms of the unloaded knee. However, contact between the lateral condyle and the tibial plateau was not explicitly modelled. Instead a linear load with a distribution increasing from lateral to medial was applied to the lateral condyle. Therefore, the effect of the relative geometries of the articulating surfaces on load transmission through the joint was not modelled. Various 2D elastic plane strain models have been used to model contact at impact loads (Li et al., 1995; Anderson et al., 1990). These studies incorporated both articular surfaces and the contact between them. However, since the cartilage was modelled as an elastic single-phase material the load sharing between the fluid and solid could not be investigated. All of the above plane strain models were limited in that they did not account for out-of-plane irregularities in geometry.

Modelling with accurate 3D geometry was challenging. There were increased computing requirements, due to the size of the models, as well as convergence problems, contact modelling issues and boundary condition issues associated with modelling the cartilage as a biphasic material. For these reasons, 3D models typically have treated the cartilage as a single phase elastic solid. Heegard et al. (1995) developed a 3D model of the human PF joint using CT scans. The elastic model was used to investigate the contact pressures and kinematics of the joint. The model was used to investigate the kinematics of the joint, and contact patterns. The model was not used to study the effects of changes in patellar position on cartilage stress. Since, the model was elastic, the load sharing between the fluid and solid phases in cartilage could not be investigated.

In summary, models representing articular joints used various geometric assumptions.

In general, the simpler geometrical models were used with more elaborate biphasic and finite deformation theories. Although useful in studying cartilage behaviour, these models did not accurately represent the complex geometry of the joint surfaces or the resulting contact mechanics. There were a number of added complexities involved in modelling 3D contact mechanics with the biphasic theories. As a result, the more complex geometrical models typically used simpler single-phase elastic assumptions. These models were useful in characterizing global joint kinematics and contact stresses, however, they did not allow the study of solid and pore fluid interactions. Biphasic analysis of geometrically accurate models under physiologic loading would provide valuable information about joint biomechanics. This type of model would be necessary to investigate the relation between patellar orientation and cartilage stresses.

4.1.5 Boundary Conditions

As well as material properties and geometry, the boundary conditions of a model were also important. Two types of boundary conditions will be discussed: kinematic and hydraulic. Kinematic boundary conditions were applied to include the effect of structures that were not explicitly included in the model. For example, the subchondral bone affected the behaviour of cartilage. There was some debate on how to model its effect on cartilage mechanics. Many models used boundary conditions to fix the bone-cartilage interface in all directions (e.g., Spilker et al., 1992; Mukherjee and Wayne, 1998b). This was equivalent to assuming the bone was a rigid material, incapable of deforming. The underlying assumption in this case was that the bone was several hundred times stiffer than cartilage, and therefore bone deformation could be neglected. Conversely, many models explicitly modelled the bone as a linear elastic solid (van der Voet, 1992; Atkinson et al., 1998). Some models took into account the varying material properties in the different regions of the bone, such as the cortical and cancellous bone layers (Anderson et al., 1990; Huber-Betzer et al., 1990). Commonly used bone material properties are shown in Table 4.2.

Table 4.2: Material properties commonly used to model bone.

Reference	Type of bone	Young's modulus (MPa)	Poisson's ratio
Cowin (1989)		1100-1900	0.1-0.4
Galbraith and Bryant (1989)	Cancellous	300	0.49
Anderson et al. (1990)	Subchondral bone	2760	0.3
	Cortical bone	13800	0.3
	Cancellous bone	345-1380	0.3
Huber-Betzer et al. (1990)	Subchondral plate	3000	0.3
	Cancellous bone	1000	0.25
Eckstein et al. (1994)	Subchondral bone	1500	0.33
Heegard et al. (1995)	Cortical bone	1500	0.3
	Cancellous bone	300	0.3
Atkinson et al. (1998)	Subchondral bone	2000	0.3

A sensitivity analysis performed suggested that a significant depth of bone must be modelled, at least 15 times the tissue thickness (Galbraith and Bryant, 1989). Inadequate bone depth was found to cause a non-uniform stress distribution resulting in errors in calculated displacements and strains. Spilker et al. (1992) suggested that the large effect of the bone, in this study, was due to the large value of Young's modulus (E=12 MPa) used for cartilage. In addition, bone was represented using the modulus of cancellous bone (E=300 MPa) instead of the much larger modulus of subchondral bone, which may have influenced the results. The uncertainty in the results suggested that a sensitivity analysis should be carried out to determine the effect of bone geometry. An appropriate bone depth should be chosen so that the boundary constraints have negligible effect on the stress distribution in the cartilage.

If the cartilage is modelled as a biphasic material, hydraulic boundary conditions must be applied. There was consensus that the cartilage-bone boundary could be modelled as

impermeable (Spilker et al., 1992). However, there was debate on the appropriate hydraulic boundary conditions for the surface of the articular cartilage. One of the following four assumptions was typically used:

1. the pressure at the opposing cartilage surfaces was considered equal,
2. the surfaces were always permeable, even once contact was made,
3. the surfaces were permeable, until contact, when they became impermeable, and
4. the surfaces were sealed and impermeable.

With assumption 3, the underlying concept was that joint loads were transmitted by a thin fluid film between the surfaces, which becomes pressurized during contact, impeding fluid flow. An impermeable surface could also be visualized by consideration of the permeability of the surface layer. Experimental work has shown that the permeability of the cartilage was highest at the surface (Maroudas, 1979). Therefore, under a compressive load, fluid was exuded faster from the surface zone, than the middle or deep zones. With an amount of fluid now removed, large deformations of the matrix components in the surface zone cause an increase in drag forces, resulting in a decrease in permeability, possibly sealing the surface layer. To date, no experimental results on the effect of surface contact and loading on the surface permeability have been published.

Van der Voet (1992) performed a sensitivity analysis on the effects of hydraulic boundary conditions on the surface on a finite element model during stress relaxation and creep loading. It was reported that sealing the surface resulted in up to a three-fold increase in peak pressures and reaction forces, for a stress relaxation test in which ramp loading occurred in 500 seconds. It was suggested that the surface permeability was an important consideration when analysing the long-term loading effects on cartilage, and for models loaded slowly. As the model is loaded more quickly, fluid flow and the hydraulic boundary conditions had less effect on the short-term response of the cartilage (Kralovic, unpublished observation). During short-term response the fluid did not have time to flow. Initial investigation of the linear biphasic finite element model approximated that for a fast loading rate of 5 seconds the fluid velocity was on the order of 1×10^{-8} m/s (Kralovic, unpublished observation). In addition, large deformations of the solid would cause an

increase in drag forces, resulting in a further decrease in permeability, not incorporated in the model. Therefore, for large strain and strain rates when analysing short-term response of cartilage it may be reasonable to model the surfaces as impermeable.

4.1.6 The Effects of Congruence or Changes in Kinematics

In this section only those studies quantifying the effects of joint congruence or changes in kinematics on mechanics will be discussed. The research can be divided into two groups:

1. studies that perturbed the joint geometries, and calculated the resulting cartilage and bone stresses,
2. studies that perturbed the joint kinematics and calculated the resulting changes in the cartilage and bone stresses. Note that since the change in kinematics caused a shift in contact area this method indirectly led to a change in contact geometry.

The advantages and disadvantages of each will be discussed.

4.1.6.1 Perturbing Joint Geometry

Theoretical analyses of the effects of joint geometry on mechanics have been documented (Huber-Betzer et al. 1990; Eckstein et al., 1994; Stone and Yu, 1997). Eckstein et al., (1994) studied the effect of joint geometries on the stress distribution in bone. Five hemispherical and semi-elliptic joint geometries were analysed using the finite element method. It was assumed that a distribution where the stresses were minimized and uniform was optimal for joint health and function. An incongruous joint (oversized femoral head and deepened socket) resulted in the most satisfactory distribution of stresses. Although, this may be the case in a hemispherical joint such as the hip, it is unclear whether the same applies for other joints with flatter geometries, such as the PF joint. It was concluded that joint geometry was important in optimizing transmission of joint loads. A limitation of this study was that the cartilage layer was not modelled.

The compliance of cartilage was expected to change joint congruence and alter the distribution of stresses in the bone. In the following studies, the cartilage layer was modelled. The effects of flattening the tibia were studied using an elastic finite element model of the tibiofemoral joint (Huber-Betzer et al., 1990). The joint surfaces were

represented by circular arcs. Increasing the radius of the tibia, led to a large increase in peak and average pressures. A similar study was done by Stone and Yu (1997), in which a finite element model of a non-specific joint was created using circular arcs. The effect of congruence on joint stresses was studied by varying the radius of one body. Twelve geometric cases were studied and the congruence of each was defined as the ratio of the radii of curvature (R_1/R_2). A small decrease in the congruence ratio caused a large increase in compressive, shear, and von Mises stresses. For example, changing the congruence ratio from 0.99 to 0.98 caused a 25% increase in compressive stress, and a 17% increase in shear stress. These studies suggested that relative geometries of the opposing articular cartilage surfaces are important to joint function, and that incongruent geometries may lead to a sharp increase in cartilage and bone stresses.

The theoretical approaches described had a number of advantages. The geometry of the surfaces could be changed easily, allowing systematic analysis of the effects of geometry on stress. Since the geometries were simple, they were easy to classify. Therefore, a relation between congruence and the resulting stress could be established. However, while these simple models indicated general trends, they did not simulate accurately the complex surface interactions expected in real joints. In addition, only central loading was assumed. It was expected that different loading conditions could alter mechanical responses. Changing the geometric input was equivalent to modelling a different joint. Therefore, the congruence and stress conditions between different joints were calculated. However, by using the same geometry, and perturbing the kinematics, the effect of joint injury and subsequent treatment methods can be evaluated.

4.1.6.2 Perturbing Kinematics

Many clinical problems such as chondromalacia (Bentley and Dowd, 1984) and recurrent subluxation or dislocation (Paulos et al., 1980) have been related to abnormal patellar tracking. Abnormal patellar tracking has been linked to muscle imbalances (Hirokawa, 1991; Huberti and Hayes, 1984), injuries to ligaments and joint stabilizers (Ronsky et al., 1995), and joint malalignment. These clinical conditions can be simulated by altering joint

kinematics. Many experimental studies have been performed on human cadaver knees. The effects of variations of Q-angle and flexion angle on patellofemoral contact pressures have been investigated using pressure sensitive film (Huberti and Hayes, 1984). Q-angle defined the line of action of the quadriceps with respect to the shaft of the femur. Abnormal Q-angles indicates joint malalignment (e.g., tibial rotation due to excessive pronation of the foot). Both a 10° increase and a 10° decrease in the Q-angle resulted in unpredictable contact patterns and an increase in peak pressures (e.g., an average increase of 45% at 20 degrees of flexion). Changes in contact pressures in cadaver knees due to changes in partitioning of the quadriceps force have been investigated (Ahmed et al., 1983b). The magnitude and direction of quadriceps muscle force had an effect on contact patterns and contact pressures. Furthermore, the ligaments are thought to constrain the kinematics of the patella, passively. For example, rupture or transection of the ACL has been associated with altered tracking and contact patterns (Ronsky et al., 1995; Herzog et al., 1998).

These experimental results indicated that muscles and passive joint stabilizers affect joint kinematics that subsequently affects joint congruence and contact stresses. However, the resulting changes in kinematics were complex in nature and difficult to characterize. Consequently, it was difficult to establish a relation between the changes in kinematics and the changes in joint stress. In addition, with experimental techniques it was not possible to measure the distribution of stresses throughout the depth of the cartilage and bone.

Few theoretical models have been used to study the effect of perturbing kinematics on internal tissue stresses. A 3D mathematical model (Hirokawa, 1991) of the human PF joint was used to study the effects of:

- increasing and decreasing the Q angle by displacing the attachment sites of the quadriceps muscle on the femur by 1 centimetre laterally or medially,
- increasing and decreasing the length of the patellar tendon by 1 centimetre,
- displacing the position of the tibial tuberosity anteriorly by 1 centimetre.

The resulting changes in kinematics and contact force were calculated with the model.

Applying Hertzian contact theory the contact stresses were computed. Results indicated that both an increase and decrease in Q-angle caused an increase in contact stresses. Changes in the patellar tendon length showed either undulating variations or small changes in contact stress, while elevating the tibial tuberosity showed a 20 to 30% reduction in stress. In this study, the geometry was characterized using the principal curvatures of the surfaces at the initial points of contact. This simplification may have affected the results. Other mathematical models (Blankevoort et al., 1991; Heegard et al., 1995) have potential in analysing the effect of changing muscle forces and ligament properties and geometry to a greater extent. To date, they have only been used to analyse normal PF kinematics.

Clinically, a variety of conditions, including chondromalacia and patellofemoral pain syndrome are suspected to be linked to abnormal kinematics and stresses. Experimental and theoretical work suggested that joint kinematics and joint congruence play a large role in the distribution of cartilage stresses. However, the relation between changes in orientation of the patella and changes in stress had not been accurately quantified in the literature. Experimental methods were limited to peak pressure values, and were incapable of analysing the internal stresses and strain in the cartilage. There was also the difficulty of characterizing the changes in kinematics caused by changes in passive or active restraints. Due to complexities of dealing with contact modelling of 3D surfaces, the theoretical models were oversimplified, and in many cases were not representative of the complex surface interactions in-vivo. The models typically used simplified geometry and elastic assumptions. Therefore, the interactions between solid stresses and pore fluid could not be investigated. To date the effects on cartilage solid stresses and pore fluid pressures of systematically perturbing the patellar orientation have not been investigated.

4.1.7 Purpose

Despite the many finite element models used to investigate joint mechanics and cartilage behaviour, the effects of perturbing patellar alignment on cartilage stresses have not been investigated to date. Therefore the purpose of this component of the thesis was to:

- quantify the effects of lateral versus central patellar alignment on stress distribution in PF cartilage and
- determine how sensitive the results are to material properties.

Commercial finite element software (ABAQUS 5.6) was used to study a 2D plane strain finite element model. The model was based on experimentally measured geometry and in-situ loading of a cat joint at 70 degrees of flexion. It was speculated that, for the same loading conditions, lateral tracking would result in a

- decrease in contact area,
- increase in contact pressure,
- increase in pore fluid pressures
- increase in principal solid stress,
- increase in Tresca stress,
- increase in principal solid strain.

It was hypothesized that although the theoretical representation of cartilage and material properties would affect the magnitude of the results, directionally the trends would be unaffected. The results of the stress analysis were expected to be consistent with the results of the analyses of PF geometry and congruence in the first part of this thesis (Chapter 3).

4.2 METHODS

The effect of patellar orientation on the distribution of stresses and strains in the cartilage was investigated, using a 2D plane strain finite element model. Geometric and kinematic inputs were based on a 3D geometric model of a cat PF joint. The stress distribution was calculated for two orientations of the patella at 70° of knee flexion. Seventy degrees of flexion was chosen for a number of reasons. Firstly, it was approximately in the middle of the range of knee flexion during normal walking in cats (i.e., 50° to 85°) (Hasler et al., 1998b). In addition, it was of particular interest to study the joint mechanics under loading. Kinematic and EMG studies have shown that particularly for a destabilized, ACL deficient knee loading may occur from 50° to 75° (Hasler et al., 1998b). As well, the calculated overlap of the undeformed surfaces was reasonable at 70°, and reorientation of the joint using the maximum curvatures resulted in a symmetric joint position. This suggested that the measured geometry and kinematics at 70° were reasonable.

Two orientations of the patella were chosen for analysis: (1) the experimentally measured lateral tracking position, and (2) the reoriented central tracking position. The measured lateral orientation was used, because at this position the kinematics of the bones was measured, and could be used as input to drive the finite element model. With a calculated congruence index of 0.267 mm^{-1}, the lateral tracking represented an incongruent position. With a calculated congruence index of 0.015 mm^{-1} central tracking represented a congruent position. The patella was reoriented centrally using the points of maximum curvature as the initial points of contact. These two positions represented the endpoints of the range of expected patellar orientations. Therefore, the resulting joint stresses were speculated to characterize the range of possible stresses for this particular joint at this flexion angle. Both the lateral and central tracking models will be discussed in turn.

4.2.1 Lateral Tracking Model

A computer program was written in Matlab (v5.1, Mathworks Inc., Natick, MA) to write the ABAQUS input file defining the model, automatically. A schematic diagram of the lateral tracking model is presented in Figure 4.3.

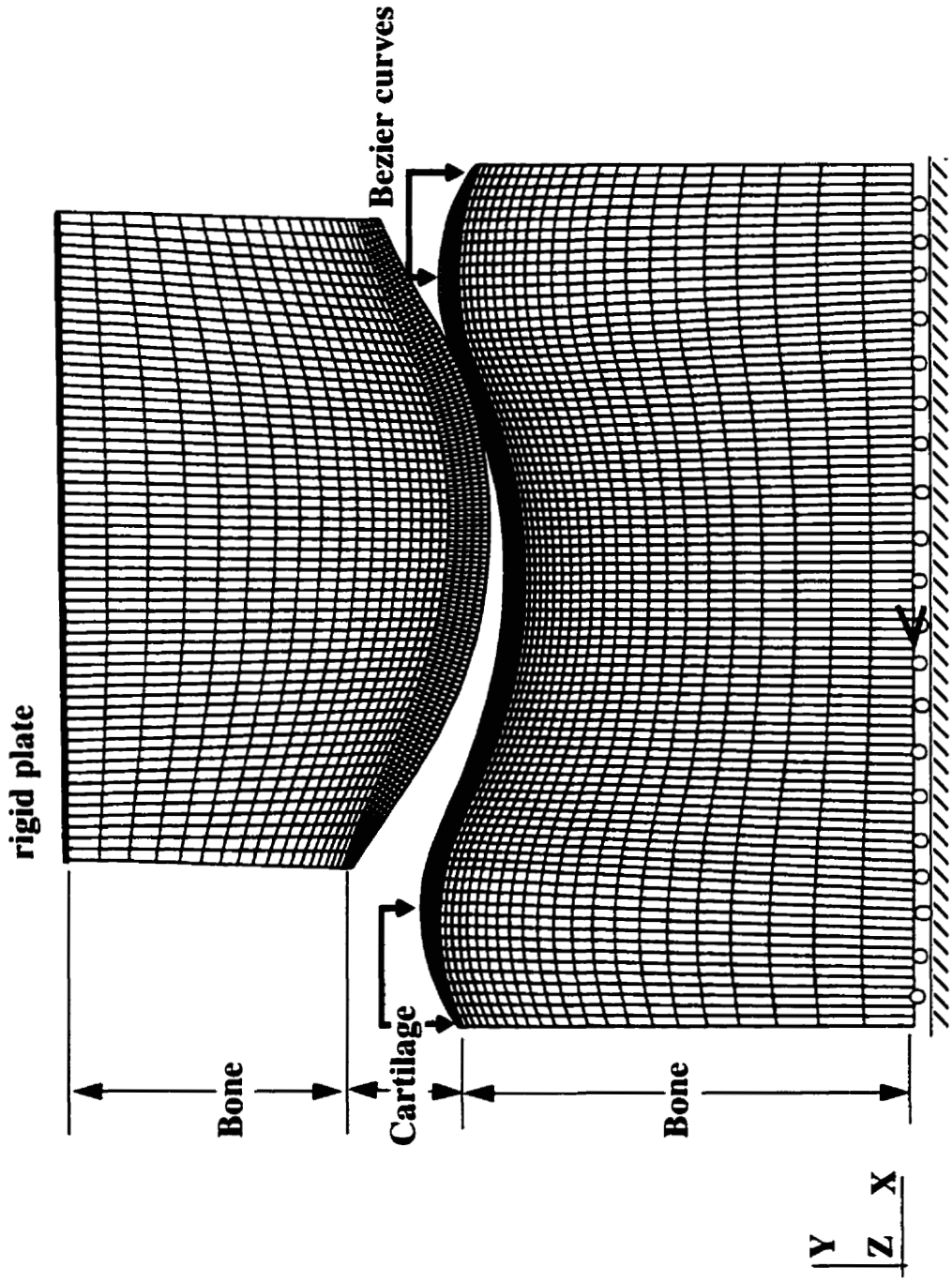

Figure 4.3:A schematic diagram of the lateral tracking finite element model.

Model inputs included: 1. geometry, 2. mesh, 3. boundary conditions, 4. contact modelling, 5. loading, and 6. element and material properties. Details regarding each of these inputs will be discussed in the following sections.

4.2.1.1 Geometry

To investigate the effect of patellar orientation and joint congruence on PF joint stresses, it was necessary to model the geometry of the opposing cartilage surfaces, as well as the geometry of the subchondral bone accurately. The non-uniform cartilage thickness has been speculated to affect joint stresses and was represented in the model. This required that complex joint specific geometry be incorporated. The geometry was derived from the 3D geometric model, that was based on photogrammetric data (Section 3.2.1).

Due to the complexities of modelling in 3D, in terms of meshing, contact modelling, model convergence, and computer storage requirements, a 2D plane strain model was used. Plane strain assumed that there was no strain in the direction normal to the plane of the model. It was equivalent to modelling a thin transverse slice through the centre of the joint, where out-of-plane geometry was constant and deformations were negligible. Previous analysis (Figure 3.13 and Figure 3.14) showed that the geometry varied little in the proximal/distal direction, and therefore plane strain was a reasonable approximation. Note that the plane strain model was given unit out-of-plane thickness.

The planar geometry was derived from the 3D geometric model by taking a slice through the centroid of the contact area with the patella and femur at 70° of flexion (Section 3.2.3.2). The slice was defined by the surface normal at the centroid based on the patellar surface and a lateral vector (Figure 3.8). The TPS algorithm was used to resample the cartilage and subchondral bone surfaces of the patella and femur on the transverse slice. The location of the resampled points depended on the desired mesh. Meshing will be described further in Section 4.2.1.2.

At the medial and lateral edges of the patella and femoral groove, as the cartilage tapers and thins, the cartilage and bone geometries were irregular and highly curved. This caused

distortions of the projected grid used with the MDPG technique for acquisition of surface geometry. With the given grid orientation, it was not possible to measure the geometry at the edges of the patella and the femoral groove accurately. For the patella, the contact occurred far enough from the edges that this did not affect the model. However, for the femur in the lateral tracking model, the contact occurred at the lateral edge, resulting in large deformations of the edge cartilage, possibly affecting the calculated contact area and cartilage stresses. Therefore, the geometry was mathematically extended to model the thinning of the cartilage. From the digital photographs it was determined that the cartilage tapered off in approximately 2 millimetres. Four (two medial and two lateral) weighted Bezier curves (Farin, 1996) were added to approximate how the cartilage and bone surfaces might taper off in 2 millimetres. The Bezier curves were continuous with the existing measured data. Weighting factors of 1.0 and 0.7 were used for edges of the bone and cartilage, respectively, to adjust the shape of the curves. The weighting factors were chosen to flatten the curves so that the cartilage thickness was constantly decreasing. Extending the geometry resulted in the desired reduction of cartilage deformation on the lateral edge. A sensitivity analysis to different weighting factors resulted in negligible differences of 2% in reaction force. Even smaller differences were noted in the peak pore pressure and peak principal stress and strain values. This indicated that the results were not sensitive to small changes in the geometry of the medial and lateral sides.

A number of sensitivity analyses to determine the effects of model variables (e.g., geometry, mesh sensitivity, boundary conditions, and loading time) was necessary to justify the inputs to the model. Therefore, the final model inputs were arrived at by an iterative procedure, by analysing each input in turn. In the final lateral tracking model (Figure 4.3) the patella was displaced 0.119 mm in a loading time of 5 seconds. The loading protocol will be developed in detail in Section 4.2.1.5. The cartilage was modelled as a biphasic material with the following material properties; E=0.5 MPa, v=0.15, and $k=5\times10^{-8}$ mm/s. The material properties represented approximately the middle of the range reported in the literature. All sensitivity analyses will be presented for this main lateral tracking model. The lateral tracking model was used, because it was expected to

result in higher stresses and be more sensitive to changes in model input variables.

4.2.1.2 Mesh

Finite element models divide complicated structures into a collection of smaller elements with simpler geometry. Typically, increasing the density of elements leads to a better approximation of the solution. However, a high density of elements increases the complexity of the model, computational time, and computer storage requirements. Therefore, there is a trade-off between accuracy and model efficiency. In the absence of stress concentrations, there is a mesh density for which a further increase in element density yields negligible changes in model results. For this mesh the results are said to converge, and are an adequate approximation of the solution. Therefore, three mesh densities were analysed to determine the lowest mesh density for which the results converged.

Table 4.3: The effects of mesh density on reaction force, peak pore pressure, and peak minimum principal stress in the patellar cartilage.

Model	# of elements through width of the patella *	Total # of elements in the model	Reaction force (N)	Peak pore pressure in the patella (MPa)	Peak minimum principal stress in patella the (MPa)
1	60	1615	1.16	0.55	-0.25
2	120	4769	1.19	0.56	-0.20
3	200	11310	1.20	0.56	-0.20

* The same number of elements were used through the width of the femoral groove not including the elements added to cap off the cartilage.

An increase in mesh density from model 2 to model 3 had a negligible effect on results (i.e., a change of less that 1% in reaction force and peak pore pressure, and peak principal stress and strain) and therefore a mesh density of model 2 was chosen.

The mesh was created so that the nodes were placed through the thickness of the cartilage along the normal to the cartilage surface. This allowed results to be analysed as a function of cartilage thickness. Nodes and elements were defined automatically in the Matlab

program, by the following sequence of steps. First, the cartilage surfaces were resampled at the appropriate intervals using the TPS algorithm, and the 2D surface normals at the resampled points were calculated using differential geometry. Next the points where the surface normals intersected the subchondral bone surfaces were calculated using the TPS algorithm. Finally, ABAQUS commands were used to fill in the nodes and to generate the elements (ABAQUS, 1994c). The distortion of the elements was checked, and it was found that the height to width ratio was between 0.1 and 10, which was recommended for the most reliable performance (ABAQUS, 1994b). In addition, the meshing program ensured that nodes were located at the initial points of contact for both the lateral and central tracking positions. This enabled results to be analysed at the initial points of contact.

4.2.1.3 Boundary Conditions

Two types of boundary conditions were required: kinematic and hydraulic. Although the bone is much stiffer than cartilage, literature suggests that treating it as a rigid boundary may affect model results. Therefore the subchondral bone was explicitly modelled. The bone was modelled as a homogeneous isotropic linear elastic solid. Eight-node isoparametric displacement elements were used (CPE8). Eight-noded elements were chosen because the quadratic shape functions are more robust. A Young's modulus of 15 GPa and Poisson's ratio of 0.3 were used. This corresponded well with values presented in the literature (Table 4.2). The literature suggested that the depth of the bone modelled may have an effect on the model results. Therefore, a sensitivity of the results for bone depths of 40%, 60%, and 80% 100% of the width of the patella were analysed. The depths of bone analysed had negligible effect on the reaction force, peak pore pressure, and peak principal stress and strain. Although bone depth did not affect the loading response of cartilage, the stress distribution in the bone was affected. At a bone depth of 60% of the patellar width, qualitative analysis showed that the distribution of the stresses in the bone close to the cartilage were unaffected by the boundary conditions. Therefore, a bone depth of 60% of the patellar width was chosen. In retrospect, since the bone stresses were not analysed a smaller bone depth would have been sufficient.

Along the base of the femur, all nodes were modelled as roller supports, constraining the displacement in the global Y direction (Figure 4.3). One node in the middle of the base was also restrained in the global X direction to prevent uncontrolled displacement in the X direction. The top of the patella was modelled as a rigid plate (i.e., no relative displacement was allowed between the nodes at the top of the patella). To model the top as a roller support would have been complicated because in the lateral orientation the patella was not aligned with the global XYZ coordinate system. A sensitivity analysis showed the rigid plate versus roller support on the top of the patella in central tracking resulted in a negligible difference of less than 1% in reaction force, peak pore pressure, and peak principal stresses and strain. Multi-point constraints were used to constrain the degrees of freedom at the midside nodes where the mesh was refined across the bone to cartilage interface (ABAQUS, 1994c).

The boundary between the cartilage and subchondral bone was modelled as sealed and impermeable. In addition, the surface of the patellar and femoral cartilage was also modelled as impermeable. Modelling the surface cartilage as impermeable was a reasonable assumption for a number of reasons. Firstly, it was hypothesized that for the regions in contact, flow out of the cartilage is prevented by a thin pressurized fluid layer. Secondly, it was hypothesized that the loading time, in this study, was too small for fluid flow to have a large effect on the results. Analysis showed that as the loading time was decreased, the hydraulic surface boundary conditions had less effect on the results. Thirdly, results were only analysed at peak loading, fluid flow effects associated with stress relaxation or creep were not analysed in this study. Finally, large cartilage strains close the surface were expected to further decrease the permeability of the cartilage, due to increased drag forces.

4.2.1.4 Contact Modelling

A surface based contact formulation was used to model the surface interaction between the patellar and femoral cartilage. This was the most general contact formulation available in ABAQUS (ABAQUS, 1994c). The direction of contact, and which nodes come into

contact were not predefined. Therefore, the meshes on the contacting bodies did not need to match. The nodes on the femoral and patellar cartilage surfaces were defined as the master and slave surfaces, respectively. The slave surface could not penetrate the master surface. However, the master surface could penetrate the slave surface and the contact direction was always normal to the master surface. In retrospect, the femoral surface should have been chosen as the slave surface, because the femoral mesh density was larger. However, the choice of master/slave surface definitions had a negligible effect on the final results. Small sliding frictionless contact formulation was used. This was an acceptable assumption as the coefficient of friction between the cartilage surfaces is extremely low (~0.0025) (Shrive and Frank, 1994).

4.2.1.5 Loading

The experimentally measured kinematics of the PF joint at 70° was used to drive the lateral tracking finite element model. Recall that the undeformed geometry of the PF surfaces and joint kinematics were combined to develop a 3D geometric model (Section 3.2.1 and Section 3.2.2). The finite element geometry was derived from the 3D geometric model by taking a slice through the centroid of the contact area at 70° flexion. The slice was defined by the surface normal at the centroid of the patellar surface and a lateral vector. The overlap between the undeformed cartilage surfaces (0.119 mm) was calculated as the distance along the surface normal projected from the centroid of the contact area on the patellar cartilage surface to its intersection with the femoral cartilage surface. The initial unloaded position of the model was obtained by translating the patellar along the surface normal at the centroid until the patella was in initial contact with the femur. Subsequently, to load the model, the patella was translated by the amount of overlap of the undeformed surfaces (0.119 mm) into the femur along the surface normal to the centroid. Note that during the experiment the joint was loaded in-situ with the patella sliding along the femur as extension occurred. Although the final positions were the same, the model was an approximation of the complicated experimental loading regime.

In the experiment, 70° of flexion was achieved in approximately 0.125 seconds. It was

difficult to model such a fast loading rate. For transient soils analysis in ABAQUS a backward difference operator was used to step through the time history of the simulation. This integration procedure required a minimum recommended time step. If time increments smaller that this critical value were used, instabilities and oscillations may have appeared in the solution. The minimum recommended time step was dependent on the material properties and the size of the mesh near the applied load as follows,

$$\Delta t \geq \frac{\gamma_w}{6kE}(\Delta h)^2 \tag{34}$$

where γ_w was the specific weight of the fluid, k was the permeability, and Δh was the smallest dimension of a poroelastic element in the loaded region of the model (ABAQUS, 1994c). If the problem required analysis with smaller time increments, a finer mesh was required. For the present model, the minimum recommended time step was 0.05 seconds. Numerous loading times were analysed (Table 4.4) for the lateral tracking model.

Table 4.4: The effects of loading time on reaction force, peak pore pressure, and peak minimum principal stress in the patellar cartilage.

Loading time (s)	0.125	1	5	10	50	500
Minimum time step used	$\Delta t<0.05$	$\Delta t<0.05$	$\Delta t>0.05$	$\Delta t>0.05$	$\Delta t>0.05$	$\Delta t>0.05$
Reaction Force (N)	1.22	1.21	1.19	1.16	0.99	0.47
Peak Pore pressures in the patella (MPa)	0.61	0.59	0.56	0.53	0.40	0.14
Peak minimum principal stress in the patella (MPa)	-0.22	-0.21	-0.20	-0.19	-0.16	-0.12

For loading times less than 5 seconds convergence was only achieved using time steps shorter than the minimum recommended time step. The mesh density required to decrease the recommended time step to that required for model convergence was not appropriate due to the increase in computation time and computer storage requirements. It was unclear how ignoring the minimum recommended time step affected the reliability of the results.

In addition, as the loading time decreased, the loading time had a smaller effect on the results. Decreasing the loading time from 5 to 0.125 seconds, which meant that the pore fluid was more confined and had less time to flow, increased the reaction force by 3%, and increased the peak pore pressures and peak minimum principal stress in the patellar cartilage by less than 10%. As the effect of the loading time between 5 and 0.125 seconds on results was relatively small, a loading time of 5 seconds was chosen as a reasonable approximate of the experimental loading.

4.2.1.6 Element and Material Properties

Cartilage is predominantly modelled as either an elastic or biphasic material. The appropriate choice for cartilage element properties depends on the loading conditions and the desired output variables. Studies suggested that linear elastic behaviour could be assumed for analysing the instantaneous response of cartilage provided the strain rate was larger that 0.5 s^{-1}. Given that the average strain rate, in the present study, was estimated at 1.36 s^{-1}, a single-phase elastic model was appropriate. An advantage of the single-phase elastic model was that it was less complex. However, the biphasic theory allows the calculation of the solid stress and pore fluid pressure. Understanding load sharing between the solid and fluid phase provides valuable information on the interaction between the solid and fluid phases. It was not clear how the cartilage element properties would affect the differences in joint mechanics between lateral and central tracking. Therefore, a sensitivity analysis was performed to determine how linear biphasic and elastic assumptions affected the model results. Note that strain dependent behaviour introduced with the finite deformation theory was not incorporated for two reasons. Firstly, the combined deformation of the patellar and femoral cartilage was 0.119 mm. The thickness of the patellar and femoral cartilage at the initial points of contact was 0.48 mm and 0.19 mm respectively, resulting in an average strain of 18%. The literature suggested that models with strain up to 25-30% may be reasonably approximated by the linear biphasic theory. Secondly, reliable strain dependent material properties have not been established in the literature. Introducing more complicated material properties would increase the uncertainty of the results.

The reported range of biphasic and elastic material properties used to model cartilage was very large. There is, to date, little consensus on the values of the material properties used to model cartilage. It was expected that the material properties chosen would have an effect on the results. In light of the uncertainty introduced by the material properties, the differences in loading response of cartilage between the lateral and central tracking model were analysed for 9 different material property cases; 6 linear biphasic cases and 3 elastic cases.

For all of the biphasic models, the cartilage was modelled as a linear biphasic material using soils consolidation transient analysis. Eight-node poroelastic elements (CPE8P) were used. The solid phase was modelled as isotropic and linearly elastic. Young's modulus and Poisson's ratio were used to characterize the solid phase. The initial fluid to solid ratio was 4 to 1 and was uniform throughout the entire layer. The fluid phase was modelled with a density of 9.81 kN/m^3, equal to that of water, and an isotropic permeability that was held constant. In all cases automatic time incrementation was used, where the maximum pore pressure change permitted in any increment was 0.05 MPa. A baseline Case A was chosen as the representative biphasic case study. For the baseline Case A, the Young's modulus was 0.5 MPA, the Poisson's ratio was 0.15, and the permeability was 5×10^{-8} mm/s (Table 4.5). These material properties values represented approximately the middle of the range presented in the literature. The permeability of the cartilage was decreased (Case Klo) and increased (Case Khi), respectively, representing the range reported in the literature. The value for Young's modulus was increased four-fold representing the higher end of the reported range (Case Ehi). The value for Poisson's ratio was increased (Case Vhi) and decreased (Case Vlo), respectively.

For the elastic case studies, the cartilage was modelled as a linear isotropic elastic material using eight-node elastic elements (CPE8). Young's modulus and Poisson's ratio were used to characterize the behaviour of the cartilage. These material properties accounted for the behaviour of the solid as well as pore fluid. For the three elastic cases (Cases EL1, EL2, and EL3) the value for the Young's modulus was progressively increased. The focus of this component of the study was to determine the difference between lateral and central

Table 4.5: The material properties and loading for the nine case studies for the displacement driven lateral tracking model.

Model type	Case Study	Young's modulus (MPa)	Poisson's ratio	Permeability (mm/s)	Displacement (mm)
biphasic	A	0.5	0.15	5×10^{-8}	0.119
	Klo	0.5	0.15	1×10^{-10}	0.119
	Khi	0.5	0.15	5×10^{-7}	0.119
	Ehi	2.0	0.15	5×10^{-8}	0.119
	Vhi	0.5	0.25	5×10^{-8}	0.119
	Vlo	0.5	0.05	5×10^{-8}	0.119
elastic	EL1	2	0.45	n/a	0.119
	EL2	10	0.45	n/a	0.119
	EL3	20	0.45	n/a	0.119

tracking, and how material properties and element assumptions affected those differences.

In each of the 9 case studies the bone was modelled as a homogeneous isotropic linear elastic solid. Eight-node isoparametric displacement elements were used (CPE8) with a Young's modulus of 15 GPa and a Poisson's ratio of 0.3.

4.2.2 Central Tracking Model

The geometry, mesh, boundary conditions, and contact modelling used for the central tracking model were identical to those described for the lateral tracking models in the previous sections (Figure 4.4). The only differences between the central tracking and lateral tracking model were:

- the central versus lateral orientation of the patella,
- the force versus displacement driven loading, and
- the added boundary conditions on the top of the patella.

The patella was reoriented centrally so the points of maximum 2D curvature were the initial points of contact, and the in-plane surface normals at these points were aligned vertically.

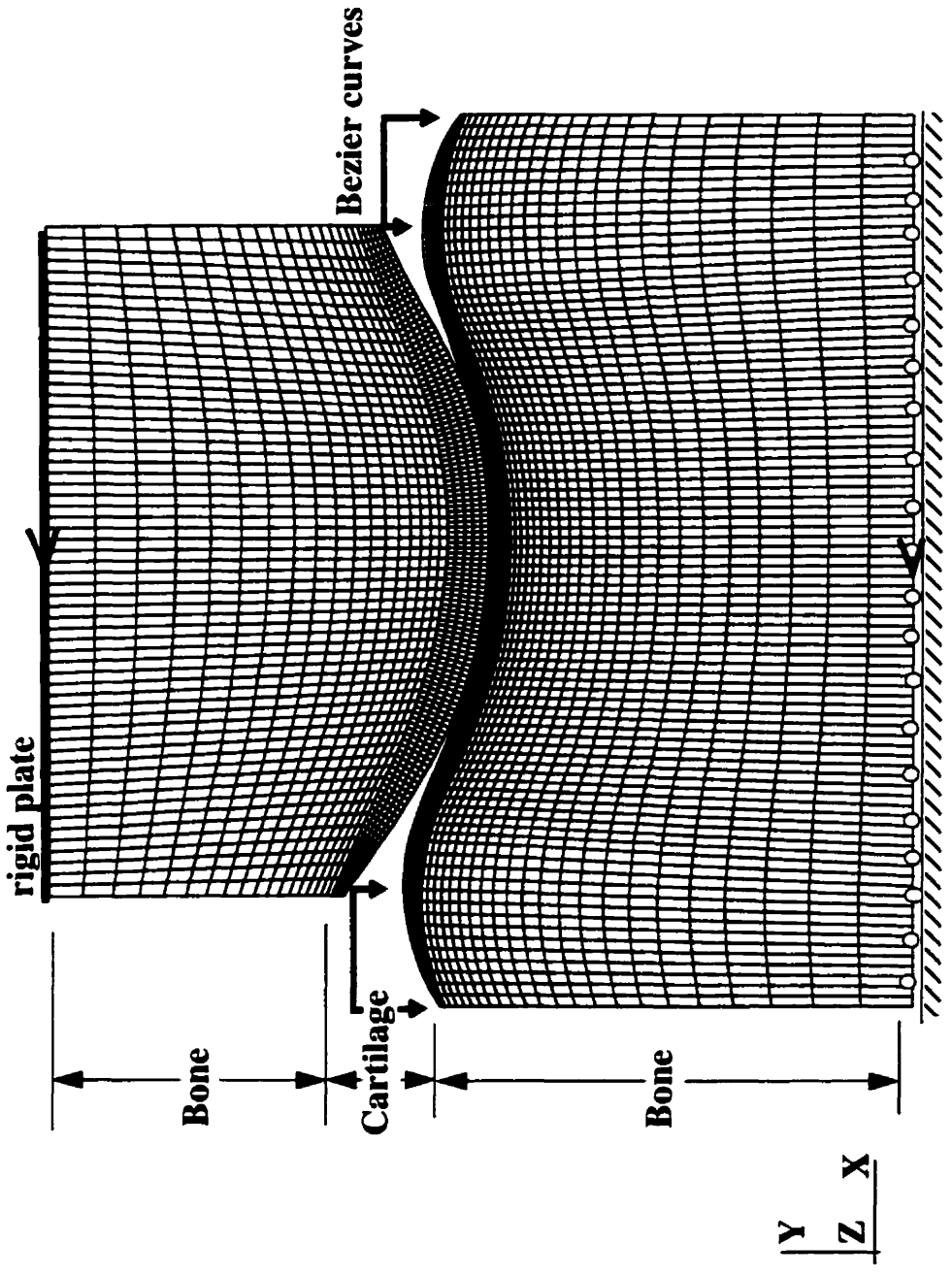

Figure 4.4:A schematic diagram of the central tracking finite element model.

To compare the resulting stress distributions, the same loading conditions were used for both the lateral and central tracking models. Therefore, any differences between the stress distributions were strictly a function of the geometry of the articular cartilage layers in the regions of contact. Therefore, the total magnitude of the reaction force needed to cause the applied displacement in the lateral tracking model was used to drive the central tracking model. The force was applied normal to the initial point of contact, in this case along the vertical axis. This was equivalent to assuming that the magnitude of the muscular force causing the displacement of the patella is the same in both tracking conditions. Therefore, the direction of force application caused the different patellar tracking patterns. An extra boundary condition was added to restrain the patella from translating horizontally by constraining the horizontal displacement of nodes at the top edge of the patellar bone.

The same nine element and material property case studies were analysed for central tracking (Table 4.6).

Table 4.6: The material properties and loading for the nine case studies for the force driven central tracking model.

Model type	Case Study	Young's modulus (MPa)	Poisson's ratio	Permeability (mm/s)	Displacement (mm)
biphasic	A	0.5	0.15	5×10^{-8}	1.189
	Klo	0.5	0.15	1×10^{-10}	1.218
	Khi	0.5	0.15	5×10^{-7}	0.9834
	Ehi	2.0	0.15	5×10^{-8}	4.425
	Vhi	0.5	0.25	5×10^{-8}	1.097
	Vlo	0.5	0.05	5×10^{-8}	1.298
elastic	EL1	2	0.45	n/a	1.463
	EL2	10	0.45	n/a	7.212
	EL3	20	0.45	n/a	14.18

4.2.3 Model Analysis

The following variables were analysed at peak loading (i.e., 5 seconds) to characterize the effect of lateral versus central tracking:

- contact area/unit width,
- contact pressure,
- pore pressure (biphasic case studies only),
- minimum and maximum principal stress,
- Tresca stress,
- minimum and maximum principal strain.

Contact area/unit width, contact pressure and reaction force were especially useful to compare with experimental measuring techniques, geometric models, as well as 2D and 3D models based on force and moment equilibrium. Therefore, these variables were useful in evaluating the model. For the biphasic models the pore pressures were analysed, to indicate the load sharing between the solid and fluid phases. Pore fluid velocities were analysed qualitatively to better understand the interaction between the fluid and solid matrix. The distribution of principal and Tresca stresses in the patellar and femoral cartilage were analysed, because they were independent of the orientation of the coordinate system and provided an indication of the general state of stress at a point. For a general loading case, stress at a point may be represented by six components of stress. However, these components of stress are dependent on the coordinate system chosen. The general state of stress may be represented by Mohr's circle, where the principal stresses are the stress in the directions where shear stress is zero, and Tresca stress is defined as twice the maximum shear stress. The directions of the principal stresses indicated how the stress was transmitted and distributed in the cartilage. Note that for the biphasic case studies, the stresses in the solid phase were presented. In contrast, for the elastic case studies, the stress represented the total stress in the solid and fluid phases. Principal strains were analysed to indicate the local deformations in the cartilage layers.

The contour plots illustrating the distribution of the stresses and strains for lateral and central tracking were qualitatively compared for all 9 material property cases. Contour plots for Case A and Case EL1, represented typical distributions of the biphasic and elastic

case studies, respectively, and will be presented. In addition, the peak values of the output variables for all cases were analysed. The percentage change in the peak values caused by lateral tracking was used to quantify the differences between lateral and central tracking for the 9 case studies.

4.3 RESULTS

The results are presented with emphasis on comparing the effects of lateral tracking versus central tracking on each of the output variables. Where applicable, the distribution of the variables within the patellar and femoral cartilage will be presented for Case A and Case EL1. Case A and Case EL1 represented typical distributions in the biphasic and elastic models, respectively. The absolute value of the variables varied considerably between case studies. To compare the influence of the material and element assumptions, the peak values of the output variables for central and lateral tracking are presented. Peak values within the patellar and femoral cartilage are reported. The percentage change in the central values caused by lateral tracking are presented in Table 4.7.

4.3.1 Contact Area

For all the case studies analysed, the contact area per unit width for the lateral tracking model was smaller than for the central tracking model (Figure 4.5). For Case A, lateral tracking reduced the contact area by 38%. All biphasic models yielded similar results.

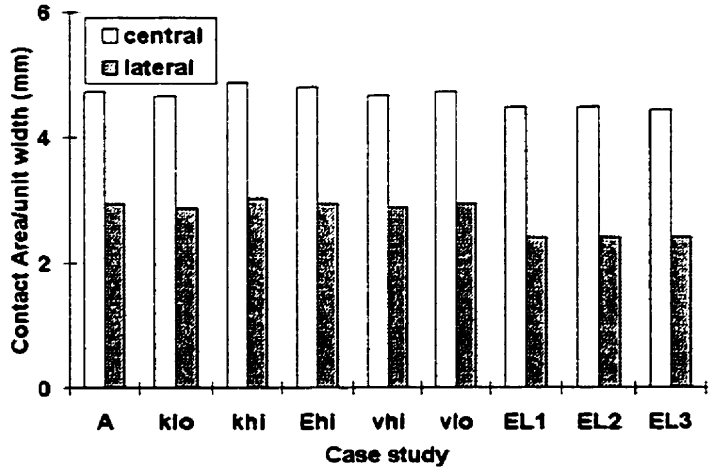

Figure 4.5: Biphasic and elastic models: Contact area per unit width for central and lateral tracking.

For all the elastic models contact area decreased by 46% with lateral tracking. The contact area/unit width for the elastic models was lower than for the biphasic models.

4.3.2 Contact Pressure

The lateral tracking model resulted in larger contact pressures distributed over a smaller contact area for all cases studied (Figure 4.6).

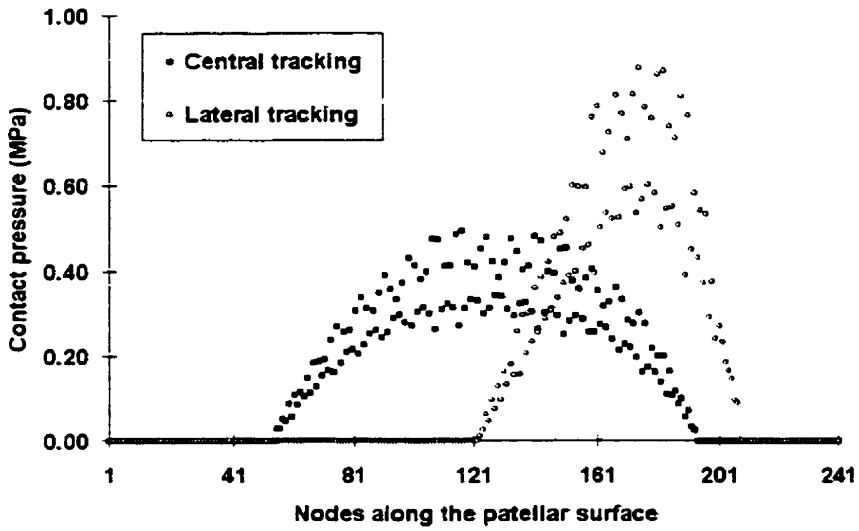

Figure 4.6: Biphasic model (Case A): Contact pressures versus the distance along the patellar surface for central and lateral tracking.

The peak contact pressure was consistently larger for lateral tracking than for central tracking. For all biphasic models lateral tracking increased the peak contact pressure by 70-80% (Figure 4.7). The Young's modulus had the largest effect on contact pressure. Increasing the Young's modulus (Case Ehi) of the solid phase four-fold, increased the peak contact pressure by more than 3.5 times. Increasing the permeability of the cartilage (Case Khi) decreased the peak contact pressure, while decreasing the Poisson's ratio of the solid phase (Case Vlo) increased the contact pressures.

For the elastic cases, increasing Young's modulus caused an increase in peak contact pressure (Figure 4.8). However, regardless of the Young's modulus, the percentage increase in peak contact pressure for lateral tracking was consistently around 120%. The peak contact pressures were generally larger for the elastic cases than the biphasic cases.

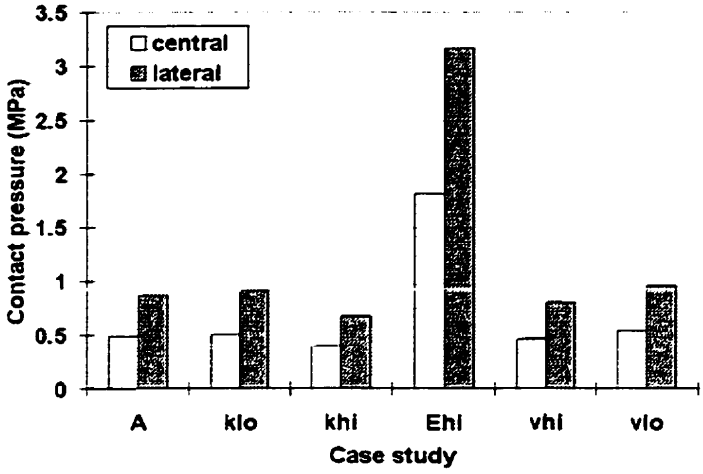

Figure 4.7: Biphasic models: Peak contact pressure for central and lateral tracking.

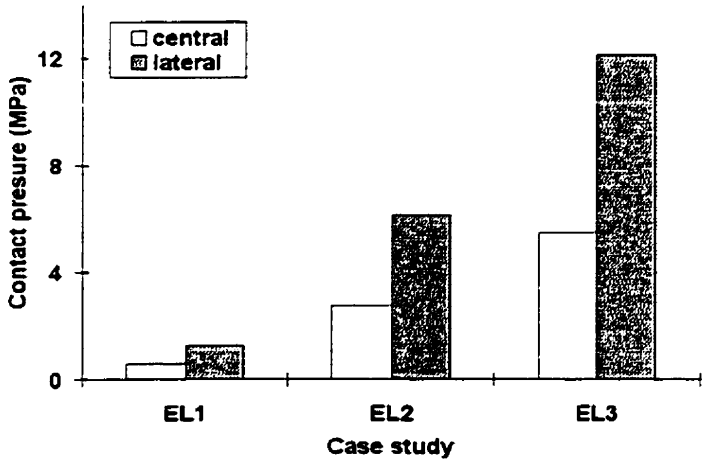

Figure 4.8: Elastic models: Peak contact pressure for central and lateral tracking.

4.3.3 Pore Pressure (Biphasic models)

Pore pressure was highest in the region of initial contact for both central and lateral tracking models (Figure 4.9). The vertical isobars illustrated that the pressure was uniform through the thickness of the cartilage layer, while a steep gradient appeared toward the periphery of the joint. Lateral tracking resulted in larger pore pressures, and a steeper gradients toward the periphery of the joint. Lateral tracking increased peak pore pressure in the patellar and femoral cartilage by 55 to 75% and 70%, respectively (Figure 4.10).

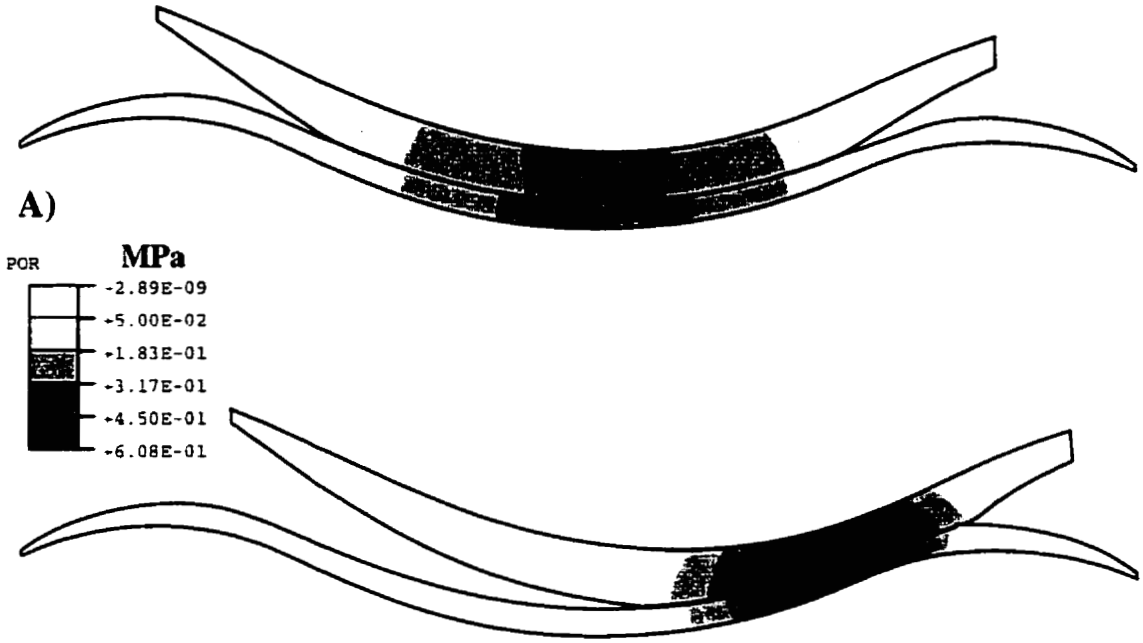

Figure 4.9: Biphasic model (Case A): Distribution of pore pressure in the patellar and femoral cartilage for A) central and B) lateral tracking.

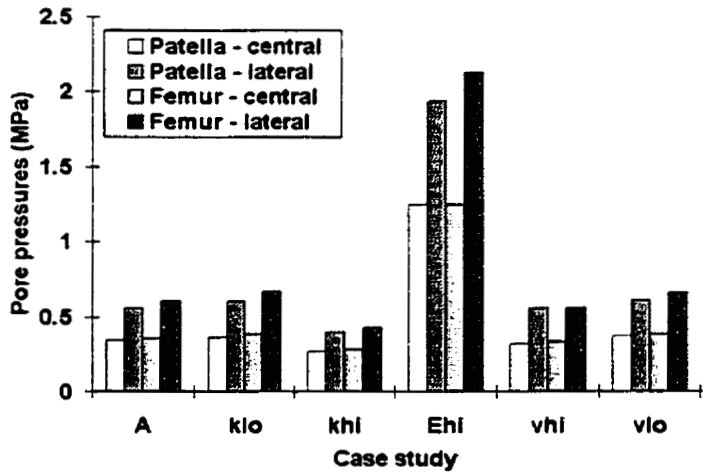

Figure 4.10: Biphasic models: Peak pore pressures in the patellar and femoral cartilage for lateral and central tracking.

4.3.3.1 Pore Fluid Velocity (Biphasic models)

To understand the interaction between the fluid and the solid matrix the horizontal and vertical pore fluid velocities were qualitatively analysed. Fluid velocity was small due to the relatively small loading time and that the surface was impermeable and the pore fluid was confined. In both the lateral and central tracking models, under compression, the fluid flowed laterally out of the contact region (Figure 4.11 and Figure 4.12). Fluid flow in the vertical direction was much smaller. The fluid was expected to flow up towards the cartilage surface where bulging would occur. This trend was not seen in the present model for two reasons; the cartilage surface was modelled as sealed and impermeable and the matrix was modelled with isotropic permeability. In reality the permeability decreases with depth, promoting fluid flow towards the surface. Lateral tracking resulted in fluid velocities two to three times greater than during central tracking.

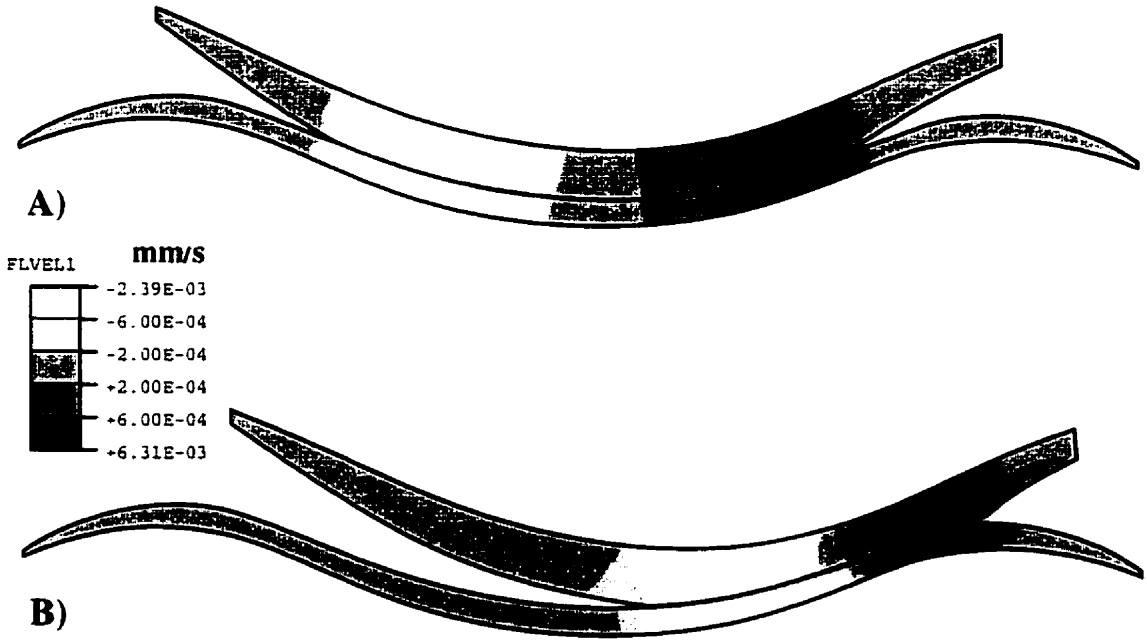

Figure 4.11: Biphasic model (Case A): Horizontal fluid velocity in the patellar and femoral cartilage for A) central and B) lateral tracking.

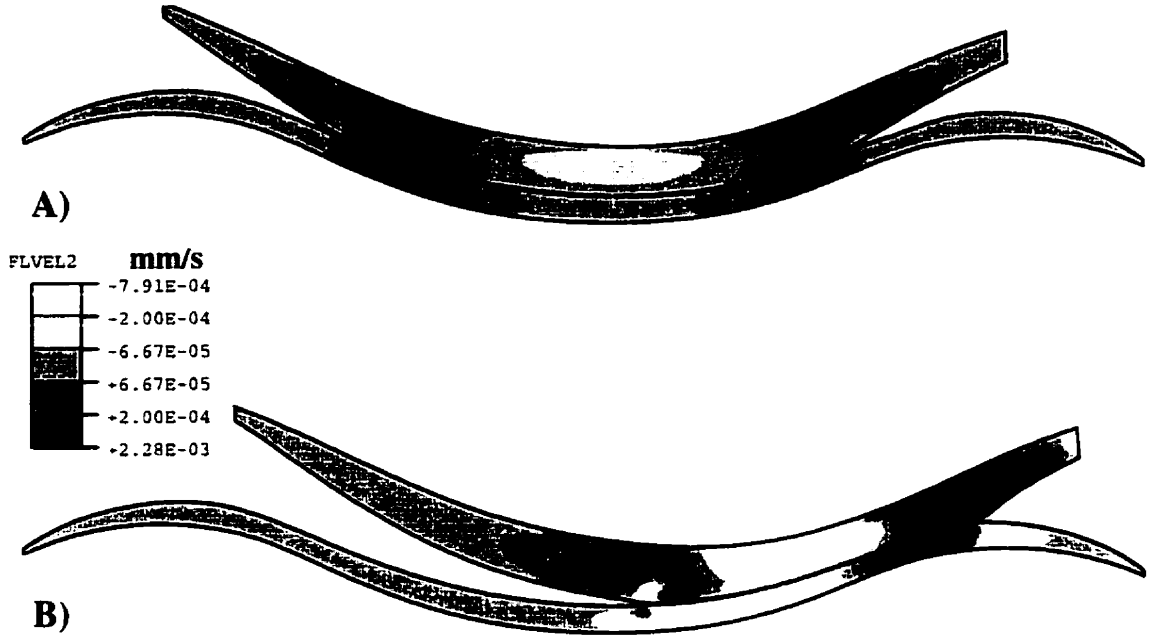

Figure 4.12: Biphasic model (Case A): Vertical fluid velocity in the patellar and femoral cartilage for A) central and B) lateral tracking.

4.3.4 Minimum Principal Stress

Lateral tracking resulted in a different distribution of minimum principal stress throughout the patellar and femoral cartilage for all case studies. All biphasic case studies resulted in similar distributions of principal stress in the solid phase of the cartilage (Figure 4.13). A large negative minimum principal stress indicated a large compressive principal stress. For the central tracking model, the compressive principal stress was highest in the patellar cartilage on the medial and lateral sides adjacent to the subchondral bone. Although a similar trend was present in the lateral tracking model, there was an additional region of high compressive principal stress on the patellar surface where initial contact was made. Lateral tracking increased compressive principal stress. Comparing the pore pressures to the stress in the solid phase, the load sharing in the fluid to solid phase was approximately 2.5 to 1. All elastic case studies resulted in similar distributions of total principal stress in the cartilage (Figure 4.14). Similar to the biphasic case studies, lateral tracking increased compressive principal stress.

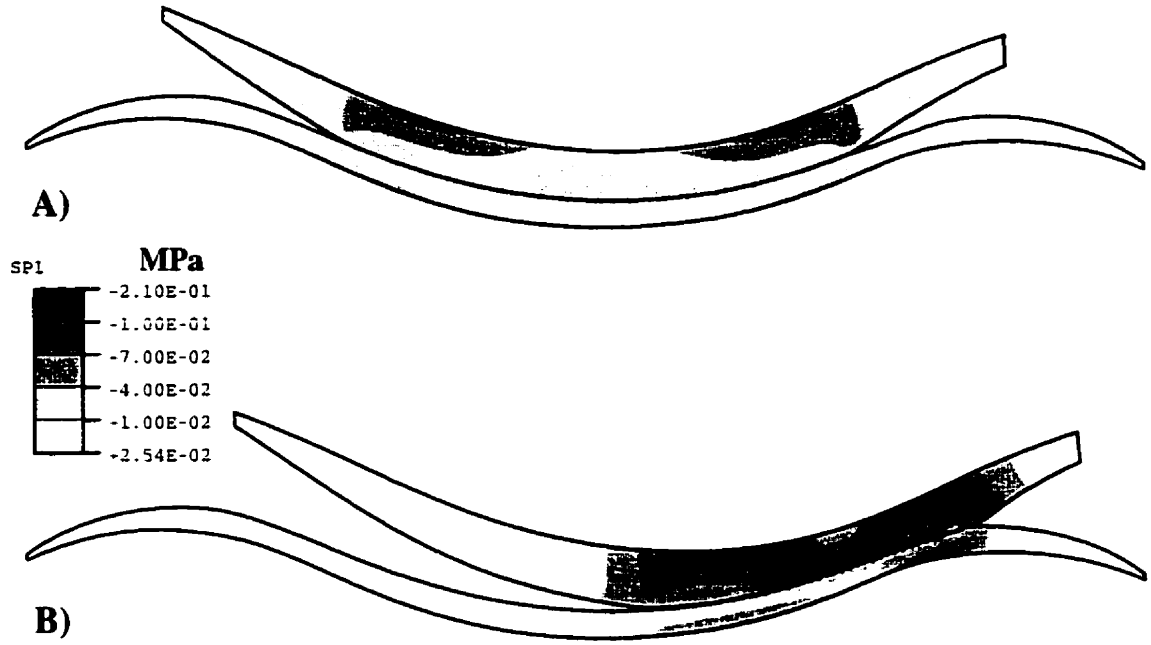

Figure 4.13: Biphasic model (Case A): Minimum principal stress distribution in the solid phase of the patellar and femoral cartilage for A) central and B) lateral tracking. Dark regions indicate high compressive stress.

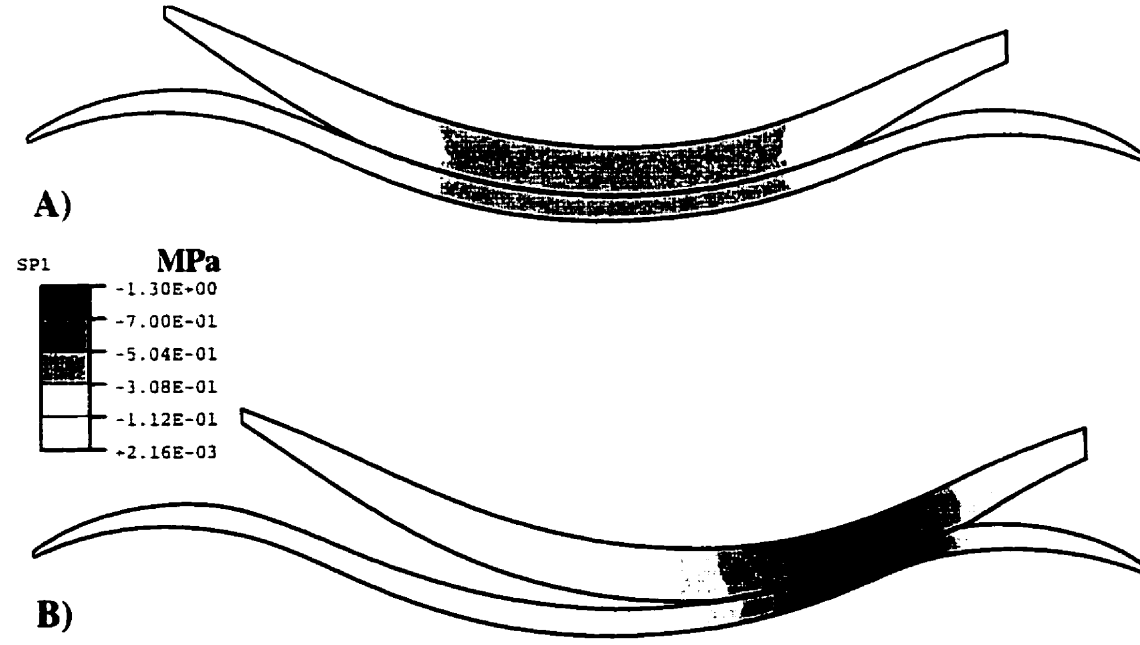

Figure 4.14: Elastic model (Case EL1): Minimum principal stress distribution in the patellar and femoral cartilage for A) central and B) lateral tracking. Dark regions indicate high compressive stress.

However, total compressive principal stress was distributed similarly to the pore fluid pressures in the biphasic models, indicating that the majority of load was taken by the fluid phase. In the elastic models, the compressive stress was highest in the contact region and the stress was uniformly transmitted through the thickness of the cartilage to the subchondral bone.

The directions of principal stress are useful in understanding the distribution of stress (Figure 4.15 and Figure 4.16).

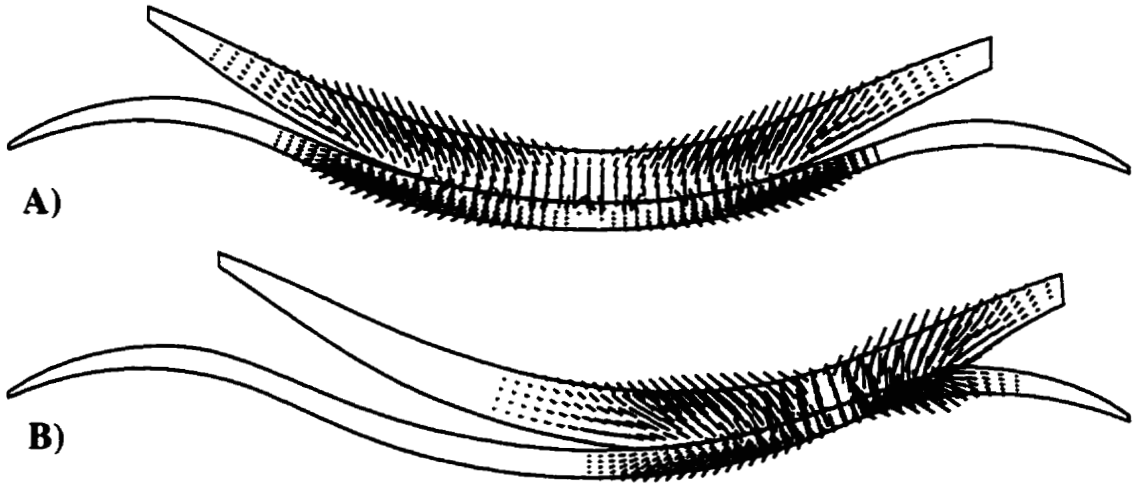

Figure 4.15: Biphasic model (Case A): Directions of minimum principal stress distribution in the patellar and femoral cartilage for A) central and B) lateral tracking.

In all case studies, at the cartilage surface and through the thickness of the cartilage under the region of initial contact, compressive principal stresses were oriented perpendicular to the cartilage surface. Peripheral to the region of initial contact compressive principal stresses were angled laterally and adjacent to the subchondral bone the compressive principal stresses were approximately 45 degrees to the bone interface.

For all the case studies, lateral tracking increased the magnitude of the peak compressive principal stress (Figure 4.17 and Figure 4.18).

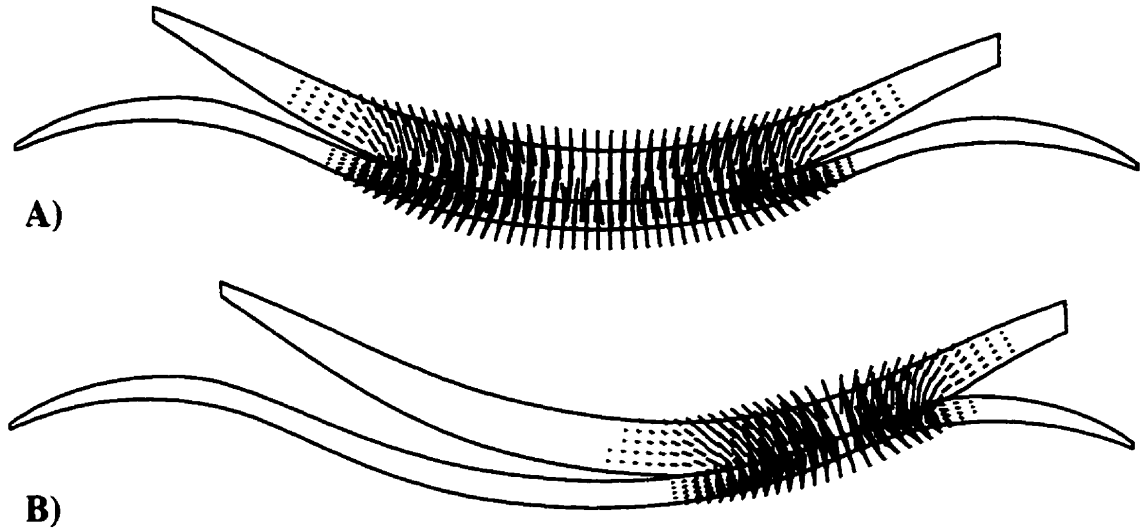

Figure 4.16: Elastic model (Case EL1): Directions of minimum principal stress distribution in the patellar and femoral cartilage for A) central and B) lateral tracking.

For the biphasic analysis the magnitude of the peak compressive principal stress increased due to lateral tracking by 100 to 120% and 175 to 195%, respectively, in the patellar and femoral cartilage. For the elastic models, lateral tracking increased the maximum patellar and femoral compressive principal stress by 125% and 133%, respectively. Young's modulus (Case Ehi) had the largest effect on the values of compressive principal stress.

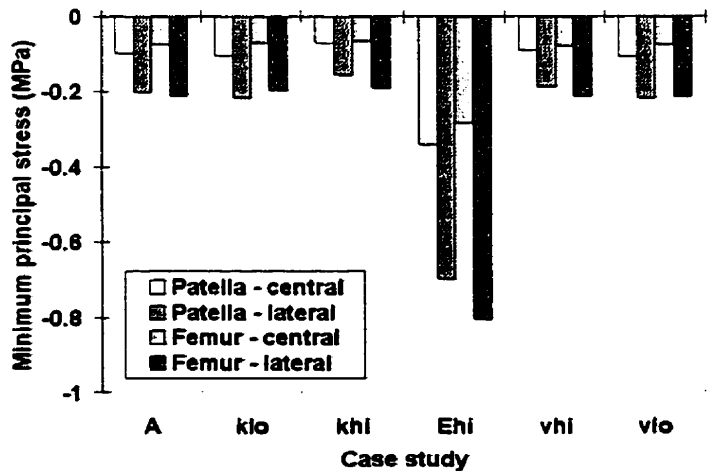

Figure 4.17: Biphasic models: Peak minimum principal stresses in the solid phase of the patellar and femoral cartilage during central and lateral tracking.

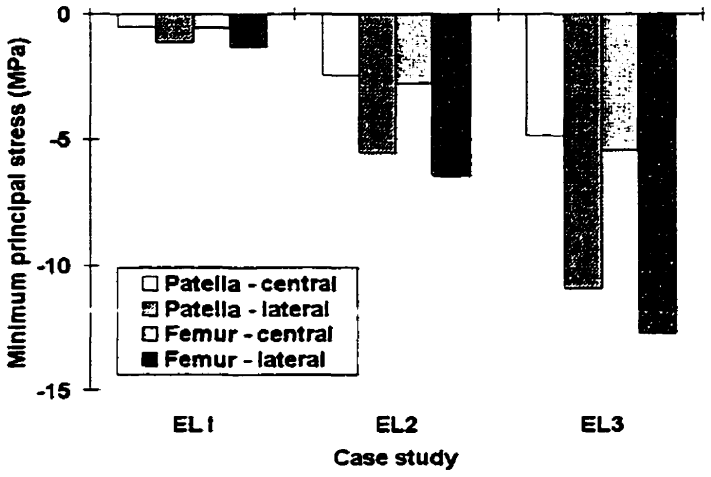

Figure 4.18: Elastic models: Peak minimum principal stresses in the patellar and femoral cartilage during central and lateral tracking.

4.3.5 Maximum Principal Stress

All biphasic cases resulted in similar distributions of maximum principal stress in the solid phase of the cartilage (Figure 4.19). A large positive maximum principal stress indicated large principal tensile stress. For the central tracking model, the maximum principal stress was highest in the patellar cartilage on the medial and lateral sides adjacent to the subchondral bone. A similar trend was present in the lateral tracking model, with the addition of a region of high maximum tensile principal stress on the patellar surface where initial contact was made. The maximum principal stresses were higher in the lateral tracking model. All elastic case studies resulted in similar distributions of total principal stress in the cartilage (Figure 4.20). The main difference between the elastic and biphasic models was that in the contact region of the elastic models the maximum principal stress was compressive (i.e. negative value). In addition, the total maximum principal stress was distributed similarly to the pore fluid pressures in the biphasic models, indicating that the majority of load is taken by the fluid phase. In the elastic models, the maximum principal stress was highest in the contact region and the stress was uniformly transmitted through the thickness of the cartilage to the subchondral bone. Similar to the biphasic case studies, lateral tracking increased the magnitude of the maximum principal stress.

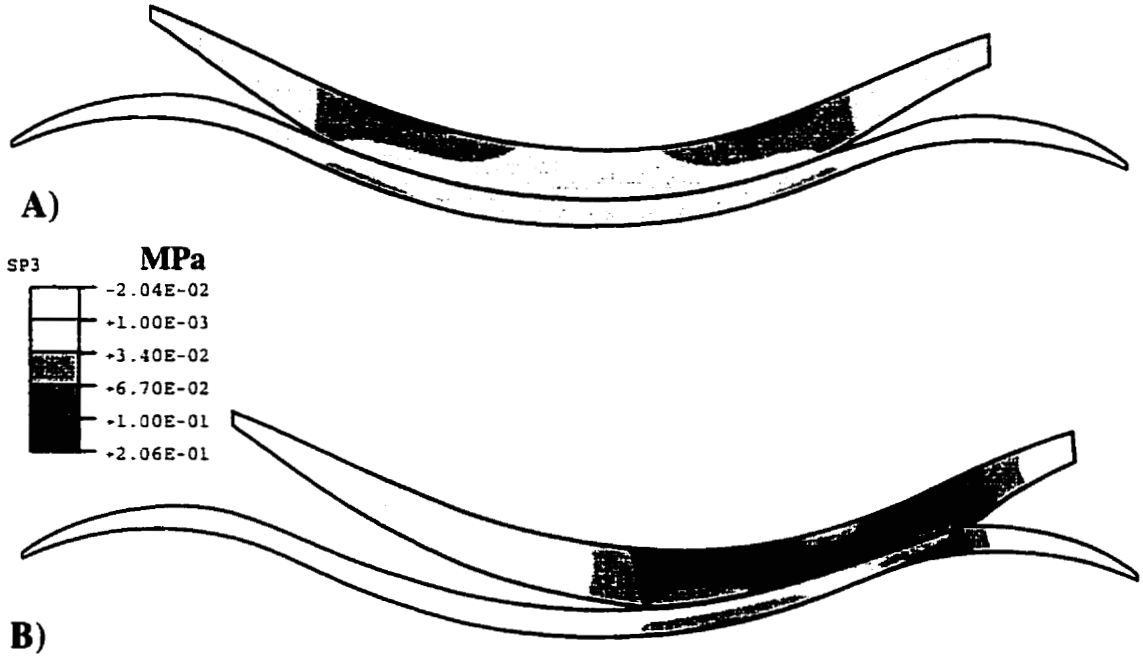

Figure 4.19: Biphasic model (Case A): Maximum principal stress distribution in the solid phase of the patellar and femoral cartilage for A) central and B) lateral tracking. Dark regions indicates high tensile stress.

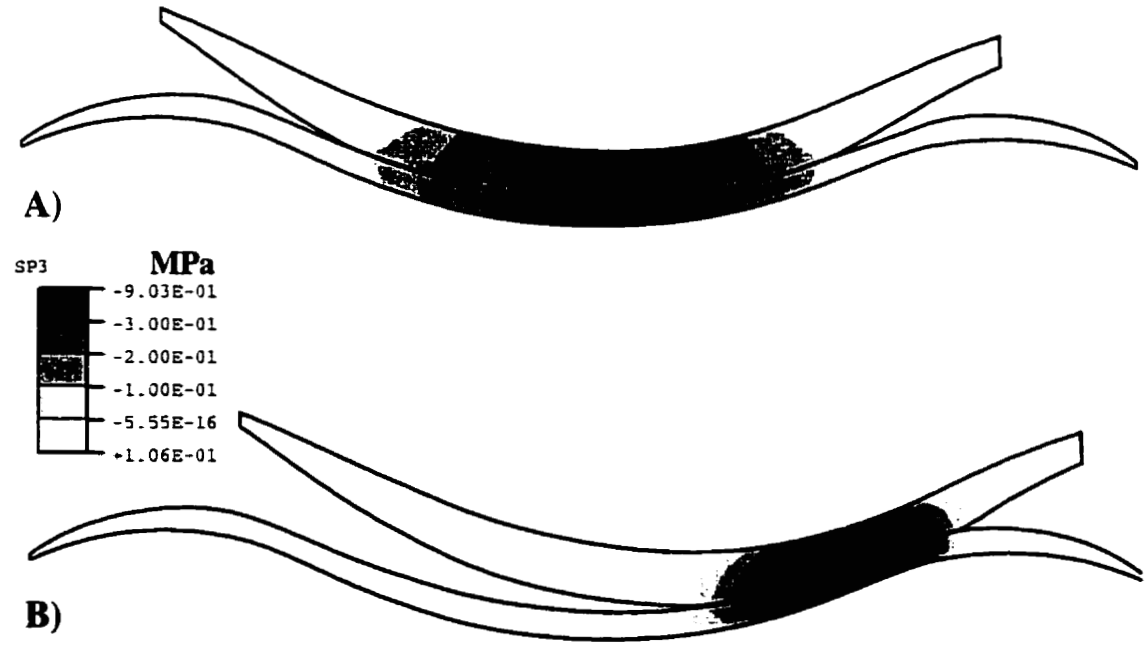

Figure 4.20: Elastic model (Case EL1): Maximum principal stress distribution in the patellar and femoral cartilage for A) central and B) lateral tracking. Dark regions indicate high tensile stress.

By definition, the maximum principal stresses are directed perpendicular to the minimum principal stresses. Therefore, in all case studies, at the cartilage surface and through the thickness of the cartilage under the region of initial contact, maximum principal stresses were oriented parallel to the cartilage surface (Figure 4.21 and Figure 4.22).

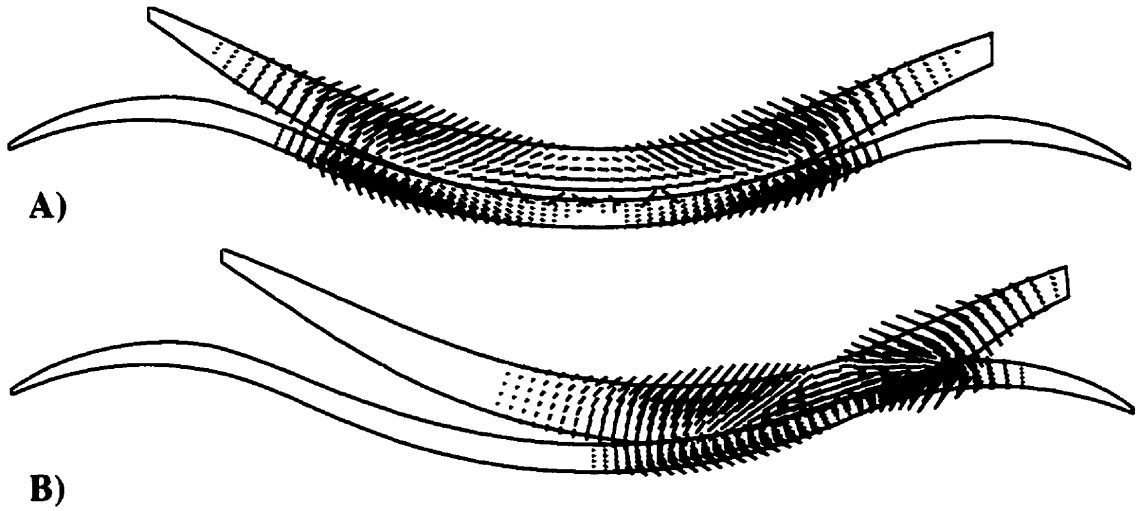

Figure 4.21: Biphasic model (Case A): Directions of maximum principal stress distribution in the patellar and femoral cartilage for A) central and B) lateral tracking.

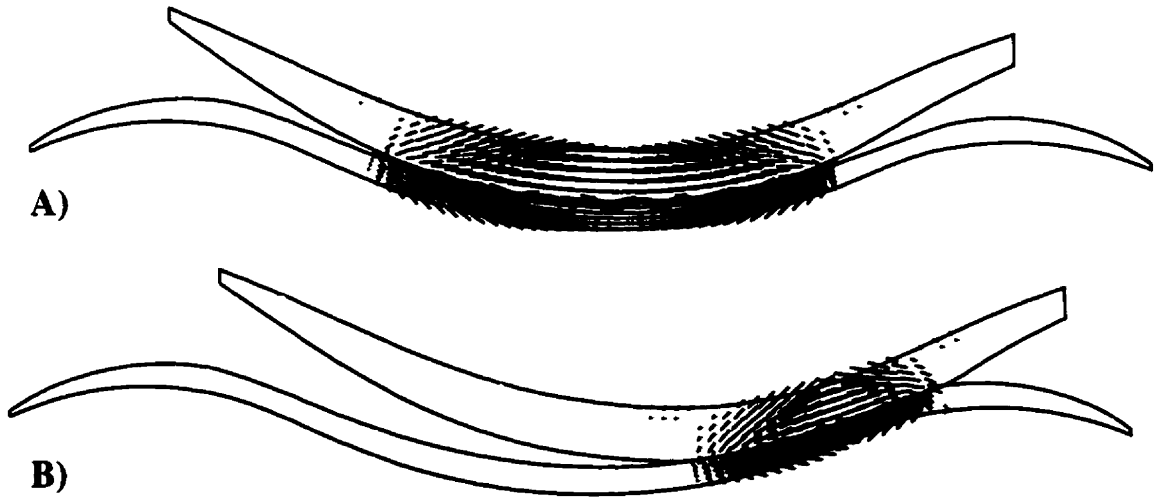

Figure 4.22: Elastic model (Case EL1): Directions of maximum principal stress distribution in the patellar and femoral cartilage for A) central and B) lateral tracking.

Peripheral to the region of initial contact compressive principal stresses were directed laterally and adjacent to the subchondral bone the maximum principal stresses were

approximately 45 degrees to the bone interface. Lateral tracking consistently increased peak values of tensile principal stress (Figure 4.23 and Figure 4.24). In the biphasic models, lateral tracking increased patellar and femoral peak maximum principal stress by 100-120%, and 175-230%, respectively. In the elastic models the increases in patellar and femoral maximum principal stress were consistently 94% and 325-335%, respectively. Young's modulus (Case Ehi) had the largest effect on peak tensile principal stress.

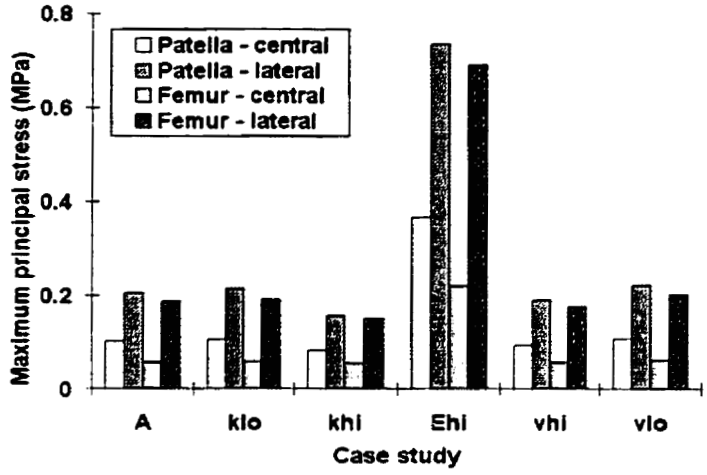

Figure 4.23: Biphasic models: Peak maximum principal stresses in the solid phase of the patellar and femoral cartilage for central and lateral tracking.

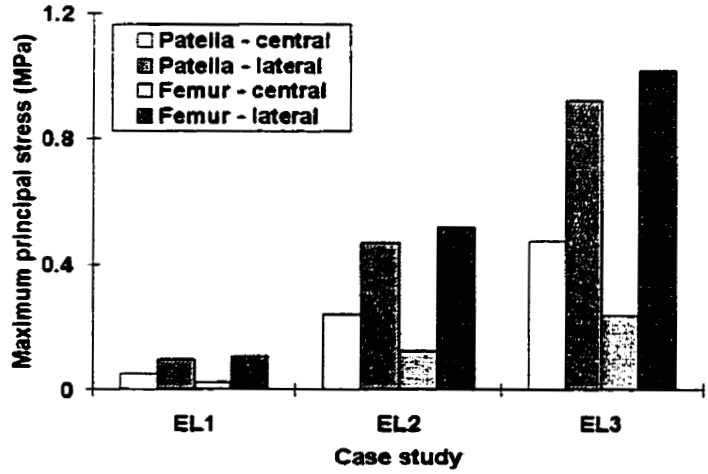

Figure 4.24: Elastic models: Peak maximum principal stresses in the patellar and femoral cartilage for central and lateral tracking.

4.3.6 Tresca Stress

The distribution of Tresca stress was similar for all biphasic and elastic cases. (Figure 4.25 and Figure 4.26).

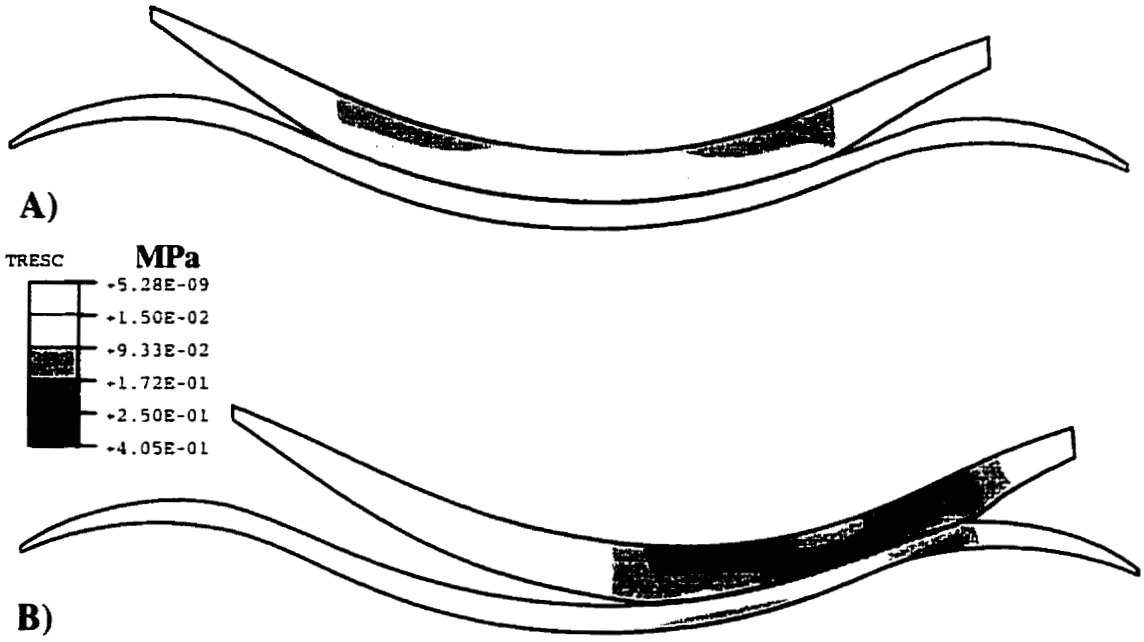

Figure 4.25: Biphasic model (Case A): Tresca stress distribution in the solid phase of the patellar and femoral cartilage for A) central and B) lateral tracking.

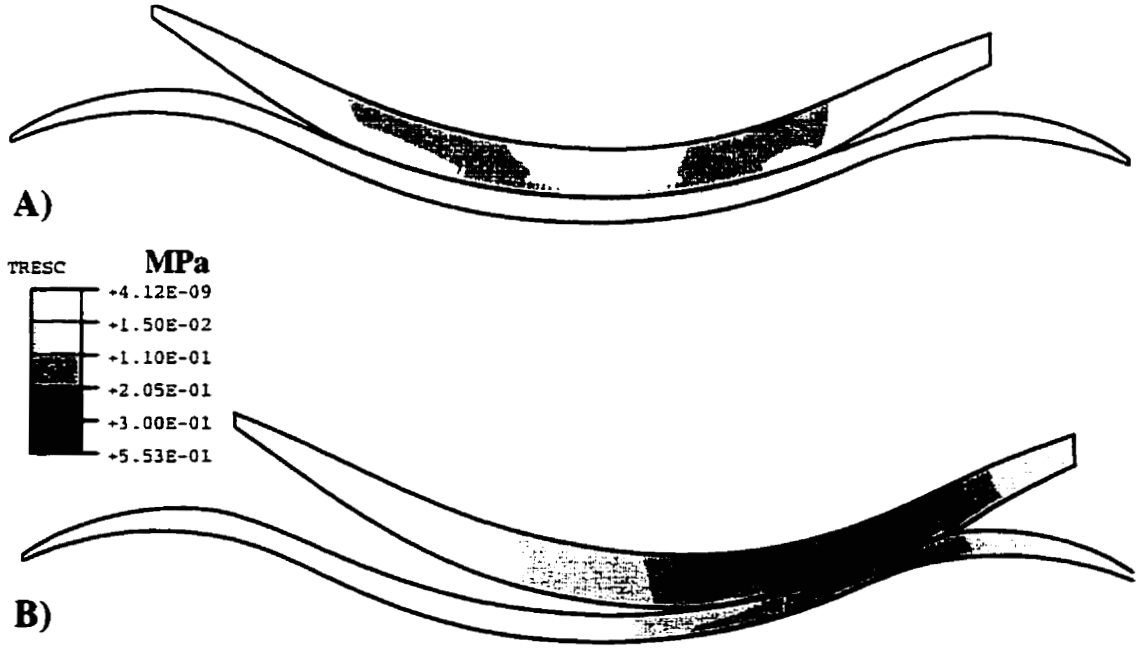

Figure 4.26: Elastic model (Case EL1): Tresca stress distribution in the patellar and femoral cartilage for A) central and B) lateral tracking.

The Tresca stress was highest in the patellar cartilage by the subchondral bone in the central tracking models. In the lateral tracking models there was an additional region of high stress at the patellar surface.

In the biphasic model, lateral tracking increased peak Tresca stress by 95-105% in the patella, and 205-230% in the femoral cartilage (Figure 4.27). For the elastic models, lateral tracking increased patellar and femoral peak Tresca stress by 119%, and 228% respectively (Figure 4.28).

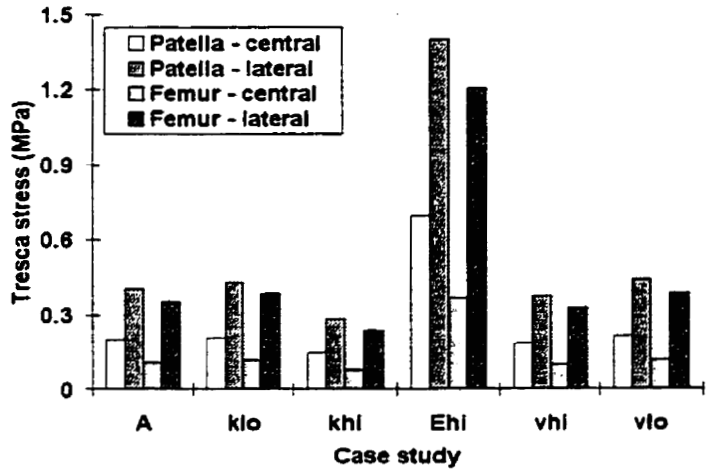

Figure 4.27: Biphasic models: Peak Tresca stresses in the solid phase of the patellar and femoral cartilage for central and lateral tracking.

4.3.7 Minimum Principal Strain

The distribution of minimum principal strain was similar for all biphasic and elastic case studies (Figure 4.29 and Figure 4.30). A large negative minimum principal strain indicated the compressive deformation of the cartilage. The lowest minimum principal strain occurred close to the subchondral bone on either side of the contact area. For lateral tracking the magnitude of the compressive principal strain was much higher than for central tracking, and there was an additional region of high compressive strain at the surface of the patella. The magnitude of the minimum principal strain for the biphasic cases was consistently larger than for the elastic case studies.

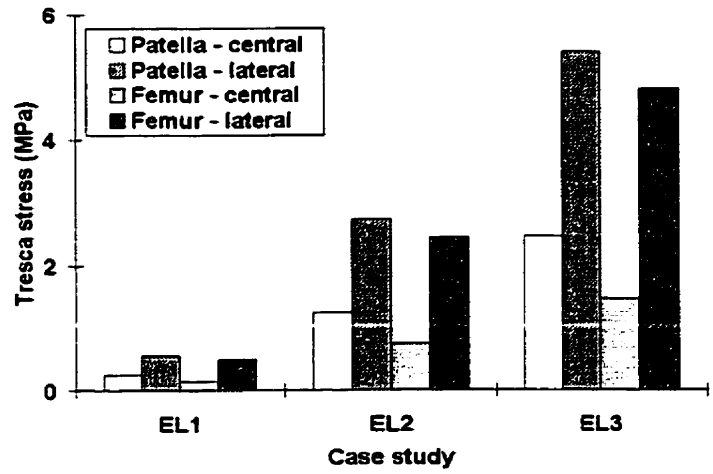

Figure 4.28: Elastic models: Peak Tresca stresses in the patellar and femoral cartilage for central and lateral tracking.

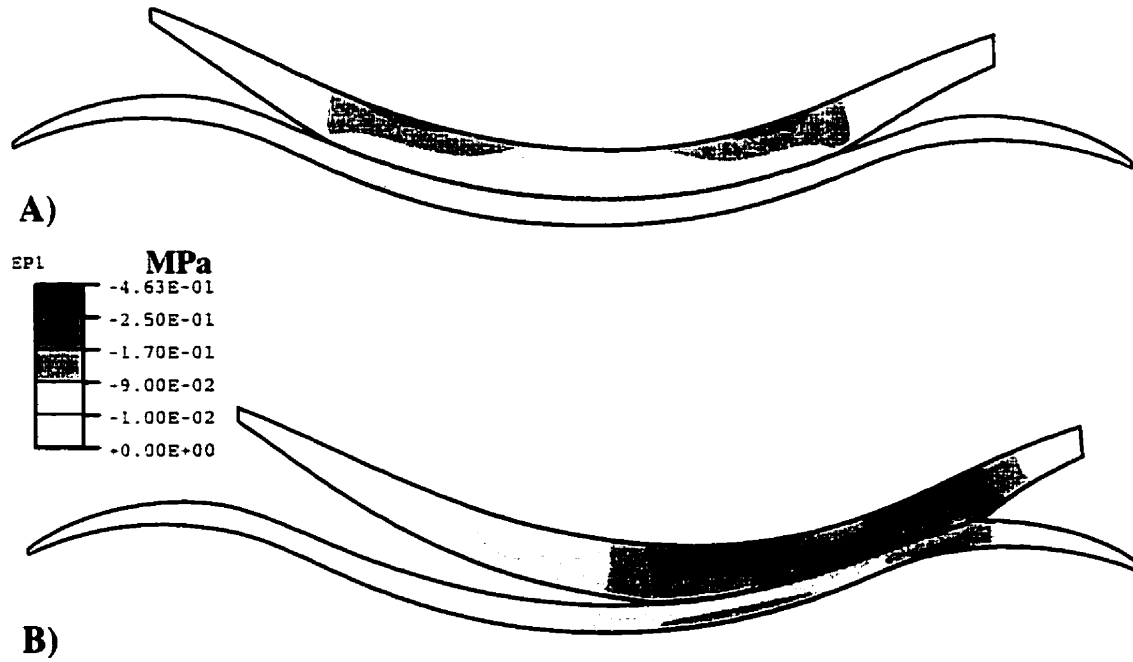

Figure 4.29: Biphasic model (Case A): Minimum principal strain distribution in the solid phase of the patellar and femoral cartilage for A) central and B) lateral tracking. Dark regions indicate high compressive strain.

Note, that although the local strain for the biphasic cases was as high as 45% in the lateral tracking model, the majority of cartilage experienced compressive strain less than 25-30%. Therefore, it was assumed that the linear biphasic theory provided a reasonable approximation.

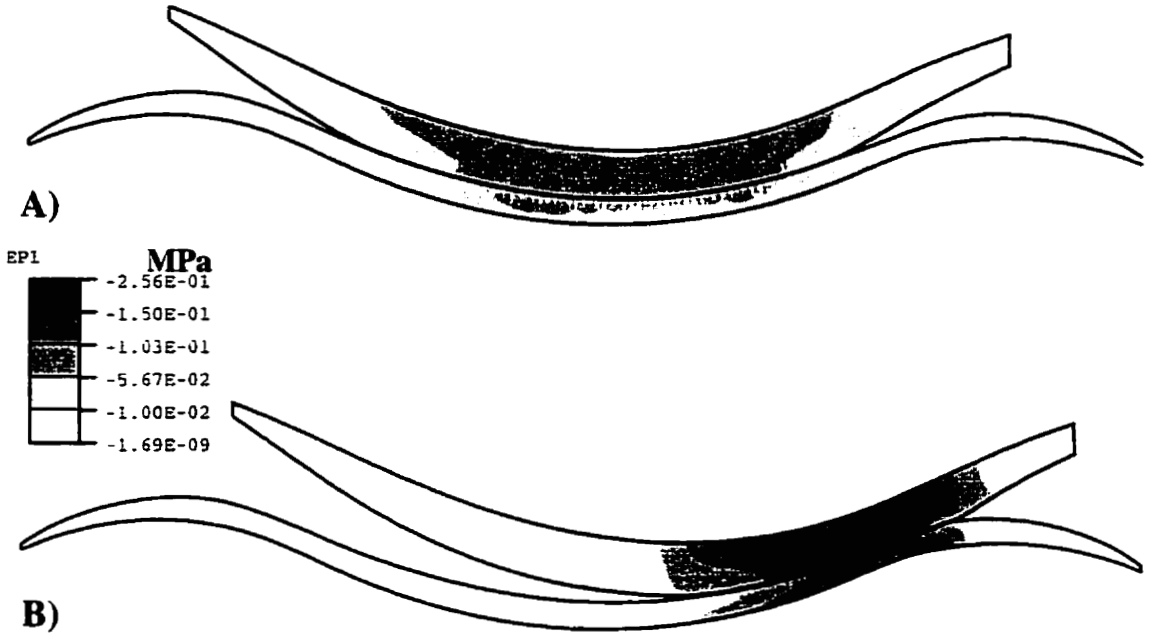

Figure 4.30: Elastic model (Case EL1): Minimum principal strain distribution in the patellar and femoral cartilage for A) central and B) lateral tracking. Dark regions indicate high compressive strain.

In the biphasic models, lateral tracking increased the peak compressive principal strain in the patellar and femoral cartilage by 105% and 180-225% respectively (Figure 4.31). For the elastic models, lateral tracking resulted in a 144% and 155% increase in patellar and femoral peak compressive principal strains, respectively (Figure 4.31). Changing the permeability (Cases Khi and Klo) had the largest effect on cartilage strains in the biphasic model. In general, the elastic models yielded far smaller compressive principal strains.

4.3.8 Maximum Principal Strain

The distribution of maximum principal strain was similar for all biphasic and elastic case studies (Figure 4.32 and Figure 4.33). A large positive maximum principal strain indicated the tensile deformation of the cartilage. Close to the subchondral bone on either side of the contact area was the region of the highest tensile deformation. For lateral tracking the maximum principal strain was higher than for central tracking, and there was an additional region of high principal strain at the patellar surface. The tensile principal strain was much larger in the biphasic than elastic models.

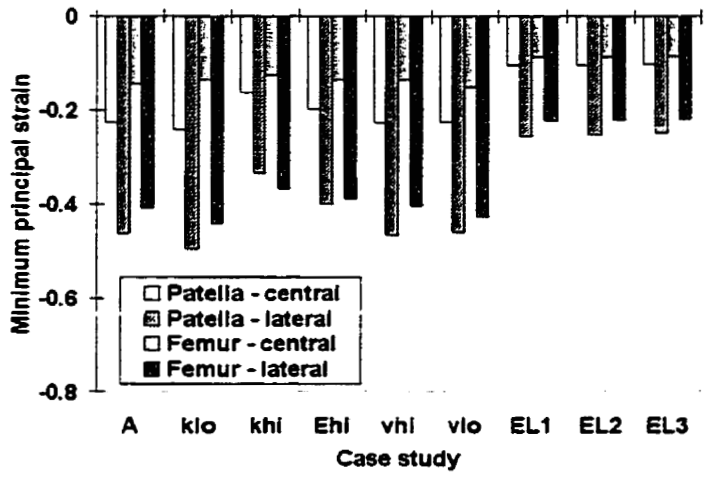

Figure 4.31: Biphasic and elastic models: Peak minimum principal strains in the patellar and femoral cartilage for central and lateral tracking.

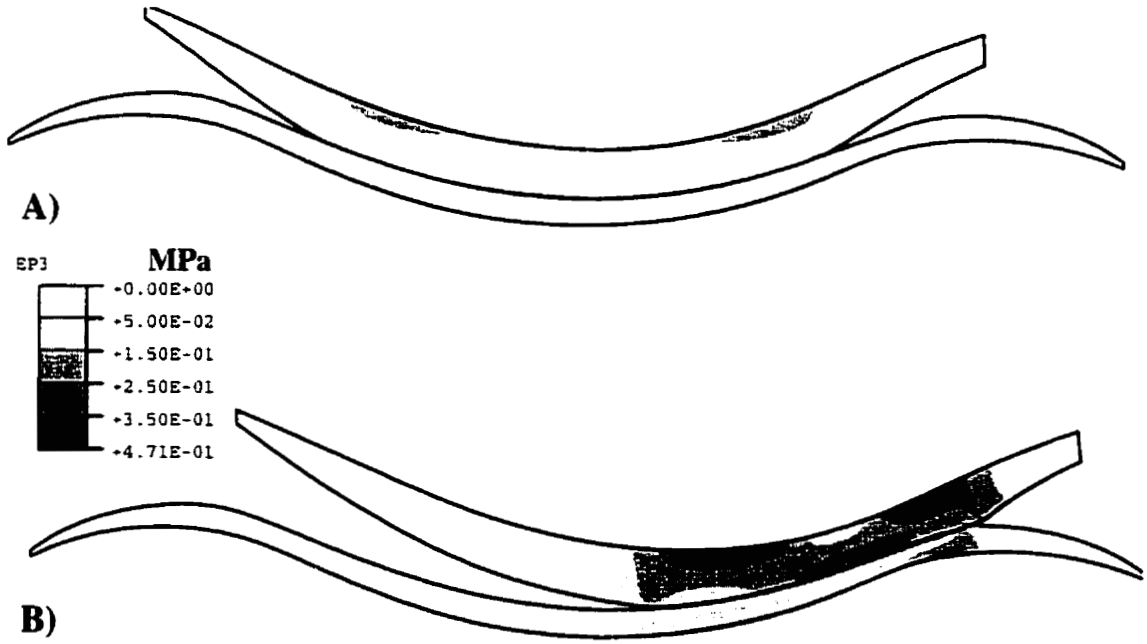

Figure 4.32: Biphasic model (Case A): Maximum principal strain distribution in the solid phase of the patellar and femoral cartilage for A) central and B) lateral tracking. Dark regions indicate high tensile strain.

In the biphasic model, lateral tracking increased in the peak value of maximum principal strain in the patellar and femoral cartilage by 95 to 105%, and 180 to 230% respectively (Figure 4.34).

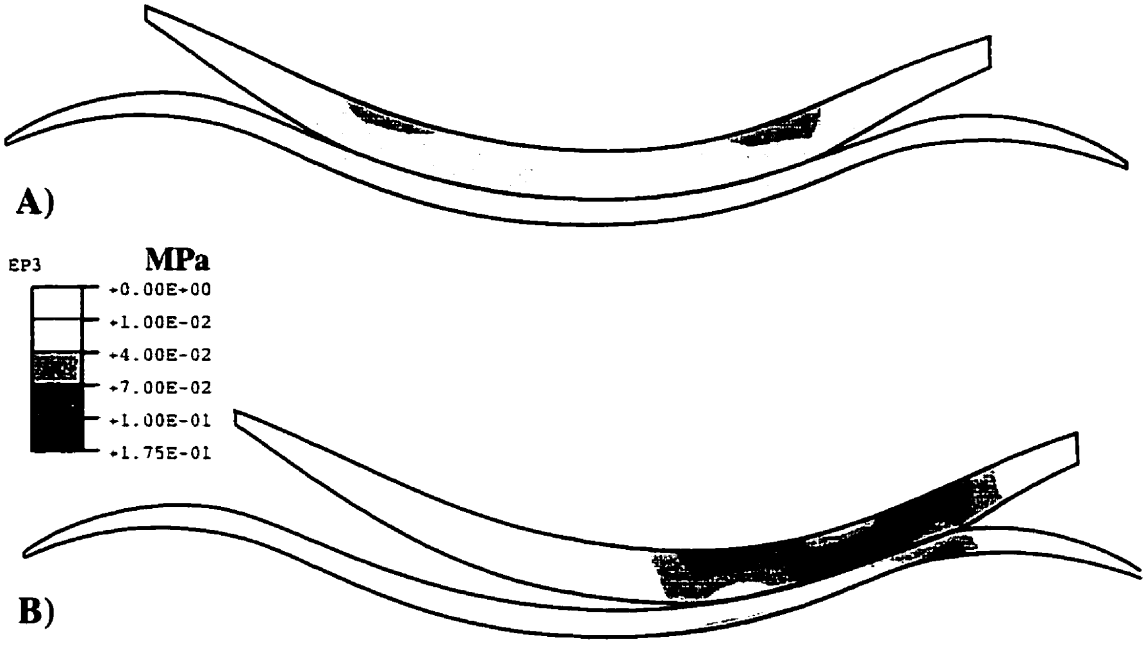

Figure 4.33: Elastic model (Case EL1): Maximum principal strain distribution in the patellar and femoral cartilage for A) central and B) lateral tracking. Dark regions indicate high tensile strain.

For the elastic models, lateral tracking resulted in an increase of 117%, and 240% in patellar and femoral maximum principal strains, respectively (Figure 4.34). Again decreasing the permeability had the largest effect on cartilage strains in the biphasic models. Also note that the elastic models, being much stiffer, resulted in substantially lower strains than the biphasic models.

4.3.9 Summary of Results

Regardless of the element and material properties chosen, all case studies showed similar differences between central and lateral tracking. Table 4.7 illustrates the percentage change based on central values caused by lateral tracking for all the output variables studied. In all cases, lateral tracking caused a

- decrease in contact area,
- increase in contact pressure,
- increase in pore pressures,
- increase in absolute magnitude of principal stresses,
- increase in Tresca stress,
- increase in absolute magnitude of principal strains.

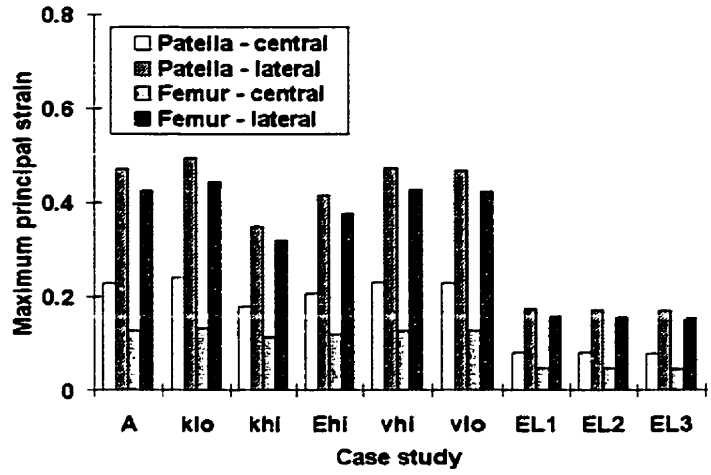

Figure 4.34: Biphasic and elastic models: Peak values of maximum principal strain in the patellar and femoral cartilage during central versus lateral tracking.

Table 4.7: Summary of the percentage change in selected finite element model output variables due to lateral versus central tracking (Lateral - Central) / Central x 100%.

Output variable	Patellar cartilage		Femoral cartilage	
	Biphasic	Elastic	Biphasic	Elastic
Contact area	-38%	-46%	-	-
Contact pressure	70-80%	120%	-	-
Pore pressures	55-75%	n/a	55-70%	n/a
Minimum principal stress	100-120%	125%	175-195%	133%
Maximum principal stress	95-105%	94%	175-230%	325-335%
Tresca stress	95-105%	119%	205-230%	228%
Minimum principal strain	105%	144%	180-225%	155%
Maximum principal strain	95-105%	117%	180-230%	240%

Although the percentage differences of these variables for central to lateral tracking were similar, the absolute values of some of the variables changed considerably between case studies. Contact area was relatively insensitive to changes in material properties, although it was generally less for the elastic models than the linear biphasic models. For the biphasic models, permeability had the largest effect on strain. Increased permeability caused a reduction in the magnitude of principal strains in the cartilage solid phase. Contact pressure and principal and Tresca stress were most sensitive to stiffness or Young's modulus of the cartilage. Increased stiffness led to an increase in cartilage stress. Permeability and Poisson's ratio had a far smaller effect. Increased permeability caused a decrease in the magnitude of biphasic cartilage stresses. Likewise, a decrease in Poisson's ratio resulted in an increase in magnitude of cartilage stresses.

4.4 DISCUSSION

The effects of lateral versus central patellar orientation on contact geometry and cartilage stress were investigated. It was hypothesized that the less congruent lateral orientation would lead to a smaller contact area, resulting in higher cartilage stresses and strains. A plane strain finite element model was developed to investigate the hypothesis. The model geometry was based on a geometric model (Boyd, 1997) constructed from experimentally collected surface and kinematic data from the PF joint of one cat specimen. Two patellar orientations were analysed; a central tracking orientation with a congruence index of 0.015 mm^{-1}, representing a highly congruent joint orientation, and a lateral tracking orientation with a congruence index of 0.267 mm^{-1}, representing a less congruent position. At 70° of flexion, with the PF reaction force held constant, lateral tracking, as compared to central tracking, resulted in a

- decrease in contact area,
- increase in contact pressure,
- increase in pore pressures,
- increase in absolute magnitude of principal stresses,
- increase in Tresca stress, and an
- increase in absolute magnitude of principal strains.

The plots of contact pressure illustrated that lateral tracking resulted in a smaller contact area with larger peak contact pressures. The contour plots of principal stresses and strains, indicated that smaller regions of larger stresses and cartilage deformation were induced by lateral tracking. The percentage change in peak values of the variables were used to indicate changes in cartilage stress and strain distributions due to patellar positions (Table 4.7).

Since data from only one specimen were used, the results could not be generalized. To establish relations between patellar alignment, contact geometry, and cartilage stresses further studies need to be done involving a larger sample size. Furthermore, only two patellar orientations, central and lateral, at a flexion angle of 70°, were analysed. This was not sufficient to establish a relation between joint alignment and cartilage stresses. To establish this relation it would be necessary to study the effects of contact geometry

throughout a full range of flexion angles. It would also be necessary to study a full range of patellar reorientations incorporating out-of plane patellar rotation and tilt as well as the reorientation within the transverse plane, that was the focus of this study. Therefore, the following discussion is limited to using this case study to explore aspects of joint alignment, contact geometry and cartilage stresses. The possible effects of these aspects on tissue function and health will be speculated. The discussion is presented in eight sections.

4.4.1 Validation and Evaluation of Results

Evaluation and validation of numerical models are very important. Simplifying assumptions made regarding geometry, and element and material properties limit the validity of the models. Since material properties were not measured in this study it was not possible to validate the model completely. Instead the model was evaluated by comparing the present results to literature values. Although it was difficult to compare results between studies due to differences in loading protocol, specimen geometry, and patellar orientation, reported values were useful in providing a general estimate of the order of magnitude of the results. As the contact area was insensitive to the material properties it was used in model evaluation. The contact area/unit width calculated for lateral tracking at 70° was an average of 2.76 mm. This was in good agreement with the contact length calculated using the geometric model (Boyd, 1997). Assuming that overlap of the undeformed surfaces indicated contact, the contact length was calculated as 2.43 mm. To compare contact areas with values in the literature the contact area/unit width was multiplied by a contact width of 3.63 mm, calculated from the geometric model. The total contact area, estimated from the finite element model was 10 mm^2 for lateral tracking. This was in good agreement with contact areas measured with pressure sensitive film (Herzog, unpublished data). Contact areas were measured for five cat PF joints during stimulation of the quadriceps nerve, while a restraining bar fixed the knee flexion angle. For a 20% stimulation, as was used in the present experiment, the average contact area at a flexion angle of 58° was 8 mm^2 to 10 mm^2. Other studies (Ronsky et al., 1995) reported a much larger average contact area of 41.3 mm^2. However, this may be because the

measurement was taken during 60% stimulation of the quadriceps nerve. Micro-indentation transducers were used to study contact area in cadaver knees while loading the quadriceps (Ahmed et al., 1983b). Twenty-five to 30% of the patellar surface was in contact at 70° flexion. In the present study, given that the total patellar cartilage surface area was approximately 87 mm^2, the contact area for lateral tracking was 12% of the total area. It is suspected that this value was low due to the non-central patellar orientation in the present study. Using the contact area /unit width of 4.65 mm calculated for the central tracking model, and assuming the contact length was 75% of the contact width (i.e., the same proportion as for lateral tracking), the contact area corresponding to central tracking was estimated as 28.1 mm^2. This resulted in a contact area of approximately 32% of the total patellar surface area for central tracking, which was in good agreement with Ahmed et al. (1983b).

It was more difficult to evaluate PF contact forces, contact pressures, and cartilage stresses, due to the dependence of these variables on the material properties. As well, with differences in geometry and loading conditions a comparison of results between studies was not always useful. A comparison of contact pressures with another study involving similar loading conditions and geometry was made to put the present results into perspective. The range of peak PF contact pressures for central tracking calculated in the present study ranged from 0.4 to 1.8 MPa for the biphasic models, and 0.6 to 5.5 MPa for the elastic models. Herzog (unpublished data) measured an average of 13 MPa peak pressure in 5 cats with pressure sensitive film, at 20% stimulation. It was speculated that the differences between the model and experimentally measured peak pressure were primarily due to the assumption of plane strain made for the model, as well as differences in specimen geometry, patellar tracking, and loading conditions. Although comparison with pressure sensitive film data was useful, recall that it has been estimated that pressure sensitive film data are associated with 25% error.

It would be useful to construct a joint model based on geometry and force equilibrium to provide an estimate of the PF contact force. This would help our ability to evaluate the model. In addition to the unconstrained extension, during experimental data collection

(Boyd, 1997) a number of trials were taken in which a restraining bar was used to fix the flexion angle of the knee. The bar was instrumented to measure the force. As well, an implantable force transducer was used to measure the force in the patellar tendon. The force measurements and geometry may be used as inputs to a joint model, to provide an estimate of the PF contact force. Validation of the model would be complicated by the simplifying assumptions of the joint model and measurement accuracy of the implantable force transducer.

In the present study the less congruent lateral patellar tracking resulted in smaller contact area, and larger stresses and strains in the cartilage than the more congruent central tracking. It was difficult to compare the magnitude of the changes in mechanics with values presented in the literature because of differences in joint geometry, loading conditions, and joint orientations between studies. Likewise, typically the contact geometries have not been quantified making a direct comparison of results impossible. However, the general trends of decreasing contact area and increasing stress with non-central tracking have been observed in the literature.

Differences in contact mechanics due to ACL transection in cat PF joints have been studied using pressure sensitive film (Herzog et al., 1998). Contact areas and peak pressures were measured at different flexion angles for different knee extensor forces, produced by stimulation of the femoral nerve. In general, the contact area in ACL intact knees was oriented laterally, whereas in the ACL transected joints the contact area was more centrally located. Pressure sensitive film indicated that for central position the contact area was 22% higher and the peak pressures were 55% lower than for lateral contact. The same trends were observed in the present study. The magnitude of the effect of contact geometry cannot be commented on since the geometry of the surfaces and congruence was not quantified. In addition, although the stimulation was the same for both the ACL intact and ACL transected knees, the ACL integrity is suspected to affect the PF contact force. Previous studies of unrestrained locomotion of cats suggested that the PF contact forces are reduced by approximately 30% in ACL deficient knees (Hasler et al., 1998a). Therefore, the changes in contact mechanics may be due to a combined

effect of decreased loading as well as changes in contact geometry.

Many studies perturbing muscle forces and joint alignment have resulted in increased contact pressure due to non-central loading. The effects of varying tension in the components of the quadriceps muscle on pressure distribution in the PF joint of humans was studied using micro-indentation transducers (Ahmed et al., 1983b). Removing the tension in the vastus medialis oblique and vastus lateralis, in turn, caused lateral and medial contact, respectively. Contact area decreased for non-central tracking. The magnitude of the change in contact area and pressure distributions was not quantified. The effects of varying Q-angle on cartilage contact pressures have been analysed using a 3D mathematical model of the human PF joint in conjunction with a Hertzian elastic model (Hirokawa, 1991). Both increasing and decreasing the Q-angle resulted in non-central pressure distributions, leading to an overall increase in PF contact stress. The contact geometry, contact area magnitude and location were not reported. Similar findings were reported using pressure sensitive film to study the effect of Q-angle in human cadaver knees (Huberti and Hayes, 1984). Both increasing and decreasing the Q-angle resulted in less uniform contact pressure distributions. A 10% increase and decrease in Q-angle resulted in up to a 45% and 53% increase in peak PF contact pressures, respectively. Two different non-central contact patterns were associated with changes in Q-angle. The contact area either shifted laterally or peripheral high pressure was found on both the lateral and medial facet, with a nearly complete unloading of the central region.

To date, few numerical analyses have been done to determine the effect of perturbing PF joint alignment and orientation on cartilage stress and strain distributions. However, several studies, using finite element models, have reported large changes in contact area and contact stresses associated with changes in joint geometry. Stone and Yu (1997) represented a joint using circular arcs. The contact area, and contact stresses were analysed for twelve geometric cases by varying the ratio of radii of the bodies (R1/R2). A small decrease in R1/R2 from 0.99 to 0.98 caused a 25% increase in compressive stress and a 17% increase in shear stress. In a similar study, Eckstein et al. (1994) analysed five hemispherical and semielliptical joint geometries. The model with a flatter socket (i.e., the

socket was semielliptical and the radius of the inlet was 2.5% greater that the radius of the head) resulted in a 65% increase in peak von Mises stresses. It was concluded that very slight variations in the geometry of the articular surfaces may have a profound effect on the stress distribution in joints.

Therefore, previous studies support the results of the present study that contact geometry and joint orientation affect the contact mechanics. Results reported in the literature support the general trend that non-central joint alignment is associated with a decrease in contact area, an increase in contact pressure and an increase in cartilage stress. It was difficult to compare results between studies directly, due to differences in geometries, loading, and material properties between studies. However, in general the percent change in stresses and strains were much larger in the present study than values reported in the literature. It was speculated that the experimental studies did not perturb joint position as extremely as in this study, and therefore, the resulting change in joint congruence was not as large. Theoretical studies, approximating the joint geometries with circular arcs are expected to overestimate joint congruence. The present approach of incorporating specific joint geometry and kinematics may have been more representative of joint surface interaction.

The distribution of stresses and strains provided information on how the joint functions to transmit loads. The stress distributions will be discussed and compared to distributions presented in the literature. This discussion primarily presents the results of the biphasic models (i.e., the stresses and strains in the solid phase). However, recall that the total principal strains and Tresca stress calculated by the elastic models demonstrated the same trends as the biphasic models. Only the total principal stresses differed between the elastic and biphasic cases, because pore fluid pressure was taken into account in the elastic models. As well, although the magnitude of the variables was different between the material case studies, the distributions were not sensitive to material property changes. Therefore, this discussion applies to all the case studies.

For central tracking, regions with the highest magnitude of principal stress, principal

strain, and tresca stress were located at the subchondral bone interface, peripheral to the initial point of contact. Regions of high stress adjacent to the subchondral bone interface have been reported in the literature (Eberhardt et al., 1990; Atkinson et al., 1998; Newberry et al., 1998; Donzelli et al., 1999). Maximum shear stress has been reported at the subchondral bone interface at a radius of approximately 3/4 the contact radius (Eberhardt et al., 1990). Similar trends were reported by Atkinson et al. (1998), who investigated impact with a planar elastic model.

The locations of high stress and strain correlated well with the observed horizontal cracking at the cartilage subchondral bone interface in diseased joints (Meachim and Bentley, 1978). It has been suggested that shear stresses may be responsible for the horizontal cracking (Eberhardt et al., 1990). For central tracking the principal stresses and strains were oriented approximately 45° to the bone interface, indicating large shear stresses. This was in good agreement with the results reported in the literature. Principal stresses were directed approximately 45° to the subchondral bone interface for a transversely isotropic axisymmetric model (Donzelli et al., 1999). Similarly, the principal strains in the cartilage were oriented 40° to the subchondral bone interface using an elastic model (Li et al., 1995). Therefore, the results for principal directions of stress agree with other models, as well as known failure patterns in joints. Note that although the location of maximum stresses was similar for this model and impact injury models, due to the loading conditions, the magnitude of the stresses were much lower for this model. Even though the increase in stresses from central to lateral tracking was large, it is not known whether it was sufficient to lead to damage, perhaps after repetitive loading. For comparison, it would be of interest to establish the changes in stresses associated with normal range of motion and small perturbations in alignment.

As well as horizontal cracking, vertical splitting and fraying at the cartilage surface have been observed in diseased joints (Meachim and Bentley, 1978). In the central tracking models, in the present study, no regions of high stress and strain were observed at the articular surfaces. However, lateral tracking resulted in high stresses and strains at the articular surface in the contact region as well as at the subchondral bone interface

peripheral to the initial point of contact. This type of distribution was observed for principal stress, principal strain, and Tresca stress. Other studies have found secondary regions of high stresses and strains on the cartilage surface. An elastic impact model (Newberry et al., 1998) predicted that as well as high shear stress at the bone interface, there was a concentrated area of high maximum shear stress near the articular surface under the impact zone. Histological analysis of slices of cartilage showed that articular cartilage fissures were found in areas of high surface shear stress. Peak stresses at the cartilage surfaces were observed in a transversely isotropic biphasic model, but not in the isotropic biphasic model (Donzelli et al., 1999). It has been suggested that high tensile stress may be responsible for vertical splitting at the cartilage surface (Eberhardt et al., 1990). The direction of the maximum principal stresses was parallel and perpendicular to the surface, with the highest tensile stresses tangent to the surface. Similar principal stress directions were reported by Donzelli et al. (1999). Therefore, the distribution and direction of stresses in the lateral and central tracking model agree with the literature and known failure patterns in joints.

4.4.2 Comparison of Congruence Index and Finite Element analysis

Congruence index was a measure of the 3D local geometry at the initial points of contact. Where as the finite element analysis accounted for the global geometry in a 2D slice as well as the cartilage and bone material properties. Comparing the results of both analyses, the finite element results correlated well with the assumptions made regarding the effect of congruence on joint mechanics in Chapter 3. It was assumed that a less congruent joint exhibits smaller contact area, resulting in larger stresses and strains. As expected, the less congruent lateral tracking position decreased contact area by approximately 40%, and increased peak stresses and strains between 100% and 200%. This suggests that congruence index may be useful in comparatively indicating cartilage stresses, as well as characterizing contact geometry. The central and lateral patellar positions represent the range of congruence indices that result from perturbations in patellar tracking of the PF joint at 70° of flexion. Therefore, all other positions analysed may yield stresses and strains within the range determined by the central and lateral tracking positions. However,

cartilage stresses were only analysed for two extreme positions. The relation between congruence index and cartilage stresses is still unclear. It is expected that the relation between congruence index and cartilage stresses depends on joint geometry, joint loading, and material properties. Analysis of a range of patellar orientations under a variety of conditions would increase understanding of the relation between congruence index and cartilage stresses.

4.4.3 Comments on the Structure and Function of Cartilage

Analysing the internal mechanics of the tissue allow further insight on how the structure of the cartilage affects its function. Two of the main functions of cartilage are to transmit and distribute compressive joint loads. Therefore, it is necessary to have a compression carrying material under the load. The architecture of the cartilage surface is not conducive to carry these loads due to the poor compressive properties of collagen. However, the main component of cartilage is tissue fluid (60-80%). Hydrostatic fluid pressure is the most efficient way of transmitting and distributing compressive loads through a fluid filled tissue. This was shown in the biphasic models where isobars of pore pressure ran the full depth of the cartilage to the subchondral bone (Figure 4.9). At peak loading the fluid protected the solid matrix by taking 2 to 3 times more load than the solid matrix. The distribution of total stresses in the elastic case studies were very similar to the distribution of pore pressures in the biphasic models, indicating that at peak loading the fluid phase played a dominant role in carrying compression.

To carry compressive loads, the tissue fluid must be sufficiently confined. The impermeability of the solid matrix helped confine the tissue fluid. It is also speculated that the surface layer of the cartilage impedes fluid flow, due to a thin layer of pressurized fluid where contact occurs. In addition, as fluid flows the remaining matrix and negatively charged proteoglycans are compressed together, increasing drag forces which impede further fluid flow. The confined conditions ensure that the cartilage maintains its shape during cyclic loading. If very large shape changes occur quickly ploughing friction may impede joint movement. However, a certain amount of matrix permeability allows the

redistribution and exudation of tissue fluid. Fluid flow may contribute to changes in joint geometry that increase joint congruence. For example, lateral fluid movement away from the contact region caused bulging at the periphery of the contact region, effectively increasing the contact area and reducing contact pressures. Bulging peripheral to the contact region may be one reason why the elastic models resulted in consistently lower contact areas than the biphasic models. Exudation of fluid also maintains a thin layer of pressurized fluid and near frictionless contact. Fluid flow also is thought to contribute to tissue health in the movement of nutrients and cell wastes.

One of the advantages of the biphasic finite element analysis, was that the results provided insight on the interaction between the solid and fluid components of the cartilage, and helped define their functional roles. Under compression, the fluid flowed laterally under the contact region. Due to the impermeability of the solid matrix, the fluid exerted drag forces on the matrix. The drag forces caused tensile stress in the solid matrix. The tensile stresses were oriented in the same directions as pore fluid movement. For example, the principal tensile stresses were oriented parallel to the cartilage surface under the contact region in the surface layer, and 45 degrees to the subchondral bone in the deep layer. Lateral tensile stresses were observed in all biphasic models. In the elastic models tensile stresses within the contact region were absent because the fluid flow was not modelled.

Collagen fibres are the main tension carrying component in the cartilage matrix. To carry tensile stresses effectively the collagen fibres are oriented parallel to the direction of the tensile stress field. Therefore, at the cartilage bulging peripheral to the contact region and lateral tension caused by drag from fluid flow are restrained by collagen fibres oriented parallel to the surface. Similarly, in the deep zone, where fluid is flowing away from the bone, the collagen fibres are perpendicular to the bone. In addition, the principal stresses were oriented 45 degrees to the subchondral bone inducing shear stresses. The fibres also reinforce the cartilage to withstand these shear stresses. Through the middle or transitional layer, the collagen fibres have a random orientation to deal with lateral flow under the contact region and flow towards the cartilage surface on the periphery of the contact region. Therefore, there is evidence that there is a strong relationship between the

anatomical structure and the stresses carried by the components of cartilage.

4.4.4 Speculations on the Effects of PF Tracking on Cartilage Health

The large differences in magnitude and distribution of stresses and strains between lateral and central tracking suggest that patellar orientation may play a large role in cartilage function and health. It has been suggested that there is a window of optimal loading to maintain cartilage health and that loading outside this window may contribute to the onset of PF disorders and disease, such as chondromalacia, patellofemoral pain syndrome, and osteoarthritis. In this study, peak cartilage stresses and strains increased by 100% to 200%, as a result of lateral tracking. Although the increase in cartilage stresses is large, their effect on cartilage function and health is not fully understood. How does the range of cartilage stresses induced by perturbing patellar tracking correspond to the window of optimal loading? Is the increase in cartilage stresses sufficient to affect cartilage health adversely? Further research on the long term effects of changes in stress of this magnitude are necessary to establish the effects on cartilage health and function.

Mechanical loading maintains cartilage health by affecting nutrition of the solid matrix and cartilage cells. Loading causes pressure gradients within the cartilage, promoting interstitial fluid flow. The pore fluid movement causes an influx of nutrients and an efflux of wastes. It has also been proposed that mechanical loading affects the metabolic activity of cartilage cells. In the lateral tracking model the contact area and region of high pore pressures was small. The lack of mechanical stimuli may adversely affect the unloaded regions. In contrast, for central tracking the stresses and pore pressures were distributed over a large area affecting most of the cartilage. A uniform distribution of stresses over a large region may promote better nutrition and increased cell metabolism. The optimal patellar tracking alignment to promote effective transmission of loads and cartilage health has not been established. It has been shown that a perfectly congruent system on a global scale does not distribute loads well (Greenwald and O'Conner, 1971; Eckstein et al., 1994). The optimal joint congruence for the most efficient load transmission and distribution is also not currently known. It has been suggested that a certain amount of

incongruence is necessary to promote movement of synovial fluid and to allow joint movement. Knowledge of the stresses associated with normal joints, and the sensitivity of stresses resulting from perturbations in alignment may provide a basis for further understanding optimal tracking and the sensitivity of the PF joint.

4.4.5 Effects of Element and Material Property Assumptions

The range of element and material properties used to model cartilage in the literature was large. Variations in material properties have been attributed to

- natural variation of tissue structure and composition,
- variation between species,
- variation in specific testing protocol,
- methods of storing cartilage, and
- theoretical approach used (i.e., lack of appropriate constitutive equations).

To date it is not well established which assumptions most accurately model the behaviour of articular cartilage. Due to the uncertainty in the element and material property assumptions, nine cases were analysed: 6 linear biphasic cases, and 3 elastic cases. The peak values of the output variables were used to indicate changes in the loading response of the models. The percentage change of the peak values of each of the variables was used to quantify the effect of the element and material property assumptions on the difference between lateral and central tracking (Table 4.7). All cases showed trends of similar magnitude. On average, the percentage change was larger in the femoral cartilage than the patellar cartilage and was larger for the elastic models. Therefore, the differences between lateral and central tracking were relatively insensitive to the element and material properties assumed. One of the strengths of this comparative study was that the results did not depend on the absolute value of stress, but rather on the relative changes in stress and strain due to lateral versus central tracking.

Although the element and material properties did not affect the change in contact mechanics between lateral and central tracking greatly, the absolute value of some of the output variables varied considerably. Contact area was higher for the linear biphasic models than the elastic models, but was relatively insensitive to changes in material

properties. The cartilage in the biphasic models investigated was generally more compliant than in the elastic models. As well, tangential fluid flow caused bulging at the edges of the contact area, possibly increasing the contact area.

For the biphasic cases, changes in permeability had the largest effect on solid strains. The strains were substantially lower for the elastic models, due to increased stiffness. However, for the biphasic models the strains in the solid phase were reported. In contrast, for the elastic models, the total strains of the entire cartilage were reported. Therefore, the biphasic and elastic strains cannot be directly compared. This is also true for the calculation of stresses.

Contact pressure, principal stresses, and Tresca stresses were most sensitive to the stiffness or Young's modulus of the cartilage. Increasing the stiffness increased cartilage stresses. These findings are in agreement with the literature. For example, it was found that increasing the Young's modulus by 5 times yielded a 75% increase in contact pressures (Huber-Betzer et al., 1990). However, the material property sensitivity, in their study, was analysed for a model with a 3 mm step-off fracture, which may have affected results. In the present study, the permeability and Poisson's ratio had smaller effects on results than the Young's modulus. Decreasing the permeability and the Poisson's ratio effectively made the cartilage less compliant and increased cartilage stresses.

Due to the uncertainty in element and material properties, the current role of finite element modelling of cartilage is as a comparative tool. For example, in the present study the relative effects of lateral versus central tracking were compared. The absolute values of the stresses and strains could not be commented on, because they were dependent on the element and material properties. Likewise, this study did not allow us to conclude which of the element and material property assumptions most accurately model articular cartilage behaviour. To make further advances in this area it is critical to measure the cartilage properties, evaluate the constitutive equations, and collect the experimental data necessary to validate the model assumptions.

4.4.6 Limitations

There were a number of limitations to this study. Firstly, a plane strain finite element model was used. This is equivalent to modelling a thin transverse slice through the joint, in which the out-of-plane geometry was assumed constant. Although, curvature analysis showed that the curvatures vary little in the proximal/distal direction the incorporation of out-of-plane changes in geometry, and out-of-plane variations in stress are expected to affect the model results. Using geometric model data and the automatic meshing program it is possible to create a 3D finite element model by constructing brick elements from the nodes of consecutive slices. Issues regarding contact modelling, model convergence, and computer storage time would have to be dealt with. However, it would be of interest to compare the differences between the 3D model and the plane strain model.

The uncertainty in the material properties limited the analysis. There is some debate on whether the current constitutive equations used to characterize cartilage and the indirect experiments used to determine the material coefficients are appropriate. Due to the uncertainty in the properties taken from the literature the absolute value of the stresses and strains at certain locations in the cartilage could not be determined definitively. The study was limited to comparing the relative magnitude of the variables between two patellar tracking positions. The uncertainty of the material properties also affected our ability to evaluate the model. In addition, the cartilage was assumed to be homogenous and isotropic. The cartilage is known to be heterogeneous and anisotropic. It is not known to what extent the simplifying assumptions affect the results. Finally, the linear biphasic theory was used. This is a reasonable approximation if the strains are less that 25-30%. Although the lateral tracking model showed peak strains of closer to 45-50%, these occurred in small isolated regions, and the majority of the regions had strains within the linear range. However, it would be of interest to implement the finite deformation theory to investigate the effect of incorporating strain dependent material properties.

Another limitation of the study was the loading protocol. Although the loading protocol used in the model was sufficient to investigate the effects of patellar alignment on joint

stresses, it did not fully represent in-vivo joint loading for several reasons. Recall, that the model was loaded along the normal to the surface at the initial point of contact, until the measured displacement was achieved. In-vivo, the patella slides over the femoral groove surface, potentially inducing shear stresses at the surface. Although the final positions are the same, simplification of the loading is expected to cause changes in the cartilage stresses. Secondly, to isolate the effects of relative surface geometries the loading between central and lateral tracking was constant. In-vivo, changing the patellar orientation is expected to affect the PF contact force, which would affect the induced cartilage stresses. Further research must be done to quantify the expected changes in loading with changes in patellar orientation. In addition, the kinematics was measured during 20% stimulation of the femoral nerve. The kinematics and loading are, therefore, expected to differ from physiologic in-vivo kinematics and loading. It would be of interest to quantify the joint biomechanics using normal walking kinematics.

Finally, to establish relations between patellar alignment, contact geometry, and cartilage stresses further studies need to be done involving a larger sample size. In addition, it would be necessary to study the effects of contact geometry throughout a full range of flexion angles. It would also be necessary to study a full range of patellar reorientations incorporating out-of plane patellar rotation and tilt as well as the reorientation within the transverse plane, that was focused on in this study.

4.4.7 Conclusions

In conclusion, the finite element results suggested that patellar orientation and consequently contact geometry significantly affects the loading response of cartilage. Lateral tracking, representing an incongruent joint position, decreased contact area by approximately 40%, and increased the magnitude of peak stresses and strains by 100% to 200%. These results correlated well with the assumptions made regarding the effect of congruence on joint mechanics in the previous chapter. Lateral and central tracking were associated with different distribution patterns of stresses and strains. For central tracking, regions of peak stress and strain occurred at the subchondral bone interface. However, for

lateral tracking there was a secondary region of high stress and strain at the articular surface. High tensile principal stresses in the biphasic models were oriented parallel to the surface, and high principal stresses were oriented 45° to the subchondral bone. This distribution correlated well with literature and evidence of vertical surface cracking and horizontal splitting at the subchondral bone interface in patients with osteoarthritis. The tensile stresses were a result of drag forces exerted on the solid matrix by fluid flow. The collagen fibres are oriented in the same directions as the calculated principal tensile stress field. This indicates that functional role of the collagen fibres is to carry tensile stress. Conversely, the functional role of the confined tissue fluid is to carry compressive stress.

Joint orientation and contact geometry may have significant effects on cartilage function and health. Further research must be done to establish the effect of the calculated changes in magnitude and distribution of cartilage stresses on health, to determine the optimal patellar orientation and joint congruence for the efficient transmission of joint forces. These findings have important implications in terms of treatment and rehabilitation of joint instabilities and abnormal tracking associated with ligament laxity and rupture, joint malalignment and muscle imbalances.

5.0 GENERAL SUMMARY AND CONCLUSIONS

The goal of this research was to investigate the complex relation between PF kinematics and joint mechanics. The objective was to understand how patellar orientation and position in the femoral groove affects contact geometry, and the resulting cartilage stresses and strains. Two approaches were used:

- the study of joint congruence and
- the study of cartilage stresses and strains.

Both approaches used experimentally measured surface geometry and in-situ joint kinematics of a cat PF joint (Boyd, 1997).

Joint congruence index was quantified as a function of flexion angle, and central versus a range of medial and lateral patellar tracking positions. The congruence index indicated the similarity between the local relative geometries of the joint surfaces which affects joint surface interaction. It was assumed that a highly congruent joint increases contact area, and decreases cartilage stresses and strains. The local congruence was sensitive to patellar position. Congruence varied with flexion angle and perturbations in medial-lateral patellar position. Congruence was highest in the central tracking positions and decreased with medial and lateral tracking.

To further investigate the effects of the joint congruence, a plane strain finite element model incorporating bone and cartilage material properties was created. The resulting stresses and strains in the cartilage were quantified as a function of lateral versus central patellar tracking position. The lateral position, with a congruence index of 0.267 mm^{-1}, represented an incongruent position. While the central position, with an index of 0.015 mm^{-1}, represented a congruent position. Both biphasic and elastic plane strain finite element models were investigated. Lateral tracking decreased contact area by approximately 40% and increased cartilage stresses and strains by 100% to 200%.

The finite element results correlated well with the assumptions made regarding the effect of congruence on joint mechanics in Chapter 3. As hypothesized, the less congruent lateral

position resulted in a smaller contact area, and larger stresses and strains. This suggests that congruence index may be a valuable indicator of cartilage stresses and strains. The central and lateral patellar positions were representative of the endpoints of the range of congruence indices that resulted from perturbations in patellar tracking at 70° of flexion. Therefore, all other positions analysed may yield stresses and strains within the bounds determined by the central and lateral tracking positions. Calculation of stresses and strains for a range of patellar orientations under a variety of conditions would increase understanding of the relation between congruence index and cartilage stresses.

There are advantages and disadvantages to both approaches used. Quantifying congruence index was straightforward. It could be quickly calculated for numerous joint positions and was an ideal measure to perform a sensitivity analysis. However, the measure did not account for cartilage compliance, material properties, changes in global geometry with deformation, and the thickness of cartilage. Congruence index could only be used as an indirect indicator of contact area, and cartilage stresses. In addition, the congruence index was a measure of the local geometries at the initial points of contact. It has been suggested that a measure of the global geometry would be more indicative of the interaction of cartilage surfaces. In contrast, quantifying cartilage stresses using the finite element method took into account cartilage compliance, material properties, cartilage thickness, and changes in geometry with deformation. In addition, the effects of the magnitude and rate of loading could be analysed, and the time-dependent response of cartilage could be quantified. However, finite element modelling is time consuming, and it would be difficult to perform a sensitivity analysis to various joint positions. In addition, without accurate element and material properties, finite element modelling could only be used as a comparative tool. Therefore, both methods have their advantages, and both are useful in determining the sensitivity of joints to changes in joint orientation and contact geometry.

The PF joint studied was sensitive to changes in patellar position. Lateral tracking, compared to central tracking, caused an 18 fold increase in congruence index, and a 100% to 200% increase in cartilage stresses. To determine whether these results are representative a larger number of joints need to be characterized to determine how

variations in joint geometry and patellar tracking patterns affect PF joint sensitivity to patellar position.

Although the increase in cartilage stresses was large, the effect on cartilage function and health was not fully understood. An animal model in which the medial or lateral vasti are cut to induce medial or lateral tracking would allow investigation of the effects of tracking on cartilage health in-vivo. There are a number of challenges to overcome. Firstly, resulting changes in cartilage stresses must be quantified. Since dynamic stress distributions cannot be measured directly, the use of theoretical models would be necessary. This would involve quantifying in-vivo skeletal kinematics combined with joint geometry, and material properties. However, due to uncertainties regarding modelling assumptions, finite element methods are limited to being a comparative tool. Further research must be done in terms of determining material properties, evaluating constitutive equations, and incorporating 3D geometry. The above are necessary for model validation. The ability to validate models is vital for finite element modelling to realize its full potential in terms of quantifying stresses in cartilage. Secondly, criteria must be determined to indicate tissue health. The following is a list of variables that may provide an indication of tissue health:

- material properties of cartilage,
- cartilage porosity,
- water content of cartilage,
- cell density,
- changes in geometry (thickness or surface geometry),
- biochemical analysis of cartilage,
- markers indicating cell metabolism, and
- interstitial fluid flow.

A number of these variables have been analysed previously (Wong et al., 1997; Herzog et al., 1998). The results were not conclusive due to the inadequate number of specimens analysed, large variability between specimens, and the limitations of the experimental techniques available. In addition, most studies have analysed the short-term effect of loading on tissue health. Since, cartilage and other biological tissue (i.e., ligaments and muscles) are continuously adapting it is necessary to study the long term response of

cartilage in-vivo.

Although central tracking was associated with highest joint congruence and lowest cartilage stresses, further research must be done to determine whether it is the optimal patellar orientation for efficient transmission of force and cartilage health. To determine optimal tracking further understanding of the effect of stress on cartilage health is necessary. In addition, it is necessary to study a full range of patellar reorientations incorporating out-of plane patellar rotation and tilt as well as the reorientation within the transverse plane, that was focused on in this study.

As a result of this research it is proposed that patellar alignment may be an important consideration in terms of treatment and rehabilitation of joint instabilities and abnormal tracking associated with ligament laxity and rupture, joint malalignment and muscle imbalances. Understanding the relation between kinematics, joint geometry, and mechanical function of the joint is vital in furthering insight on the effect of joint injuries and disease.

6.0 REFERENCES

ABAQUS (1994a) ABAQUS theory manual (version 5.4). Hibbit, Karlsson, and Sorenson, Inc., Pawtucket, USA.

ABAQUS (1994b) ABAQUS user manual, volume I (version 5.4). Hibbit, Karlsson, and Sorenson, Inc., Pawtucket, USA.

ABAQUS (1994c) ABAQUS user manual, volume II (version 5.4). Hibbit, Karlsson, and Sorenson, Inc., Pawtucket, USA.

Ahmed, A. M. and Burke, D. L. (1983a) In-vitro measurement of static pressure distribution in synovial joints--Part I: Tibial surface of the knee. *J Biomech. Eng.* 105(3), 216-225.

Ahmed, A. M., Burke, D. L., and Yu, A. (1983b) In-vitro measurement of static pressure distribution in synovial joints--Part II: Retropatellar surface. *J. Biomech. Eng.* 105(3), 226-236.

An, K. N., Himeno, S., Tsumura, H., Kawai, T., and Chao, E. Y. (1990) Pressure distribution on articular surfaces: Application to joint stability evaluation. *J. Biomechanics* 23(10), 1013-1020.

Anderson, D.D., Brown, T. D., Yang, K. H., and Radin, E. L. (1990) A dynamic finite element analysis of impulsive loading of the extension-splinted rabbit knee. *J. Biomech. Eng.* 112(2), 119-128.

Armstrong, C. G., Lai, W. M., and Mow, V. C. (1984) An analysis of the unconfined compression of articular cartilage. *J. Biomech. Eng.* 106(2), 165-173.

Ateshian, G. A., Soslowsky, L. J., and Mow, V. C. (1991) Quantitation of articular surface topography and cartilage thickness in knee joints using stereophotogrammetry. *J. Biomechanics.* 24(8), 761-776.

Ateshian, G. A., Rosenwasser, M. P., and Mow, V. C. (1992) Curvature characteristics and congruence of the thumb carpometacarpal joint: differences between female and male joints. *J. Biomechanics.* 25(6), 591-607.

Ateshian, G. A. (1993) A B-spline least-squares surface-fitting method for articular surfaces of diarthrodial joints. *J. Biomech. Eng.* 115(4A), 366-373.

Ateshian, G. A., Kwak, S. D., Soslowsky, L. J., and Mow, V. C. (1994) A stereophotogrammetric method for determining in situ contact areas in diarthrodial joints, and a comparison with other methods. *J. Biomechanics.* 27(1), 111-124.

Ateshian, G. A., Warden, W. H., Kim, J. J., Grelsamer, R. P., and Mow, V. C. (1997) Finite deformation biphasic material properties of bovine articular cartilage from

confined compression experiments. *J. Biomechanics* 30(11-12), 1157-1164.

Athanasiou, K. A., Rosenwasser, M. P., Buckwalter, J. A., Malinin, T. I., Mow, V. C. (1991) Interspecies comparisons of in situ intrinsic mechanical properties of distal femoral cartilage. *J. Orthop. Res.* 9(3), 330-340.

Atkinson, T. S., Haut, R. C., and Altiero, N. J. (1998) Impact-induced fissuring of articular cartilage: an investigation of failure criteria. *J. Biomech. Eng.* 120(2), 181-187.

Beck, J. M., Farouki, R. T. and Hinds, J. K. (1986) Surface analysis methods. *IEEE CG&A*. 6, 18-36.

Bentley, G. and Dowd, G. (1984) Current concepts of etiology and treatment of chondromalacia patellae. *Clin. Orthop.* 189, 209-228.

Biot, M. A. (1941) General theory of three-dimensional consolidation. *J. of Applied Physics*. 12, 155-164.

Blankevoort, L., Kuiper, J. H., Huiskes, R., and Grootenboer, H. J. (1991) Articular contact in a three-dimensional model of the knee. *J. Biomechanics* 24(11), 1019-1031.

Boyd, S. K. (1997) A 3D in-situ model for patellofemoral joint contact analysis in the normal and anterior cruciate ligament deficient knee. MSc. Thesis, University of Calgary, Calgary, AB.

Boyd, S. K., Ronsky, J. L., Lichti, D. D., Salkauskas, K., and Chapman, M. A. (1999) Joint surface modelling with thin-plate splines. *J. Biomech. Eng.* 121(5), 525-532.

Brown, T. D. and Muratori, D. R. (1979) Miniature piezoelectric transducers for transient soft-body contact stress problems. *Exp. Mech.* 19, 214-219.

Brown, T. D. and Shaw, D. T. (1983) In vitro contact stress distributions in the natural human hip. *J. Biomechanics* 16(6), 373-384.

Brown, T. D. and DiGioia, A. M. (1984) A contact-coupled finite element analysis of the natural adult hip. *J. Biomechanics* 17(6),437-448.

Brown, T. D. and Shaw, D. T. (1984) In vitro contact stress distribution on the femoral condyles. *J. Orthop. Res.* 2(2), 190-199.

Brown, T. D., Singerman, R. J. (1986) Experimental determination of the linear biphasic constitutive coefficients of human fetal proximal femoral chondroepiphysis. *J. Biomechanics* 19(8), 597-605.

Bullough, P., Goodfellow, J., and O'Conner, J. (1973) The relationship between degenerative changes and load-bearing in the human hip. *J. Bone Joint Surg.*

55B(4), 746-758.

Bullough, P. G. and Jagannath, A. (1983) The morphology of the calcification front in articular cartilage. Its significance in joint function. *J. Bone Joint Surg.* 65B(1), 72-78.

Bullough, P. G. (1992) The Pathology of osteoarthritis. In Osteoarthritis: Diagnosis and medical/surgical management, 2nd Ed., 39-69. (edited by Moskowitz, R. W., Howell, D. S., Goldberg, V. M., and Mankin, H. J.), W. B. Saunders, Philadelphia.

Cowin, S. C. (1989) Bone Mechanics. 102. CRC Press, Boca Raton, Florida.

Dekel, S. and Weissman, S. L. (1978) Joint changes after overuse and peak overloading of rabbit knees in vivo. *Acta. Orthop. Scand.* 49(6), 519-528.

Donzelli, P. S., Spilker, R. L., Ateshian, G. A., and Mow, V. C. (1999) Contact analysis of biphasic transversely isotropic cartilage layers and correlations with tissue failure. *J. Biomechanics* 32(10), 1037-1047.

Eberhardt, A. W., Keer, L. M., Lewis, J. L., and Vithoontien, V. (1990) An analytical model of joint contact. *J. Biomech Eng.* 112(4), 407-413.

Eckstein, F., Merz, B., Schmid, P., and Putz, R. (1994) The influence of geometry on the stress distribution in joints--a finite element analysis. *Anat. Embryol.* 189(6), 545-552.

Edwards, J. (1967) Physical characteristics of articular cartilage. *Inst. Mech. Engrs. Proc.* 181, 16-24.

Essinger, J. R., Leyvraz, P. F., Heegard, J. H., and Robertson, D. D. (1989) A mathematical model for the evaluation of the behaviour during flexion of condylar-type knee prostheses. *J. Biomechanics* 22(11-12), 1229-1241.

Farin, G. (1996) Curves and surfaces for computer aided geometric design (4th ed.). Academic Press.

Ferguson, A. B., Brown, T. D. , Fu, F. H., and Rutkowski, R. (1979) Relief of patellofemoral contact stress by anterior displacement of the tibial tubercle. *J. Bone Joint Surg.* 61A(2), 159-166.

Ficat, R. P. and Hungerford, D. S. (1977) Disorders of the patello-femoral joint. Masson, Paris.

Frank, C. B. and Shrive, N. G. (1994) Ligament. In *Biomechanics of the Musculo-skeletal System*, 106-132. (edited by Nigg, B. M. and Herzog, W), Wiley, New York.

Fujikawa, K., Seedhom, B. B., and Wright, V. (1983) Biomechanics of the patello-femoral

joint. Part I: A study of the contact and the congruity of the patello-femoral compartment and movement of the patella. *Eng. Med.* 12(1), 3-11.

Fukubayashi, T. and Kurosawa, H. (1980) The contact area and pressure distribution pattern of the knee. A study of normal and osteoarthrotic knee joints. *Acta. Orthop. Scand.* 51(6), 871-879.

Fulkerson, J. P. and Shea, K. P. (1990) Mechanical basis for patellofemoral pain and cartilage breakdown. In Articular Cartilage and Knee Joint Function: Basic Science and Arthroscopy. 93-101. (edited by Ewing, J. W.), Raven Press, Ltd., New York.

Galbraith, P. C. and Bryant, J. T. (1989) Effects of grid dimensions on finite element models of an articular surface. *J. Biomechanics* 22(4), 385-393.

Goldsmith, A. A., Hayes, A., and Clift, S. E. (1996) Application of finite elements to the stress analysis of articular cartilage. *Med. Eng. Phys.* 18(2), 89-98.

Goodfellow, J. and Mitsou, A. (1977) Joint surface incongruity and its maintenance: an experimental study. *J. Bone Joint Surg.* 59B(4), 446-451.

Greenwald, A. S. and O'Connor, J. J. (1971) The transmission of load through the human hip joint. *J. Biomechanics* 4(6), 507-528.

Hamilton, G. R. (1996) Joint congruity and the congruous range of motion applied to displaced intra-articular calcaneal fractures. PhD. Thesis, University of Calgary, Calgary, AB.

Hasler, E. M. and Herzog, W. (1998a) Quantification of in vivo patellofemoral contact forces before and after ACL transection. *J. Biomechanics* 31(1), 37-44.

Hasler, E. M., Herzog, W., Leonard, T. R., Stano, A., Nguyen, H. (1998b) In vivo knee joint loading and kinematics before and after ACL transection in an animal model. *J. Biomechanics* 31(3), 253-262.

Haut, R. C., Ide, T. M., and De Camp, C. E. (1995) Mechanical responses of the rabbit patello-femoral joint to blunt impact. *J. Biomech. Eng.* 117(4), 402-408.

Haut, T. L., Hull, M. L., and Howell, S. M. (1998) A high-accuracy three-dimensional coordinate digitizing system for reconstructing the geometry of diarthrodial joints. *J. Biomechanics* 31(6), 571-577.

Hayes, W. C., Keer, L. M., Herrmann, G., Mockros, L. F. (1972) A mathematical analysis for indentation tests of articular cartilage. *J. Biomechanics* 5(5), 541-551.

Heegaard, J., Leyvraz, P. F., Curnier, A., Rakotomanana, L., and Huiskes, R. (1995) The biomechanics of the human patella during passive knee flexion. *J. Biomechanics* 28(11), 1265-1279.

Herzog, W., Diet, S., Suter, E., Mayzus, P., Leonard, T. R., Muller, C., Wu, J. Z., and Epstein, M. J. (1998) Material and functional properties of articular cartilage and patellofemoral contact mechanics in an experimental model of osteoarthritis. *J. Biomechanics* 31(12), 1137-1145.

Hirokawa, S. (1991) Three-dimensional mathematical model analysis of the patellofemoral joint. *J. Biomechanics* 24(8), 659-671.

Howell, D. S., Treadwell, B. V. and Trippel, S. B. (1992) Etiopathogenesis of osteoarthritis. In *Osteoarthritis: Diagnosis and medical/surgical management*, 2nd Ed., 233-262. (edited by Moskowitz, R. W., Howell, D. S., Goldberg, V. M., and Mankin, H. J.), W. B. Saunders, Philadelphia.

Huber-Betzer, H., Brown, T. D., and Mattheck, C. (1990) Some effects of global joint morphology on local stress aberrations near imprecisely reduced intra-articular fractures. *J. Biomechanics* 23(8), 811-822.

Huberti, H. H. and Hayes, W. C. (1984) Patellofemoral contact pressures. The influence of Q-angle and tendofemoral contact. *J. Bone Joint Surg.* 66A(5), 715-724.

Huberti, H. H. and Hayes, W.C. (1988) Contact pressures in chondromalacia patellae and the effects of capsular reconstructive procedures. *J. Orthop. Res.* 6(4), 499-508.

Hughston, J. C. (1968) Subluxation of the patella. J. Bone Joint Surg. 50A(5), 1003-1026.

Huiskes, R., Kremers, J., de Lange, A., Woltring, H. J., Selvik, G., and van Rens, T. J. (1985) Analytical stereophotogrammetric determination of three-dimensional knee-joint geometry. *J. Biomechanics* 18(8), 559-570.

Insall, J., Goldberg, V., and Salvati, E. (1972) Recurrent dislocation and the high-riding patella. *Clin. Orthop.* 88, 67-69.

Insall, J., Falvo, K. A., and Wise, D. W. (1976) Chondromalacia Patellae. A prospective study. *J. Bone Joint Surg.* 58A(1), 1-8.

Jurvelin, J., Kiviranta, I., Tammi, M., and Helminen, J. H. (1986) Softening of canine articular cartilage after immobilization of the knee joint. *Clin. Orthop.* 207, 246-252.

Kempson, G.E., Freeman, M. A. R., and Swanson, S. A. V. (1968) Tensile properties of articular cartilage. *Nature* 220, 1127-1128.

Kempson, G. E., Freeman, M. A., and Swanson, S. A. (1971) The determination of a creep modulus for articular cartilage from indentation tests of the human femoral head. *J. Biomechanics* 4(4), 239-250.

Koskinen, S. K., Hurme, M., and Kujala, U. M. (1991) Restoration of patellofemoral

congruity by combined lateral release and tibial tuberosity transposition as assessed by MRI analysis. *Int. Orthop.* 15(4), 363-366.

Kwak, S. D., Colman, W. W., Ateshian, G. A., Grelsamer, R. P., Henry, J. H., and Mow, V. C. (1997) Anatomy of the human patellofemoral joint articular cartilage: surface curvature analysis. *J. Orthop. Res.* 15(3), 468-472.

Lai, W. M. and Mow, V. C. (1980) Drag-induced compression of articular cartilage during a permeation experiment. *Biorheology* 17(1-2), 111-123.

Lai, W. M., Mow, V. C., and Roth, V. (1981) Effects of nonlinear strain-dependent permeability and rate of compression on the stress behavior of articular cartilage. *J. Biomech. Eng.* 103(2), 61-66.

Lancaster, P. and Salkauskas, K. (1986) Curve and Surface Fitting: an Introduction. *Academic Press*. London.

Laurin, C. A., Levesque, H. P., Dussault, R., Labelle, H., and Peides, J. P. (1978) The abnormal lateral patellofemoral angle: a diagnostic roentgenographic sign of recurrent patellar subluxation. *J. Bone Joint Surg.* 60A(1), 55-60.

Lawrence, R. C., Hochberg, M. C., Kelsey, J. L., McDuffie, F. C., Medsger, T. A. Jr., Felts, W. R., and Shulman, L. E. (1989) Estimates of the prevalence of selected arthritic and musculoskeletal diseases in the United States. *J. Rheumatology* 16(4), 427-441.

Li, X., Haut, R. C., and Altiero, N. J. (1995) An analytical model to study blunt impact response of the rabbit P-F joint. *J. Biomech. Eng.* 117(4), 485-491.

Lur'e, A. I. (1964) Three-dimensional problems of the theory of elasticity, 314-323 (edited by Radok, J. R. M.), Interscience, New York.

Mak, A. F., Lai, W. M., and Mow, V. C. (1987) Biphasic indentation of articular cartilage--I. Theoretical analysis. *J. Biomechanics* 20(7), 703-714.

Maroudas, A. (1979) Physiochemical properties of articular cartilage. In *Adult articular cartilage.* 215-290. M. A. R. Freeman (Ed.). Pitman, London.

Matthews, L. S., Sonstegard, D. A., and Henke, J. A. (1977) Load bearing characteristics of the patello-femoral joint. *Acta. Orthop. Scand.* 48, 511-516.

McCutchen, C. W. (1962) The frictional properties of animal joints. *Wear* 5, 1-17.

Meachim, G. and Bentley, G. (1978) Horizontal splitting in patellar articular cartilage. *Arthritis Rheum.* 21(6), 669-674.

Merchant, A. C., Mercer, R. L., Jacobsen, R. H., and Cool, C. R. (1974) Roentgenographic

analysis of patellofemoral congruence. *J. Bone Joint Surg.* 56A(7), 1391-1396.

Moskowitz, R. W. (1992) Experimental models of osteoarthritis. In *Osteoarthritis: Diagnosis and medical/surgical management*, 2nd Ed., 233-262. (edited by Moskowitz, R. W., Howell, D. S., Goldberg, V. M., and Mankin, H. J.), W. B. Saunders, Philadelphia.

Mow, V. C., Kuei, S. C., Lai, W. M., and Armstrong, C. G. (1980) Biphasic creep and stress relaxation of articular cartilage in compression: Theory and experiments. *J. Biomech. Eng.* 102(1), 73-84.

Mow, V. C., Gibbs, M. C., Lai, W. M., Zhu, W. B., and Athanasiou, K. A. (1989) Biphasic indentation of articular cartilage--II. A numerical algorithm and an experimental study. *J. Biomechanics* 22(8-9), 853-861.

Mow, V. C., Ateshian, G. A., and Ratcliffe, A. (1990) Anatomic form and biomechanical properties of articular cartilage of the knee joint. In *Biomechanics of Diarthrodial Joints* (Edited by Mow, V. C.) 55-81. Springer-Verlag, New York.

Mow, V. C. and Proctor, C. S. (1989) Biomechanics of articular cartilage. In *Basic Biomechanics of the Muskuloskeletal System* (edited by Nordin, M. and Frankel, V. H.) 31-58. Lea &Febiger, Baltimare, Maryland.

Mukherjee, N. and Wayne, J. S. (1998a) Load sharing between solid and fluid phases in articular cartilage: I--Experimental determination of in situ mechanical conditions in a porcine knee. *J. Biomech. Eng.* 120(5), 614-619.

Mukherjee, N. and Wayne, J. S. (1998b) Load sharing between solid and fluid phases in articular cartilage: II--Comparison of experimental results and u-p finite element predictions. *J. Biomech. Eng.* 120(5), 620-624.

Newberry, W. N., Garcia, J. J., Mackenzie, C. D., Decamp, C. E., and Haut, R. C. (1998) Analysis of acute mechanical insult in an animal model of post-traumatic osteoarthrosis. *J. Biomech. Eng.* 120(6), 704-709.

Newman, A. P. (1998) Articular cartilage repair. *Am. J. Sports Med.* 26(2), 309-324.

Palmoski, M. J., Colyer, R. A. , and Brandt, K. D. (1980) Joint motion in the absence of normal loading does not maintain normal articular cartilage. *Arthritis Rheum.* 23(3), 325-334.

Paulos, L., Rusche, K., Johnson, C., and Noyes, F. R. (1980) Patellar malalignment: a treatment rationale. *Physical Therapy.* 60(12), 1624-1632.

Pond, M. J. and Nuki, G. (1973) Experimentally-induced osteoarthritis in the dog. *Ann. Rheum. Dis.* 32(4), 387-388.

Radin, E. L., Ehrlich, M. G., and Chernack, R. (1978) Effect of repetitive impulsive loading on the knee joints of rabbits. *Clin. Orthop.* 131, 288-293.

Ronsky, J. L. (1994) In-vivo patellofemoral joint contact. PhD. Thesis, University of Calgary, Calgary, AB.

Ronsky, J. L., Herzog, W., Brown, T. D., Pedersen, D. R., Grood, E. S., and Butler, D. L. (1995) In vivo quantification of the cat patellofemoral joint contact stresses and areas. *J. Biomech*anics 28(8), 977-983.

Ronsky, J. L., Boyd, S. K., Lichti, D. D., Chapman, M. A., and Salkauskas, K. (1999) Precise measurement of cat patellofemoral joint surface geometry with multistation digital photogrammetry. *J. Biomech. Eng.* 121(2), 196-205.

Scherrer, P. K. and Hillberry, B. M. (1979) Piecewise mathematical representation of articular surfaces. *J. Biomechanics.* 12(4), 301-311.

Schinagl, R. M., Gurskis, D., Chen, A. C., and Sah, R. L. (1997) Depth-dependent confined compression modulus of full-thickness bovine articular cartilage. *J. Orthop. Res.* 15(4), 499-506.

Setton, L. A., Mow, V. C., Muller, F. J., Pita, J. C., and Howell, D. S. (1994) Mechanical properties of canine articular cartilage are significantly altered following transection of the anterior cruciate ligament. *J. Orthop. Res.* 12(4), 451-463.

Shrive, N. G. and Frank, C. B. (1994) Articular Cartilage. In *Biomechanics of the Musculo-skeletal System*, 79-105. (edited by Nigg, B. M. and Herzog, W), Wiley, New York.

Simon, B. R. (1992) Multiphase poroelastic finite element models for soft tissue structures. *Appl. Mech. Rev.* 45(6), 191-218.

Spilker, R. L., Suh, J. K., and Mow, V. C. (1992) A finite element analysis of the indentation stress-relaxation response of linear biphasic articular cartilage. *J. Biomech. Eng.* 114(2), 191-201.

Stone, J. J. and Yu, H. (1997) Computational contact analysis of joint congruency. *Biomed. Sci. Instrum.* 34, 368-373.

Stergiou, P. (1996) Biomechanical factors associated with patellofemoral pain syndrome in runners. MSc. Thesis, University of Calgary, Calgary, AB.

Suh, J. K., Spilker, R. L., and Holmes, M. H. (1991) A penalty finite element analysis for nonlinear mechanics of biphasic hydrated soft tissue under large deformation. *Int. J. Num. Methods in Eng.* 32, 1411-1439.

Suh, J. K. and Spilker, R. L. (1994) Indentation analysis of biphasic articular cartilage:

nonlinear phenomena under finite deformation. *J. Biomech. Eng.* 116(1), 1-9.

van der Voet, A. F. (1992) Finite element modelling of load transfer through articular cartilage. Ph. D. Dissertation, The University of Calgary Press, Calgary, Canada.

van Eijden, T. M. , Kouwenhoven, E., Verburg, J., and Weijs, W. A. (1986) A mathematical model of the patellofemoral joint. *J. Biomechanics* 19(3), 219-229.

Wismans, J., Veldpaus, F., Janssen, J., Huson, A., and Struben, P. (1980) A three-dimensional mathematical model of the knee-joint. *J. Biomechanics* 13(8), 677-685.

Woltring, H. J. (1986) A FORTRAN package for generalized cross-validatory spline smoothing and differentiation. *Advances in Engineering Software* 8(2). 104-113.

Wong, M., Wuethrich, P., Buschmann, M. D., Eggli, P., and Hunziker, E. (1997) Chondrocyte biosynthesis correlates with local tissue strain in statically compressed adult articular cartilage. *J. Orthop. Res.* 15(2), 189-196.

Wu, J. Z., Herzog, W., and Epstein, M. (1998a) Evaluation of the finite element software ABAQUS for biomechanical modelling of biphasic tissues. *J. Biomechanics* 31(2),165-169.

Wu, J. Z., Herzog, W., and Epstein, M. (1998b) Effects of inserting a pressensor film into articular joints on the actual contact mechanics. *J. Biomech. Eng.* 120(5), 655-659.

Zarek, J. M. and Edwards, J. (1963) The stress-structure relationship in articular cartilage. *Med. Electron. Biol. Eng.* 1. 497-507.